Glaciers of Asia—

GLACIERS OF PAKISTAN

By John F. Shroder, Jr., *and* Michael P. Bishop

SATELLITE IMAGE ATLAS OF GLACIERS OF THE WORLD

Edited by RICHARD S. WILLIAMS, JR., *and* JANE G. FERRIGNO

CONTENTS

GLACIERS OF ASIA—

GLACIERS OF PAKISTAN[1]

By John F. Shroder, Jr.,[2] *and* Michael P. Bishop[2]

Abstract

Glaciers of northern Pakistan are some of the largest and longest mid-latitude glaciers on Earth, with an estimated area of 15,000 km². Field-based and space-based glacier studies in this region are necessary to elucidate their role in providing melt-water for irrigation, hazard potential, their role in erosion and geodynamics, and their sensitivity to climate forcing. Repeated field surveys in the 1980s, 1990s, and 2000s of several glaciers in the Hindu Kush and Swat, Kohistan region, the Nanga Parbat Himalaya, and the Karakoram Himalaya, provided reference data and verification for information extracted from satellite imagery. A number of these field assessments (*Balt Bare*, Batūra, Biafo, *Gorshai, Rāikot, Sachen*, Tirich Mir, and Yengutz Har) are reported here as case studies, thought to be representative of the diversity of glaciers and their fluctuations in the western Himalaya. A number of change-detection studies using the older Landsat satellite imagery, in some cases compared to newer ASTER imagery, provide useful comparisons.

Emphasis was also directed toward glaciers with unusual advance, retreat, or surge histories. Eight criteria were developed for recognition of different types of flow as displayed on the older imagery and then applied to 169 glaciers; many have multiple criteria. Five glaciers had strongly convoluted medial or lateral moraines; 13 glaciers had medial or lateral moraines convoluted or offset by extensive crevasses or ogives; 7 had prominent tributary ice overriding or displacing main glacier ice; 14 had marked depression of ice surface below lateral moraines or tributary glaciers; 76 had lateral and medial moraines that were slightly sinuous, lobate, or offset by crevasses or ogives; 9 had recent major melting or retreat of ice front that left light-colored deglacierized terrain behind; 106 had extensive areas of debris-covered downwasting or stagnant ice; and 47 glaciers had linear moraines and accordant tributary glaciers. Some of these conditions will have changed in the ensuing two decades since this study was done originally. Finally, the issues of complex interdependencies and scale dependencies of climate forcings, glacier erosion, and mountain geodynamics in the Himalaya of Pakistan and elsewhere are areas of active research that are currently receiving much attention by a variety of workers. Study of the role of present-day glacierization and past glaciation of the western Himalaya in these efforts is greatly augmented by the availability of some of the historical satellite imagery presented here.

Introduction

Concerns over greenhouse-gas forcing and warmer temperatures have spurred research into climate forcing and associated Earth-System responses. Considerable scientific debate concerns climate forcing and landscape response, because complex geodynamics regulate feedback mechanisms that couple climatic, tectonic and surface processes (Molnar and England, 1990; Ruddiman, 1997; Bush, 2000; Zeitler, Koons, and others, 2001; Zeitler, Meltzer, and others, 2001; Bishop and others, 2002). A significant component

[1]Editors' Footnote: This manuscript was originally written in the early 1980s to describe the glaciers of Pakistan in the late 1970s and early 1980s, the "benchmark" time period for the Satellite Image Atlas of Glaciers of the World, U.S. Geological Survey Professional Paper 1386A–K. Because there were delays in publishing, the authors updated their manuscript by adding references to more recent work while intentionally retaining the original benchmark information.

[2]Department of Geography and Geology, University of Nebraska at Omaha, Omaha, NE 68182

in the coupling of Earth's systems involves the cryosphere, as glacier-related feedback mechanisms govern atmospheric, hydrospheric and lithospheric response (Bush, 2000; Shroder and Bishop, 2000; Meier and Wahr, 2002). Specifically, snow and ice mass distributions partially regulate atmospheric properties (Henderson-Sellers and Pitman, 1992; Kaser, 2001), sea level variations (Meier, 1984; Haeberli and others, 1998; Lambeck and Chappell, 2001; Meier and Wahr, 2002), surface and regional hydrology (Schaper and others, 1999; Mattson, 2000), erosion (Hallet and others, 1996; Harbor and Warburton, 1992, 1993), and topographic evolution (Molnar and England, 1990; Brozovik and others, 1997; Bishop and others, 2002). Consequently, scientists have recognized the significance of understanding glacier fluctuations and their potential as direct and indirect indicators of climate change (Kotlyakov and others, 1991; Seltzer, 1993; Haeberli and Beniston, 1998; Maisch, 2000). In addition, the international scientific community now recognizes the need to assess glacier fluctuations at a global scale to elucidate the complex scale-dependent interactions involving climate forcing and glacier response (Haeberli and others, 1998; Meier and Dyurgerov, 2002). Satellite data products from NASA's Earth Observation System (EOS) (Hall and others, 2005) assist in the identification and characterization of those regions that are changing most rapidly and that have the most significant impact on sea level, water resources, economics, and geopolitics (Haeberli, 1998).

Mountain environments are known for their complexity and sensitivity to climate change (Beniston, 1994; Meier and Dyurgerov, 2002). Numerous mountain systems have been identified as "critical regions" and include Alaska, Patagonia and the Himalaya (Haeberli and others, 1998; Meier and Dyurgerov, 2002). Within the Himalaya, alpine glaciers are thought to be very sensitive to climate forcing due to their range in altitude and variability in debris cover (Nakawo and others, 1997). Furthermore, such high-altitude geodynamic systems are thought to be the direct result of climate forcing (Molnar and England, 1990; Bishop and others, 2002), although climate versus tectonic causation is still being debated (Raymo and others, 1988; Raymo and Ruddiman, 1992). To resolve these glaciological arguments, a fundamental understanding of the feedbacks between climate forcing and glacier response is needed (Dyurgerov and Meier, 2000). This requires detailed information about glacier distribution and ice volumes, mass-balance gradients, regional mass-balance trends, and landscape factors that significantly control ablation.

The western Himalaya is an ideal location for studying the causal interrelationships between climate, present-day glacierization, and past glaciation because the magnitude of such geodynamics is relatively high — the region has experienced dramatic climatic change, and it contains significant ice volumes (Tsvetkov and others, 1998; Bishop and others, 2002). From a practical point of view, the rapidly changing glaciological, geomorphological, and hydrological conditions of this region present a "looming crisis" to the world in terms of a decreasing water supply, increased hazard potential, and geopolitical destabilization.

Scientific progress in understanding the glaciers in Pakistan, however, has been slow because of the complex topography, paucity of field measurements, and limitations associated with information extraction from satellite imagery. Information is limited or nonexistent regarding: (1) enumeration and distribution of glaciers; (2) glacier mass-balance gradients and regional trends; (3) the contribution of glacial meltwater to the observed rise in sea level; and (4) natural hazards and the imminent threat of landslides, ice and moraine dams, and outburst flooding caused by rapid glacier fluctuations.

McClung and Armstrong (1993) have indicated that detailed studies of a few well-monitored glaciers do not permit characterization of regional mass-balance trend, the advance/retreat behavior of glaciers, or global extrapolation.

To our knowledge, the alpine glaciers in Pakistan have not been adequately studied or understood in terms of their role in mountain geodynamics, or their response and sensitivity to climate forcing, to adequately characterize existing conditions and future trends. An integrated approach to studying these glaciers, developing base-line information, and improving our understanding of climate forcing and glacier fluctuations requires the use of new remote sensing and geographic information systems (GIS) technologies (Haeberli and others, 1998; Bishop and others, 2004; Bishop and Shroder, 2004).

Much of the work for this paper was originally done over two and a half decades ago using only the Landsat Multispectral Scanner (MSS) imagery (Shroder and Bishop, 2005). Subsequent delays in publication necessitated some updating. In the intervening years since the initial research was undertaken, numerous expeditions and analyses have added to the knowledge store, but only limited such information is presented here. Furthermore, advanced numerical assessments are not included in this paper because they are presented elsewhere (Bishop and others, 1995, 1998a, 1999, 2000, 2001, 2002, 2004). Instead, this paper presents baseline information to facilitate subsequent comparative studies of glacier change. Our original work using small-scale Landsat imagery was augmented by field studies in the 1980s and 1990s, and by the use of Advanced Spaceborne Thermal Emission and Reflection Radiometer (ASTER) imagery. This work is now part of the international Global Land-Ice Measurements from Space (GLIMS) project, designed to produce quantitative information about the world's glaciers through remote sensing and field observations (Bishop and others, 2000; Kieffer and others, 2000; Bishop and others, 2004). In this paper, we first provide background information about the region and the important geoscience issues there, and discuss the role of remote sensing using the reflective region of the electromagnetic spectrum in glaciological studies. Selected glacier fluctuations and glacier hazards across the region are then discussed, with an emphasis on those glaciers on which field and remote sensing studies have been conducted. The larger glaciers in Pakistan were assessed first with 1970s MSS and RBV imagery to identify observable flow variations such as the highly deformed medial moraines characteristic of surges, as well as other features. Selected ASTER scenes were then used to look at particularly interesting features first observed on the older imagery. Finally, the important role of alpine glaciers in mountain geodynamics is dicussed, and results are summarized.

Background

Pakistan has some of the world's highest and most spectacular mountains. A total of 13 of the world's 30 tallest peaks are located there, including K2 (8,611 m), the second highest peak in the world, Nanga Parbat (8,125 m), the ninth highest peak, and Tirich Mir (7,690 m) in the Hindu Kush. Because of the numerous high mountains, and abundant precipitation characteristic of a monsoon climate, the mountains of northern Pakistan, including the Hindu Kush, Hindu Raj, Kohistan ranges, Nanga Parbat massif, and Karakoram Himalaya[3], host some of the largest and longest mid-latitude glaciers on Earth (fig. 1). The glacierized area in northern Pakistan is estimated to cover 15,000 km^2, and as much as 37 percent of the Karakoram region is covered by glaciers.

---

[3]U.S. Government publications require that official geographic place-names for foreign countries be used to the greatest extent possible. In this section the use of geographic place-names is based on the U.S. Board on Geographic Names website: *http://earth-info.nga.mil/gns/html/index.html*. The names not listed on the website are shown in italics. However, in the case of italicized names, the authors have been careful to use the most accurate transliteration of local names or generally accepted local names.
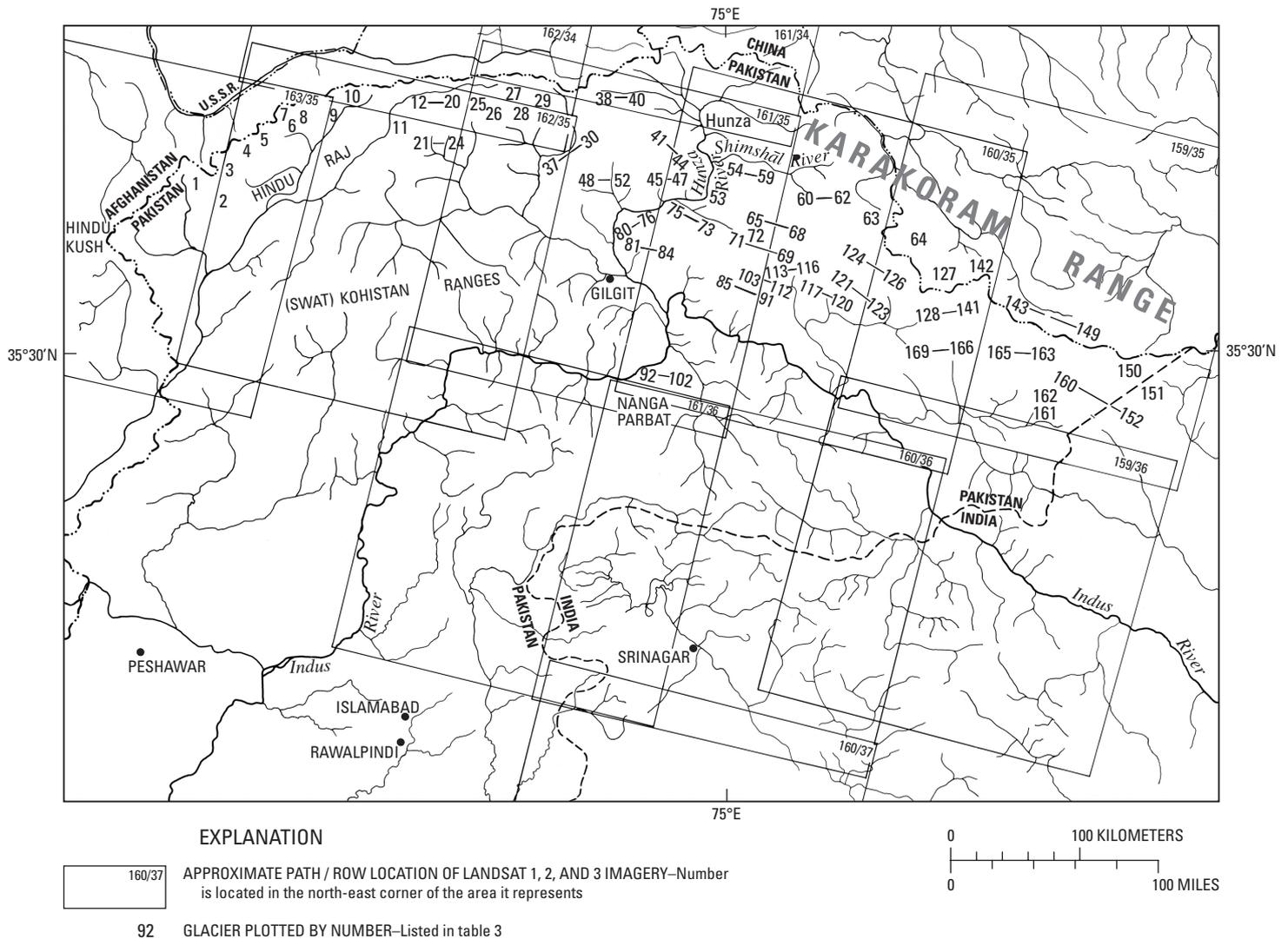
Figure 1.—*Index map of the glacierized region of Pakistan showing major geographic features, approximate Path–Row locations of Landsat 1, 2, and 3 imagery, and locations of glaciers selected for this study. Optimum Landsat images are listed in table 1 and plotted in figure 2. Glaciers selected for this study are plotted by number and listed in table 3. Small glaciers in the Hindu Kush, Hindu Raj, and Kohistan ranges were not included. Glaciers 41–169 are those of the main Karakoram Himalaya.*

The glaciers are highly variable in terms of their morphogenic and functional character. Some are mainly summer accumulation types (southwest monsoon), while others also receive mass from the westerlies. The partitioning of accumulation from both sources is thought to have dramatically changed from the past, with evidence suggesting that there was greater northward penetration of the monsoon during the Holocene (Phillips and others, 2000). Glaciers in the Himalaya have been classified according to their dominant nourishment type (Visser and Visser-Hooft, 1938; Washburn, 1939) as: (1) basin-reservoir (Firnmulden) types that are predominantly in cirques; (2) firn plateau types; (3) incised reservoir (Firnkesel) types in deep, narrow valleys with multiple catchments fed mainly by snow and ice avalanches; and (4) avalanche (Lawinen) types that lack tributary reservoirs. In practice, the latter two types are basically the same (Maull, 1938; Washburn, 1939). The huge, steep peaks of the Himalaya produce a characteristic dominance of avalanche source materials, including the copious rock debris that dominates the lower ablation regions of many glaciers in the region. The glaciers are highly variable in size, and the region has cirque, ribbon, hanging, alpine valley,

and large compound valley glaciers. An example of the later is the Baltoro Glacier [128] at K2, which is fed by about 30 tributaries and covers about 1,300 km² — almost 10 percent of the country's total glacier area. The glaciers are commonly also heavily debris-covered, with highly variable debris thicknesses and cover (Bishop and others, 1995). Given the complexity of topography, including landscape relief, slope angles and basin orientation, many glaciers exhibit highly diverse morphologies and ice-flow velocities (Shroder and others, 1999). Many have advanced to the opposite valley wall, blocking the meltwater runoff from up-valley glaciers, creating large alpine valley lake impoundments that later release catastrophically.

Various early reports of unusual features, catastrophic advances, and glacier-related floods (jökulhlaups) (Hayden, 1907; Mason, 1930, 1935; Hewitt, 1969) piqued an interest in studying these glaciers more closely, but the difficult terrain and uncertain politics allowed only intermittent observation. By the 1970s, an increasing interest in environmental changes led to several syntheses of previous work (Mercer, 1963, 1975; Horvath, 1975; Mayewski and Jeschke, 1979; Mayewski and others, 1980).

The construction of the Karakoram Highway (KKH) between Pakistan and China in 1978 provided more access to this region, and the opportunity for extensive fieldwork. This resulted in some detailed studies of glaciers in the Hunza area by the Chinese-sponsored Batūra Glacier [141] Investigation Group (BGIG; 1979, 1980), the British-sponsored International Karakoram Project (IKP) in 1980 (Miller, 1984), and the Canadian Snow and Ice Hydrology Project in the 1980s (Hewitt, 1988, 1990). Some remote sensing and glacial geomorphological studies were conducted by Shroder (1980, 1989), Bishop and others, (1995; 1998a, b; 1999), Bishop and Shroder (2000), and Shroder and Bishop (2000), although other groups from Austria, Britain, Germany, Italy, Russia, Switzerland, Nepal, and other countries including most recently Pakistan, have also made significant contributions. For example, Russian scientists used satellite imagery to evaluate glacier distribution climate regimes, equilibrium lines, and glacier surge types and locations in the western Himalaya (Kravtsova and Labatina, 1974; Desinov and others, 1982; Kravtsova, 1982; Nosenko, 1991; Lebedeva, 1993, 1995; Lebedeva and Kislov, 1993; Knizhnikov and others, 1997; Osipova and Tsvetkov, 1998, 2002, 2003). They compiled a small scale atlas of snow and ice resources over the western Himalaya and Karakoram that presented plentiful data on glaciers, glacial processes, snowmelt and runoff (Kotlyakov, 1997). Their classification of surging glaciers, similar to that used herein, was presented as: (1) identified repeated surges, with morphological features of instability, (2) some indications of pulses, (3) indications of pulses not defined, and (4) some data about massive changes in the ice zone.

In essence, however, the huge region still lacks reliable quantitative estimates of fundamental glacier parameters such as glacier distribution and ice volume, ablation rates, flow rates, ELA determinations, and has but a few detailed mass balance studies. Our field investigations and remote sensing analyses indicate that some glaciers are retreating and downwasting. Not currently known is what the regional mass-balance trend is, although we suspect a general negative mass-balance trend based upon our data and work on mass balance in other areas (Aizen and others, 1997; Fujita and others, 1997; Cao, 1998; Cogley and Adams, 1998; Bhutiyani, 1999; Meier and others, 2003; Berthier and others, 2007). Furthermore, the exact number of alpine glaciers, and their size distribution, regional ice volume, modern-day and historical spatial-distribution patterns, and sensitivity of these heavily debris-covered glaciers, is not nearly as well known in the western as in the eastern Himalaya (Mool, Bajracharya, and Joshi, 2001; Mool, Wangda, and others, 2001). Recently, however, the Government of Pakistan has finally begun to

focus on glacial assessments, using Landsat-7 Enhanced Thematic Mapper Plus (ETM+) data to study the glaciers with new appreciation of the effects of global warming (Roohi and others, 2005; Roohi, 2007). Study results are critical to the understanding of climate variability and ice-volume fluctuations, and to predicting the environmental consequences for Pakistan.

From a scientific perspective, a variety of glaciological parameters must be accurately estimated. Climate forcing has had a significant impact on this region in a relatively short period of time (Shroder and Bishop, 2000; Bishop and others, 2002). Research, however, has yet to definitively determine whether atmospheric warming will produce a negative or positive regional mass-balance trend. In addition, it is difficult to effectively characterize local variations in glacier mass balance, because the glaciers respond to a variety of climatic and geologic forcing factors (Molnar and England, 1990; Haeberli and Beniston, 1998; Dyurgerov and Meier, 2000; Shroder and Bishop, 2000). To complicate matters, the local and mesoscale topographic variations modify the regional climatic patterns and tectonic forcing (isostatic and tectonic uplift), which in turn govern climate and glacier dynamics (Hubbard, 1997; Shroder and Bishop, 2000). Consequently, glacier mass-balance gradients and the spatial distribution in the magnitude of mass balance may be highly variable, such that detailed studies of individual glaciers do not produce representative results for the region. These complex feedback mechanisms have not been adequately studied because they require sophisticated geographic information science (GISc) analyses, remote sensing, and numerical modeling of physical processes to produce information that can be integrated with climate, surface process, and tectonic physical models (Bishop and Shroder, 2000, Bishop and others, 2002).

From a resources perspective, ice masses in the Hindu Kush, Karakoram, and Nanga Parbat Himalaya constitute potential meltwater for the country, although the ice masses in India also contribute to Pakistan's water supply. As such, a far better understanding of the total volume and condition of these long- and short-term storages is critical to the management and prediction of future resource availability in both countries. Furthermore, the condition of the glacier ice mass provides important information on many factors that have significant ramifications in climate-change scenarios; these factors include glacier advance, retreat, backwasting, downwasting, surge, avalanche, debris accumulation, new meltwater lakes, and ice- and moraine-dammed lakes. Changing conditions of the regional ice mass can significantly affect irrigation, agriculture, tourism, hydroelectricity, drinking water, catastrophic floods, and cross-border conflict.

Glaciation and deglaciation in the region generate numerous hazards that can have catastrophic effects, by disrupting meltwater resources through damming and diversion, producing instabilities from mountain wall undercutting and debuttressing, and removing ice and rock supports as glaciers downwaste. A host of landforms long interpreted as Pleistocene recessional moraines have recently been reinterpreted as massive rockwall collapses which followed deglaciation and removal of wall support in a Last Glacial Maximum (LGM) (Hewitt, 1988, 1998, 1999). Furthermore, as discussed below, our prior work and that of others have now shown that the LGM in many places in the region is actually Holocene in age – much more recent and therefore more similar in conditions to the present day (Phillips and others, 2000; Shroder and Bishop, 2000).

Glacier chronologies have been attempted in the mountains of high Asia for more than a century, but only in the past two decades has any real progress been made in the western Himalaya (Derbyshire and others, 1984; Shroder and others, 1989; Gillespie and Molnar, 1995; Phillips and others, 2000; Shroder and Bishop, 2000; Owen and others, 2002). Accurate dates are required for assessing the influence of the Asian monsoon.

These recent chronologies show that a localized last glacial maximum also occurred early in the last glacial cycle. In the Swat Himalaya and the Zanskar valley, this occurred during oxygen isotope stage 5a [~91,000 to 79,000 years before the present (BP)], while in the Hunza valley, Nanga Parbat, and the Middle Indus valley, it occurred during oxygen isotope stage 3(~59,000 to 24,000 yrs BP) (Phillips and others, 2000; Richards and others, 2000; Taylor and Mitchell, 2000; Owen and others, 2002). Ice-core records from the Guliya ice cap support the view that interstadial conditions existed in western Tibet during oxygen isotope stages 3, 5a, and 5c (~111,000 to 99,000 yrs BP) (Thompson and others, 1997). The last glacial maximum in the Garhwal Himalaya occurred during oxygen isotope stage 4 (~74,000 to 59,000 yrs BP), although the large error bars suggest that it could have occurred during oxygen isotope stage 3. Extensive early glaciations have been recognized in the Khumbu and Lahul Himalaya, but these have not been numerically dated (Owen and others, 2000; Richards and others, 2000). Limited advances in the Hunza valley and middle Indus valley occurred during the global LGM in oxygen isotope stage 2 (~24,000 to 12,000 yrs BP), and advances in the Hunza valley and Lahul Himalaya occurred during the Late Glacial Interstadial (Owen and others, 2000, 2002; Richards and others, 2000). There is no evidence of glaciation during the Younger Dryas (~12,000 yrs BP) in any area of the Himalayas. In addition, as mentioned above, there is abundant evidence for an early-middle Holocene glacial advance in the Hunza valley, Nanga Parbat, Lahul Himalaya, and Khumbu Himal.

These data show that glaciation across the Himalaya appears to be broadly synchronous and that the timing of glaciation throughout the Himalaya occurred during times of insolation maxima, when the monsoon was strengthened and its influence extended further north to supply snow at high altitudes. Glaciers would have exhibited positive mass balance, allowing them to advance. Because the spatial extent of these earlier advances is not well known, it is difficult to compare them to modern glacial extents to estimate average rates of change.

Remote Sensing of Glaciers

Given the challenging logistics, geopolitical restrictions, and other uncertainties in Pakistan, many of the glaciers of Pakistan must be assessed via remote sensing. With the advent of new sensors and geographic information technologies (for example, GPS, GIS), scientists are able to estimate some glaciological parameters such as ice velocity fields and equilibrium line altitudes, and can investigate mountains and glaciers in new ways that address important scientific issues and problems (Bishop and Shroder, 2004; Bishop and others, 2004).

Remote sensing analysis of glaciers traditionally focused on simple image interpretation and the identification, characterization, and mapping of glaciers, although quantitative approaches such as image transformations and pattern recognition were used in trying to differentiate snow and glacier facies. This was characteristic of glacier studies in the 1970s (Shroder and others, 1978), including the work done originally for this paper two decades ago, which utilized Landsat 1, 2, and 3 MSS imagery. The relatively poor geometric accuracy and coarse spatial, spectral, and radiometric resolution greatly limited the use of the imagery for more than identification of the general location of moderate to large glaciers, production of general outlines of glacial extent, the identification of some glaciers that surged, and some change detection in comparisons with modern imagery. Although this information represents important base-line information (fig. 2, table 1), there was error and uncertainty associated with the information extracted.
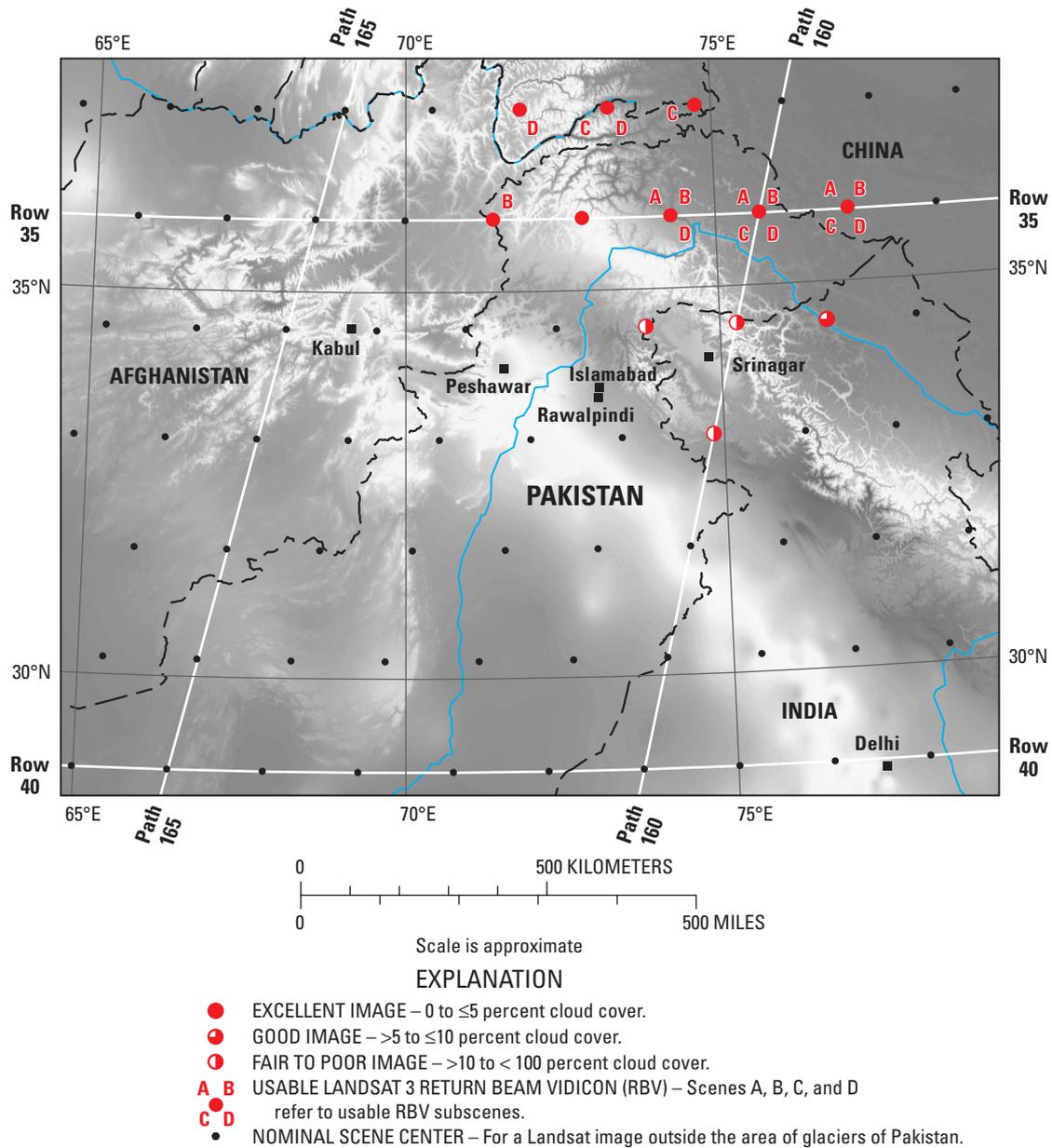
Figure 2.—Optimum Landsat 1, 2, and 3 images of the glaciers of Pakistan.

Since then, investigators have been studying glaciers using moderate to high resolution data that exhibit greater radiometric and geometric fidelity. This permits an extraction of additional information for assessing glacier conditions. For example, Aniya and others (1996) conducted an inventory of outlet glaciers of the southern Patagonia Icefield. Eleven parameters related to glacier morphology were extracted, and the results were comparable to results generated from topographic maps. Other researchers have investigated the potential of satellite imagery for mapping alpine snow (Dozier and Marks, 1987; Haefner and others, 1997), and for assessing and mapping supraglacial features (Bishop and others, 1995, 1998a, 1999) and glacier ice and snow facies (Hall and others, 1988; Williams and others, 1991). This work is commonly concerned with accurate delineation of glaciers and facies, and comparing satellite-derived surface reflectance with *in-situ* measurements. Results from these and other studies have indicated that high-resolution spectral data and topographic information are neccessary for delineating

TABLE 1.—*Optimum Landsat 1, 2, 3 MSS and RBV images of the glaciers of Pakistan*

[Abbreviations: MSS, multi spectral scanner; RBV, return beam vidicon; m, meter; μm, micrometer; km, kilometer; cm, centimeter; EROS, Earth Resources Observation and Science]

[Code column indicates usability for glacier studies; see figure 2 for explanation. —, unknown

Path-Row	Nominal scene center latitude and longitude		Landsat identification number (10 digits) or entity identification number (16 digits)[1]	Date	Code	Cloud cover (percent)	Remarks
159–35	35°58′N.	77°08′E.	3159035007819990	18 Jul 78	◒	10	
159–35	35°58′N.	77°08′E.	30531–04484 Subscenes A, B, C, D	18 Aug 79	●	0–20	Landsat 3 RBV archived by the authors[2]. Images used for figs. 20 and 21
159–36	34°32′N.	76°42′E.	3159036007819990	18 Jul 78	◒	10	Image used for fig. 25
160–35	35°58′N.	75°42′E.	2160035007721490	02 Aug 77	●	0	Image used for figs. 8*A*, 17, and 26*A*
160–35	35°58′N.	75°42′E.	2160035007723290	20 Aug 77	◒	10	
160–35	35°58′N.	75°42′E.	30532–04542 Subscenes A, B, C, D	19 Aug 79	●	5–40	Landsat 3 RBV archived by the authors[2]. Images used for figs. 13 and 20
160–36	34°32′N.	75°16′E.	2160036007723290	20 Aug 77	◑	20	
160–37	33°07′N.	74°49′E.	2160037007723290	20 Aug 77	◑	50	
161–34	37°24′N.	74°44′E.	2161034007622190	08 Aug 76	●	5	Some technical problems
161–34	37°24′N.	74°44′E.	30515–04595 Subscene C	02 Aug 79	—	—	Landsat 3 RBV archived by the authors[2]
161–35	35°58′N.	74°16′E.	2161035007622190	08 Aug 76	●	5	
161–35	35°58′N.	74°16′E.	2161035007726990	26 Sep 77	●	0	Some technical problems
161–35	35°58′N.	74°16′E.	3161035007919690	15 Jul 79	●	0	Image used for figs. 16*A*, and 22*A*
161–35	35°58′N.	74°16′E.	30515–05001 Subscenes A, B, D	02 Aug 79	●	0–20	Landsat 3 RBV archived by the authors[2]. Images used for figs. 7 and 13
161–36	34°32′N.	73°50′E.	2161036007821090	29 Jul 78	◑	0	Some technical problems
162–34	37°24′N.	73°18′E.	2162034007622290	09 Aug 76	●	0	
162–34	37°24′N.	73°18′E.	30516–05053 Subscenes C, D	03 Aug 79	—	—	Landsat 3 RBV archived by the authors[2]
162–35	35°58′N.	72°50′E.	2162035007723490	22 Aug 77	◑	20	
162–35	35°58′N.	72°50′E.	2162035007815790	06 Jun 78	●	0	Image used for fig. 6*A*
163–34	37°24′N.	71°52′E.	30553–05105 Subscene D	09 Sep 79	●	0	Landsat 3 RBV archived by the authors[2]
163–35	35°58′N.	71°24′E.	1163035007319390	12 Jul 73	●	10	Image used for fig. 3*A*
163–35	35°58′N.	71°24′E.	2163035007622390	10 Aug 76	●	5	
163–35	35°58′N.	71°24′E.	30553–05112 Subscene B	09 Sep 79	—	—	Landsat 3 RBV archived by the authors[2]

[1]Landsat images were originally assigned a unique identification number that incorporated the satellite number, the number of days since satellite launch and the time the image was acquired. All archived Landsat images are now assigned an entity (or order) identification number based on the satellite number, the path and row of the scene, and the year and Julian day of the scene acquisition.

[2] Landsat 3 RBV images of the Earth were acquired by two RBV cameras during the operation of the Landsat 3 spacecraft (launched on 5 March 1978 and deactivated on 31 March 1983). Landsat 3 RBV images have a pixel resolution of ~30 m, were acquired in a single panchromatic band (0.505–0.750 μm; spanning part of the visible and part of the near-infrared bands of the electromagnetic spectrum) by two side-by-side slightly overlapping RBV cameras. The images covered an area 98 × 98 km (4 RBV images coincide with a single MSS frame). RBV images were recorded on film media (18.5 cm × 18.5 cm) and archived as positive and negative film transparencies at the U.S. Geological Survey, EROS Data Center, Sioux Falls, S. Dak. 57198. Landsat 1 images (3 bands, 79-m pixels) and Landsat 3 RBV images (single band, 30-m pixels) are archived in film format in deep storage at the EROS Data Center. Landsat RBV images are no longer available to scientists or to the public and can only be obtained from private archives.

debris-covered glaciers, mapping glacier facies, and estimating albedo and mass balance (Hall and others, 1989; Bishop and others, 2001). Mass balance estimates can be generated by estimating the equilibrium line altitude (ELA) during the later portion of the ablation season, or using topographic information to do so (Hall and others, 1989).

The debris-covered glaciers in Pakistan and other countries are exceptionally difficult to study because they exhibit extreme spectral and topographic variability (Bishop and others, 2001; Kääb and others, 2002; Paul and others, 2002). Snow and ice facies, glacial till, and different mineral and rock types produce highly variable reflectance, making glacier mapping very difficult in the solar reflective regions of the electromagnetic spectrum. For relatively large parts of many glaciers, the supraglacial debris cannot be spectrally differentiated from the surrounding rocks and ground moraine. In these cases, it is necessary to use topographic information, because the morphometric properties of the glacier can be used for delineating the terminus and identifying supraglacial landform features (Bishop and others, 1995; Bishop and others, 1998a; Bishop and others, 2001; Paul and others, 2004).

Given our current rate of collecting glacier information in Pakistan, it is expected that far too many glaciers will significantly change or be entirely gone before we can measure and understand them adequately (Roger Barry and Wilfried Haeberli, oral comm., March 2003). This time-sensitive issue requires us to acquire global and regional coverage of glaciers via satellite imagery before they disappear. Change-detection studies using earlier baseline information generated with Landsat MSS, TM, SPOT and other data should be compared with information obtained from fieldwork and modern sensors such as ASTER. Consequently, we present several case studies here that characterize selected Pakistan glaciers and their fluctuations.

When feasible, fieldwork has been conducted to augment and validate remote sensing and GIS investigations. The field data has greatly enhanced glacier study results, because some parameters can only be reliably measured in the field.

Glacier Fluctuations and Hazards

Multi-temporal imagery and field studies document the dynamic nature of glaciers and their continual adjustment to climatic, glaciological, and geological conditions. Change-detection studies are useful for assessing basic morphological conditions (for example, advance and retreat) caused by glacier flow dynamics and mass balance variations. In addition, satellite imagery documents numerous processes and provides insights into feedback mechanisms that govern glacier fluctuations. Furthermore, the spatial context of glaciers and their spatial topological relationships to other topographic features provides valuable information about hazard potential.

Extracting such information from satellite imagery has its technical challenges and limitations caused by sensor problems and difficulties related to image texture, scale, etc. Nevertheless, higher resolution imagery can document surface features and processes, and glacier-related fluctuations, including: (1) mass movements onto glaciers; (2) spatial variation of ablation; (3) surface moisture variations; (4) influence of adjacent-terrain irradiance on ablation; (5) terminus position changes; (6) supraglacial-lake development; (7) ice-velocity variations; (8) white-ice-stream position changes; (9) glacial-lake development; and others. Commonly, however, fieldwork is required to collect information that is not easily extracted from imagery, such as the location of ice portals, features related to ablation, moulins, and other surface characteristics. When integrated with image information, a more complete picture of glacial fluctuations and sensitivity emerges.

Field Studies of Selected Glaciers

A number of glaciers in the Pakistan Himalaya were studied in the field to determine their regional variability. For each glacier, general characteristics were identified, a change detection was performed, surges and other hazards were assessed, and baseline data was developed. Background information provided in the case studies that follow can be used to establish benchmark glacier sites (Kaser and Fountain, 2001) for long-term monitoring. Information gleaned from this long-term monitoring and from analysis of ASTER or other high-resolution stereoscopic imagery allows Pakistan managers to more reliably determine the availability of water resources for irrigation and hydroelectric power, and more accurately identify potential glacier-related hazards.

Tirich Glacier

The Tirich Mir massif (7,690 m) in the Chitral area of northwestern Pakistan represents the tallest mountain in the Hindu Kush. Large glaciers radiate from it, but relatively little is known about their dynamics and mass-balance histories. Previous research indicates that the North and South Barum Glaciers on the southeastern side of the massif were confluent 50 years ago (Bateson and Bateson, 1952), and satellite imagery reveals the presence of high altitude (~4,000 m) glacier erosional and depositional surfaces. We suspect that these surfaces were formed from monsoon-enhanced glaciation between 70 and 20 K yrs BP, because similar surfaces exist at that altitude throughout the Karakoram and Nanga Parbat Himalaya, and have been dated at 60–70 K yrs BP (Phillips and others, 2000, Owen and others, 2000). Although exposure age dates for the surfaces at Tirich Mir have yet to be determined, they clearly developed during more extensive glacial conditions, and document deglaciation and valley formation. This is evident on the north side of the massif, where the large compound Tirich Glacier flows down-valley in a northeasterly direction.

Examination of Landsat MSS imagery of the Tirich Glacier reveals numerous tributary glaciers that form the large Upper Tirich Glacier [1] (fig. 3A). A variety of debris cover — ice, black slate, and granite/granodiorite — is also evident in the imagery. Upon comparison of MSS imagery with ASTER stereo pairs, a flow discontinuity was revealed that divides the Upper from the Lower Tirich Glacier [2] (fig. 3B) and has existed for more that 20 years. Presumably, this ice flow discontinuity was caused by a decrease in regional mass balance and an associated change in surface hydrology. Ground photography of this discontinuity depicts the deposition of a ground moraine and its transport by an active river originating from the terminus of a tributary glacier on the south side of the Upper Tirich Glacier (fig. 4). In addition, visual comparative analysis of satellite imagery and field observations indicates the development of large supraglacial lakes on the Upper Tirich Glacier. This observational evidence suggests that the glacier is downwasting rather than exhibiting significant retreat.

Gorshai Glacier

Gorshai Glacier, about 6 km southeast of *Matiltan* in Swat Kohistan, heads in a north-facing cirque at about 4,725 m, beneath an unnamed peak 5,254 m in elevation; this peak is south of the main Kohistan, Hindu Raj, and Hindu Kush ranges. The glacier flows 2.8 km NNW in a series of ice falls before passing, at 3,660 m (12,000 ft) in elevation, into a zone of debris cover with prominent 2-km long lateral moraines which extend down to about

A

B

N
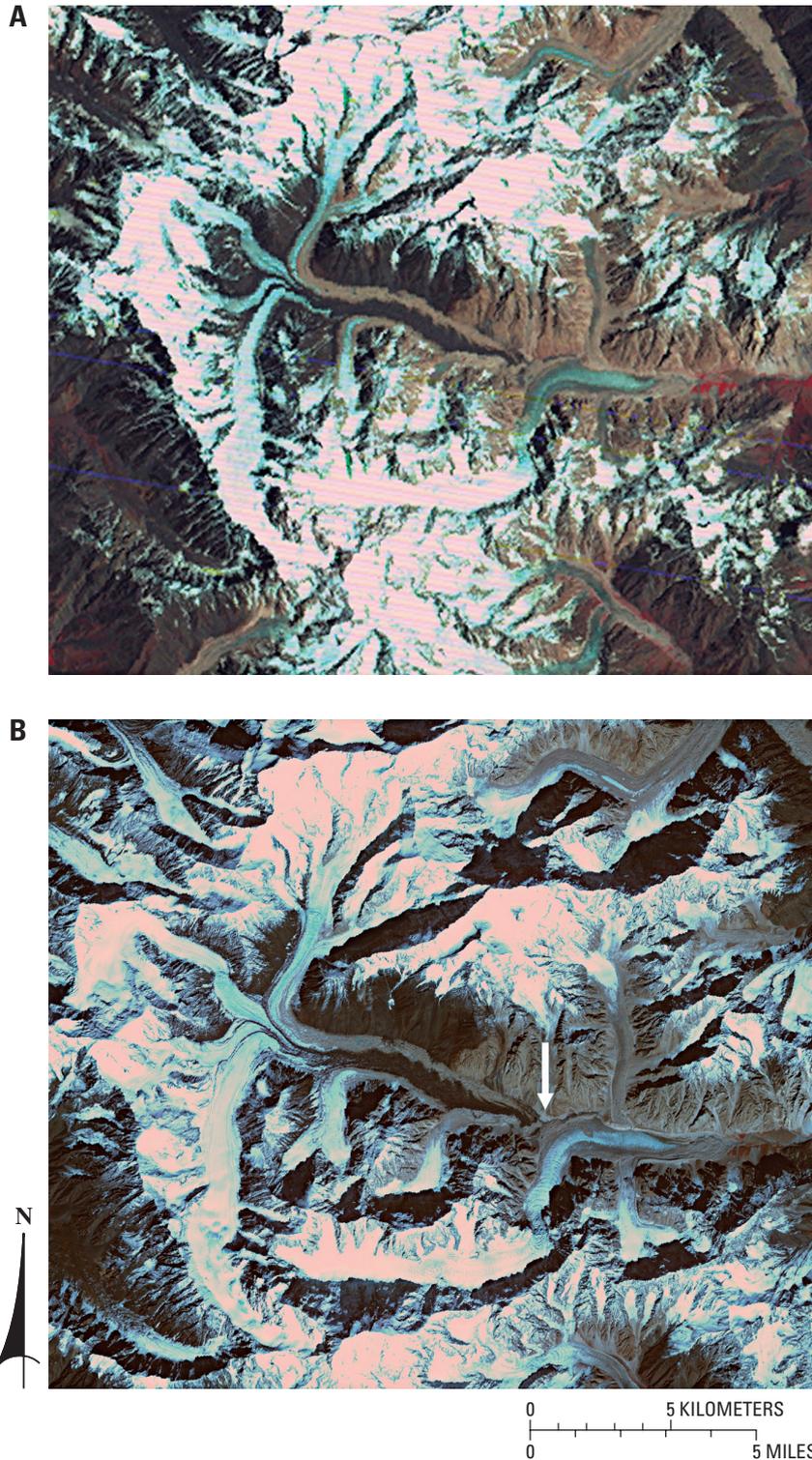
Figure 3.—A, Landsat 1 MSS false-color composite image taken on 12 July 1973, and B, ASTER image taken on 28 September 2001 of Tirich Mir glaciers (approximate lat 36°19'N., long 71°53'E.). Both scenes show that the Upper Tirich Glacier [left center] is disconnected from the Lower Tirich Glacier [right center], which is also shown in the ground photograph of this feature in figure 4. The location and direction of figure 4 are shown by the arrow. Many of the glaciers in the later ASTER scene appear somewhat larger than in the older MSS scene, but this may be only an artifact due to new snow in the late September scene. Landsat 1 MSS image no. 1163035007319390, bands 4, 5, 7; 12 July 1973; Path 163–Row 35; and ASTER image no. AST-L1B-00309282001061101111292003080213; 28 September 2001, are from the U.S. Geological Survey, EROS Data Center, Sioux Falls, South Dakota 57198.

0   5 KILOMETERS

0   5 MILES

3,000 m (~9,800 ft) in elevation (figs. 5, 6). Porter (1970, p. 1,441) noted general snowlines at elevations of 4,100–4,400 m for the Swat area. Massive snow avalanches fall from the peak above the glacier and travel down its entire length to a zone 2–3 km past the end of the lowest Neoglacial moraine. Slopes surrounding the lower moraine and avalanche chute below are heavily vegetated with grasses, birch, and conifers. The rich vegetation is caused by greater precipitation south of the main mountain ridge, in areas more exposed

Figure 4.—Photograph taken in July 1999 of the disconnection between Upper Tirich Glacier on the right and the ogives of the Lower Tirich Glacier on the left. Photograph by M.P. Bishop.
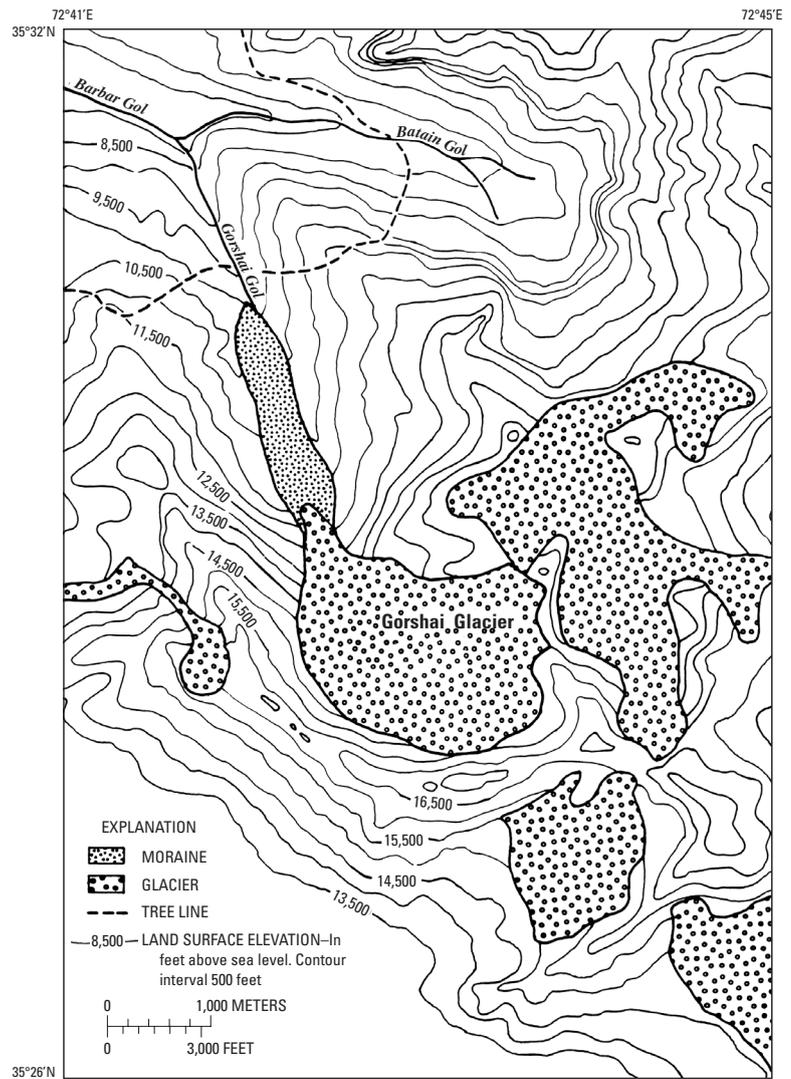
Figure 5.—Gorshai Glacier, *near* Matiltan, *Swat Kohistan. This glacier is typical of hundreds of unmapped glaciers in the Hindu Kush, Hindu Raj, and Kohistan ranges; however, it was unusual in this study because the otherwise classified large-scale aerial photographs and topographic maps of it were made available by the Government of Pakistan for this study.*

A

6 June 1978

B

13 October 2003

N

| 0 | | | | | 5 KILOMETERS |
| 0 | | | | | 5 MILES |

Scale is approximate
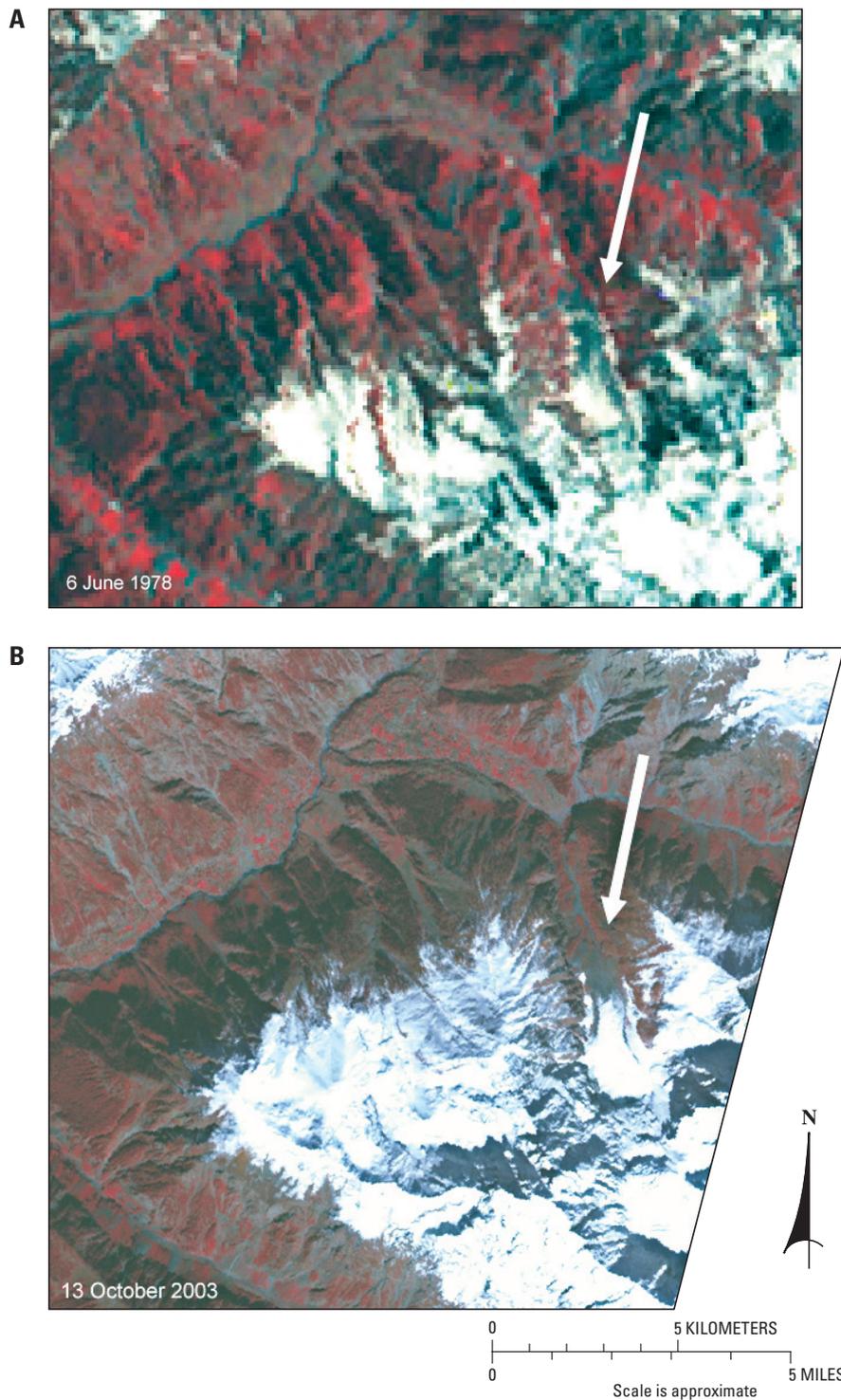
Figure 6.—Gorshai Glacier *(arrows)* *(approximate lat 35°29'N., long 72°43'E.)* **A***, Landsat 2 MSS false-color composite image taken on 6 June 1978, and* **B***, ASTER image taken on 13 October 2003 of the same area. The small size and lower pixel resolution (79 m) of the MSS imagery precludes much change detection between the two scenes. Such small and more easily accessible glaciers can, however, make good benchmark glaciers for long-term monitoring, although crevasse hazards may be a problem with this glacier. Landsat 2 MSS image no. 2162035007815790, bands 4, 5, 7; 6 June 1978; Path 162–Row 35, and ASTER image no. AST_LIB_003 10132003055911_10272003095214; 13 October 2003, are from U.S. Geological Survey, EROS Data Center, Sioux Falls, South Dakota 57198.*

to monsoon and other westerly precipitation. The result is a strong contrast between glacial features and surrounding terrain on Landsat MSS false-color composite imagery, such as the Landsat 2 MSS image used for figure 6*A*. In general, the elevations of the mountains and the aridity increase and the vegetation decreases toward the north, with the result that contrast between glaciers, moraine, and the surrounding areas declines from Swat toward the interior of the Hindu Kush, Hindu Raj, and the Karakoram Himalaya.

Glaciers of Nanga Parbat

The Nanga Parbat massif or Diāmir (8,125 m), the ninth highest mountain in the world, is located in the Indus River drainage basin and is significant in terms of its high magnitude erosion and unique mountain geodynamics (Zeitler, Koons, and others, 2001; Zeitler, Meltzer, and others, 2001). The mountain exhibits 69 glaciers that extend down to approximately 3,000 m and cover a total area of 302 km². The mountain receives less than 120 mm a^{-1} in precipitation below 2,500 m, to more than 8,000 mm a^{-1} above 4,500 m; the variation greatly influences glacier type and dynamics (Kick, 1980).

The glaciers of Nanga Parbat were first described by European explorers in the mid-1800s (Kick, 1975). The first detailed measurements, however, were made by a German expedition in 1934 (Finsterwalder and others, 1935; Finsterwalder, 1937). The German expedition produced a highly accurate 1:50,000-scale map of Nanga Parbat that is one of the most detailed maps in the western Himalaya. Additional glaciological and glacial geomorphological studies have been conducted by Pillewizer (1956), Loewe (1959, 1961), Gardner (1986), Scott (1992), Gardner and Jones (1993), Bishop and others (1999), Shroder and Bishop (2000), and Shroder and others (2000). The glaciers surrounding Nanga Parbat (figs. 7, 8) are directly exposed to high monsoon-generated precipitation and extremes of relief on cirque headwalls (3,000–4,000 m). This contributes to massive ice falls and snow avalanches that create extensive debris cover. Some of the glaciers on the steep slopes are moving rapidly in a tumbling "Blockschollen" fashion, in

Figure 7.—Part of a Landsat 3 RBV image showing Nanga Parbat massif. Many of the glaciers surrounding the massif are covered with supraglacier debris and therefore rather dark colored. Only Rākiot Glacier *[92] on the north side of the massif has much white snow-and-ice exposed.* Sachen Glacier *[95] on the northeast side was investigated in detail for this study.* Rākiot *[92] and* Chungpar Glaciers *[96] have the greatest rates of retreat since 1930. Landsat 3 RBV image no. 30515–05001, subscene D; 2 August 1979; Path 161–Row 35, was from the U.S. Geological Survey, EROS Data Center, Sioux Falls, South Dakota 57198, but is now only archived by the authors.*

A

Rāikot
Glacier

Sachen
Glacier

B

N

0   5 KILOMETERS

0   5 MILES
    Scale is approximate
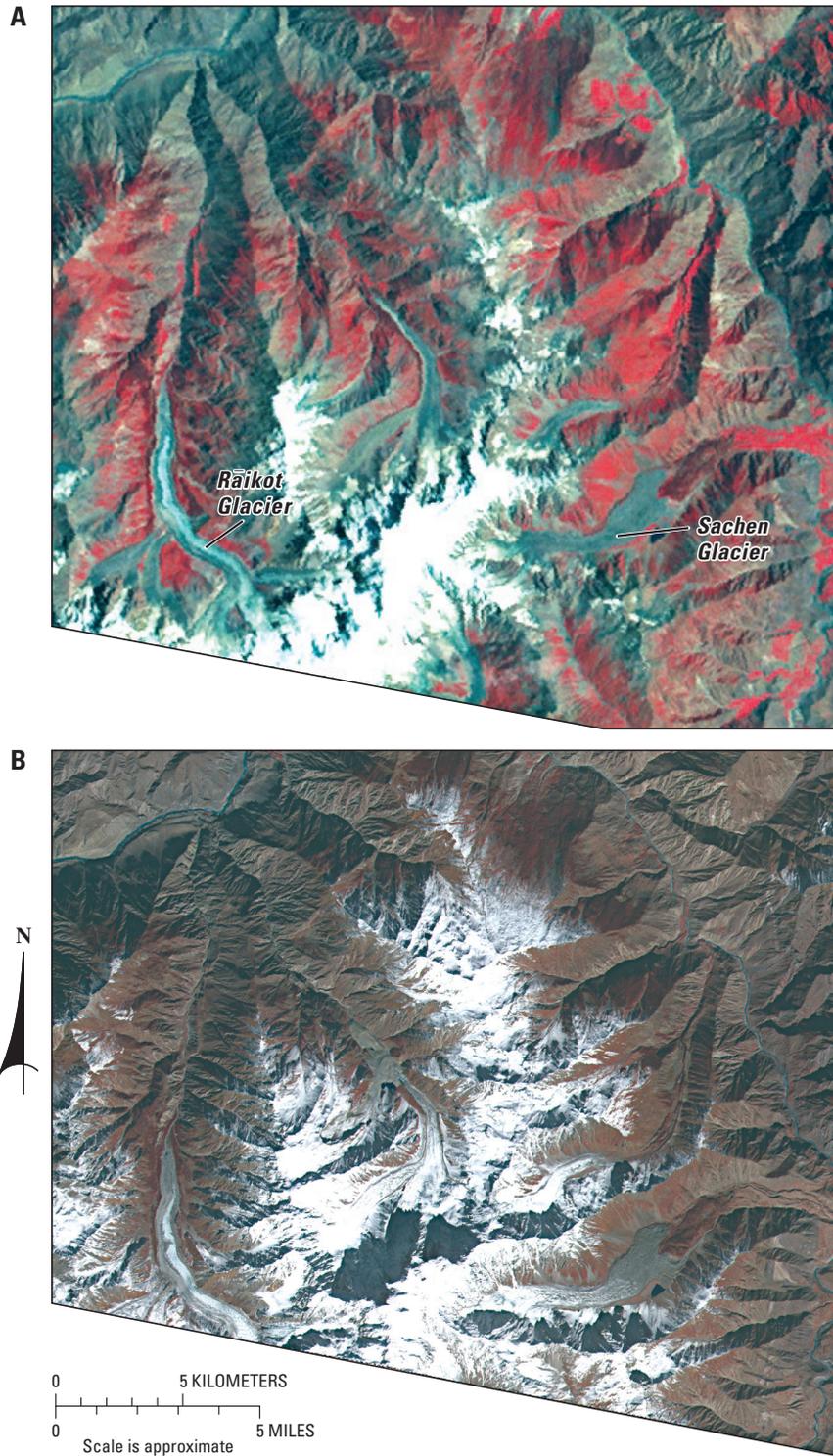
Figure 8.—**A**, *Landsat 2 MSS false-color composite image taken on 2 August 1977, and* **B**, *ASTER image taken on 29 October 2003, showing* Rāikot Glacier [92] *(approximate lat 35°20'N., long 74°35'E.) on the lower left and* Sachen Glacier [95] *(approximate lat 35°20'N., long 74°45'E.) on the lower right. Landsat 2 MSS image no. 2160035007721490, bands 4, 5, 7; 2 August 1977; Path 160–Row 35; and ASTER image no. AST_LIA_ 00310292003055903_ 11122003124818; 29 October 2003, are from the U.S. Geological Survey, EROS Data Center, Sioux Falls, S. Dak. 57198.*
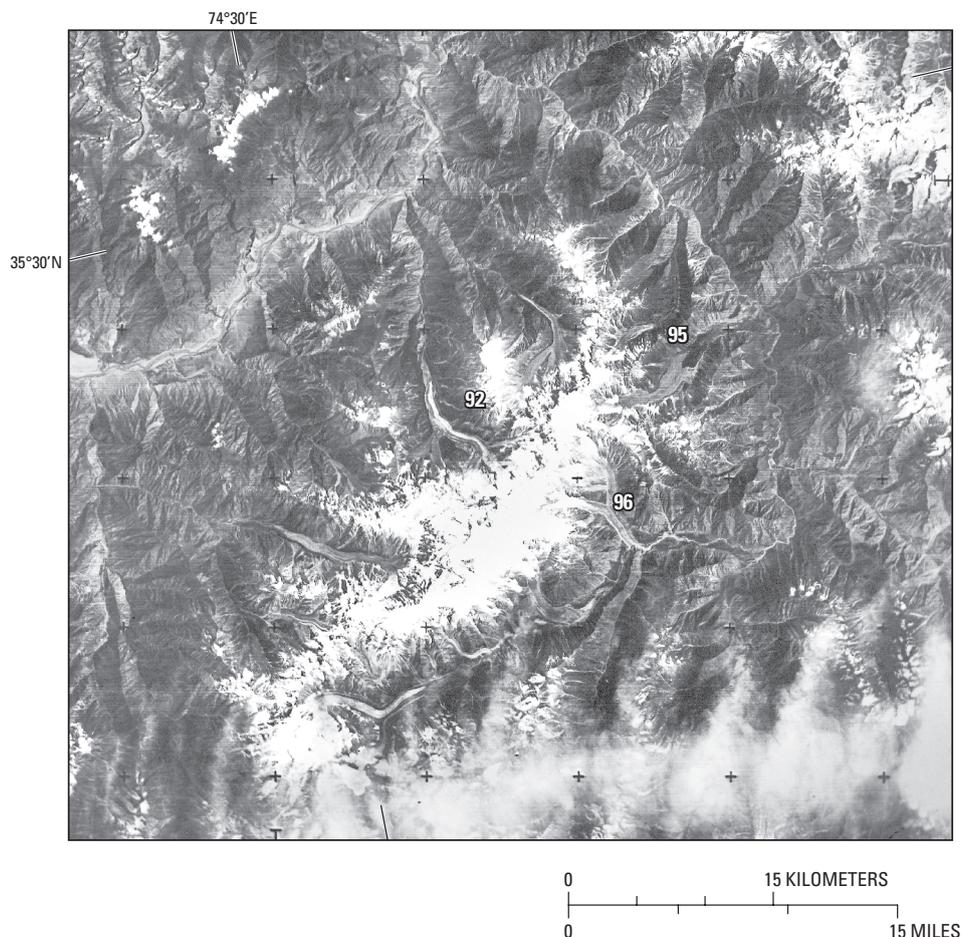
which the entire volume of the glacier is moving as a plug broken up into large ice-clods or blocks that jostle about somewhat independently (Mason, 1930; Finsterwalder and Pillewizer, 1939). The glaciers of Nanga Parbat descend from areas of fairly low accumulation to termini at about 3,000–3,800 m elevation — not into the nearby hot and arid Indus valley at 1,500 m. Elsewhere in the Karakoram, many glaciers descend from zones of large accumulation and ablate in the low, hot valleys, transporting large loads of ice and debris to lower elevations.

In general, the glaciers of Nanga Parbat have experienced a rather minor retreat since AD 1850. The two glaciers with greatest rates of retreat since 1930, *Rāikot* [*Rakhiot*] [92] and *Chungpar* [96], have had ice velocities that have increased two or more times since retreat began (Mayewski and Jeschke, 1979). At the same time, the *Sachen Glacier* [95] experienced almost no change, probably because it is a special class of glacier, a "dam glacier," that flows on its own bed of debris and raises the level of debris at the glacier bottom (Kick (1962, p. 228–229)). The lower portion of the glacier may become stagnant through excessive loading with rock debris, thereby allowing the upper portion to shear over it (Visser and Visser-Hooft, 1938; as reported by Washburn, 1939).

Sachen Glacier

Sachen Glacier [95] (Shroder and others, 2000) occurs on the northeast side of Nanga Parbat (figs. 8, 9). Its accumulation area is composed of several small firn fields and ice falls on the upper slopes of *Chongra* peak (6,891 m). Accumulation also occurs due to snow avalanches from surrounding ridges. The glacier is characterized by long, wide ablation valleys between the valley walls and large lateral moraines along both sides of the glacier. In at least four places associated with the lateral moraine, rock-glacier-like features occur, with

Figure 9.—Sachen Glacier *[95] on the northeast slopes of Nanga Parbat above* Astor *valley. The digitate terminus has five lobes that have been active at different times in the past. The presently active terminus is in the lower center of the 19 July 1984 photograph.* Lake Sango Sar *is impounded behind the inactive rock-glacier-like lobe on left. Photograph by J.F. Shroder, Jr.*

the characteristic morphology of a steep front at the angle of repose, a sharp angle between front and top, and transverse ridges and furrows. These rock glaciers either issue from the moraine at right angles to it, or come out of a tributary glacier and flow into the ablation valley.

The digitate front of *Sachen Glacier* has not backwasted significantly in 50 years, although we observed up to 25 m of recent downwasting on its northern-most front. The southern group of fronts (fig. 9) comprise two rock-glacier-like masses with steep fronts at an angle of repose that impounded lake *Sango Sar*, and two fronts of debris-covered, kettle-pocked ice. The most active front is in the center of figure 9. In 1934, this front had two arcuate moraine-covered ice lobes across its upper surface (Finsterwalder, 1937, fig 10 and topographic map), but by 1984 they had disappeared and high up on the front of the mass a large meltwater stream was flowing out.

Rāikot Glacier

The *Rāikot* (formerly *Rakhiot*) *Glacier* [92], on the north side of Nanga Parbat, is one of the best studied in the Nanga Parbat Himalaya because of the ease of access from the Karakoram Highway (KKH) at the base of the mountain. The glacier is one of the largest on the mountain, with a length of approximately 14 km, an elevation range of 3,150 to almost 8,000 m, and a total connected area of 32 km^2 (Gardner and Jones, 1993).

The *Rāikot Glacier* includes a firn basin surrounded by steep slopes above 5,500 m; it is the accumulation area and is frequently fed by snow and ice avalanches. Below the firn basin, a steep ice fall occurs between 5,500 and 4,100 m, and below that the glacier becomes increasingly debris-covered toward the glacier terminus at about 3,150 m (figs. 7, 8). Based upon measurements made by us and the Pakistan-Canada Snow and Ice Hydrology project (Gardner and Jones, 1993, and Finsterwalder, 1937), maximum ice velocities are about 900 m a^{-1} near the base of the ice fall 8 km from the terminus, 302 m a^{-1} at 2 km from the terminus, 171 m a^{-1} at 1 km from the terminus, and 94 m a^{-1} at 0.5 km from the terminus. Between 1934 and 1954, the glacier terminus thinned and retreated approximately 450 m, whereas between 1954 and 1985, it thickened and advanced approximately 250 m (Gardner, 1986). Repeat photography from 1985, 1989, 1991, 1993, 1995, 1996, and 1997 shows that the advance culminated in a thickening and steepening of the front and sides, coupled with an outburst flood in early spring, 1994, that eroded much lateral, terminal, and supraglacial debris (figs. 10, 11).

The *Rāikot Glacier* is covered with a thick mantle of supraglacial debris over most of its ablation zone (figs. 8, 10). The glacier has downwasted considerably since its most recent advance, and is therefore bordered by very steep and high lateral moraines. Most of the supraglacial debris originates from these 50- to 70-m high lateral moraines, mainly as a result of landsliding and rock-fall during rainstorms. Snow and rock avalanches also transport debris onto the glacier surface in the upper portion of the basin. Our debris-cover depth measurements taken in 1996 and 1997 indicate that glacier surface topography and debris depth is highly variable, although the supraglacial debris is thickest at the margins and terminus of the glacier, where it reaches depths of up to 4–5 m, and is thinner near the glacier center, where depths are typically 10–20 cm. Areas of shallow debris depths can be mapped via satellite imagery, because reflection in the near-infrared part of the spectrum is enhanced by ablation and melt-water production that occur in these areas.

Glacier flow dynamics and hydrology also play an important role in governing the variability of supraglacial debris depths and sediment transport. Fieldwork in 1995 led to the discovery of catastrophic glacier outburst floods

Figure 10.—(at right) **A**, *Photograph taken in July 1991 of the* Rāikot Glacier *[92] terminus (looking south). View showing generally gentle sides and plentiful lateral and terminal morainal debris. The main melt-water ice portal is in the center, with a smaller subsidiary ice portal issuing on the right (arrows). Photograph by J.F. Shroder, Jr.* **B**, *photo taken in June 1996 of the* Rāikot Glacier *terminus 2 years after the breakout flood of early spring 1994. The terminus had begun to form its steep sides from a renewed advance about 1993. The dark scar on the upper right lateral margin of the glacier (west glacier side) was the main meltwater flood ice portal in 1994. Note the removal of a considerable quantity of ice-marginal debris in the interim. Photograph by M.P. Bishop.*

Figure 11.—*Largest (47 m wide, 23 m deep) ice portal in the upper west margin of* Rāikot *Glacier [92] from the 1994 outburst flood. Three other flood outlet portals were also noted, two others on the west side, and another on the top of the terminus. The outburst flood from the four ice portals in early spring 1994 allowed the flood water to remove large quantities of ice-marginal and supraglacial debris. August 1995 photograph by J.F. Shroder, Jr.*

from four ice portals in the early spring of 1994 that originated on the surface of the glacier terminus and on the western lateral margin (Shroder and others, 2000). Presumably, internal blockage of water flow through englacial conduits led to the build-up of hydrostatic pressure, eventually causing the catastrophic outburst floods from these ice portals (figs. 10, 11). This led to the removal of significant quantities of supraglacial debris cover and the transport of sediment along the western side of the glacier, thereby increasing ablation along the exposed ice margin and over portions of the terminus.

Satellite imagery reveals that this relatively small glacier contains a limited number of supraglacial lakes, in comparison to the numerous, sizeable lakes observed on larger glaciers in Pakistan. Multitemporal imagery documents minor terminus position fluctuations, although a temporally consistent trend, of either advance or retreat, has not been observed. Comparison of SPOT panchromatic and ASTER imagery reveals that the terminus position of the glacier has not significantly changed, presumably because of summer monsoon accumulation. However, at a higher elevation two tributary glaciers, *Ganalo* and the *Chongra-Rāikot Glaciers*, were connected in the recent past; but we have observed that there is currently a disconnect between these tributary glaciers and with the *Rāikot Glacier* (figs. 8, 12).

Batūra Glacier

The large Batūra Glacier [41] to the north in the upper Hunza region is prominent on satellite imagery (fig. 13) and has been assessed in detail, in part because of its accessibility from the KKH. Batūra Glacier flows from west to east below the north side of the peaks of Batūra Muztagh (7,795 m) from 6,200 m into the upper Hunza valley at 2,516 m. The glacier is notorious for

Figure 12.—*Photograph taken in August 1997 showing the connection (arrow) between* Chongra-Rāikot Glacier *and the main* Rāikot Glacier *[92]. The two glaciers have been observed subsequently in the field and on recent imagery and are now disconnected. Photograph by M.P. Bishop.*

large avalanches (Edwards, 1960; Finsterwalder, 1960; Shi and Wang, 1980) that contribute greatly to the mass balance, as well as to the plentiful debris load. The snowline occurs at about 5,000 m, and the annual 0 °C isotherm is near 4,200 m (BGIG, 1979). The glacier is therefore cold in its upper reaches, and temperate in its middle and lower reaches, where two-thirds of the main glacier is covered with debris. Only a narrow (about 700 m) strip of white ice occurs along the south side of the glacier to within about 4 km of the terminus (fig. 14).

Chinese glaciologists (BGIG, 1979) found evidence that the Batūra Glacier was not a surging glacier, but predicted that its terminus would advance in the 1980s to threaten the KKH and then retreat in the 1990s. The predicted advance never occurred and instead the frontal ice cliff has downwasted and the portal above the main meltwater channel has backwasted (Shroder and others, 1984). The debris-covered ice is not easily seen on the imagery, but vegetation on the outwash and kettle ponds on the terminus provide good contrast (figs. 15, 16*B*).

The glacier consists of five main ice flows and more than 20 smaller tributary glaciers (fig. 16). The basin consists of heavy ice cover and snow on the higher north-facing slopes, with less extensive tributary glaciers on the north side. Extensive ablation valley complexes exist on the north side, and glacial meltwater flow and breakout floods from supraglacial ponds have been documented in these valleys.

The dominant uppermost surface of the glacier is characterized by featureless cirques that pass downward through areas of extentional flow over ice falls where the glacier breaks up into seracs. These areas are commonly below the equilibrium line, and thin medial moraines first appear from beneath the firn and pass downward into the crevasses. The western ice flow
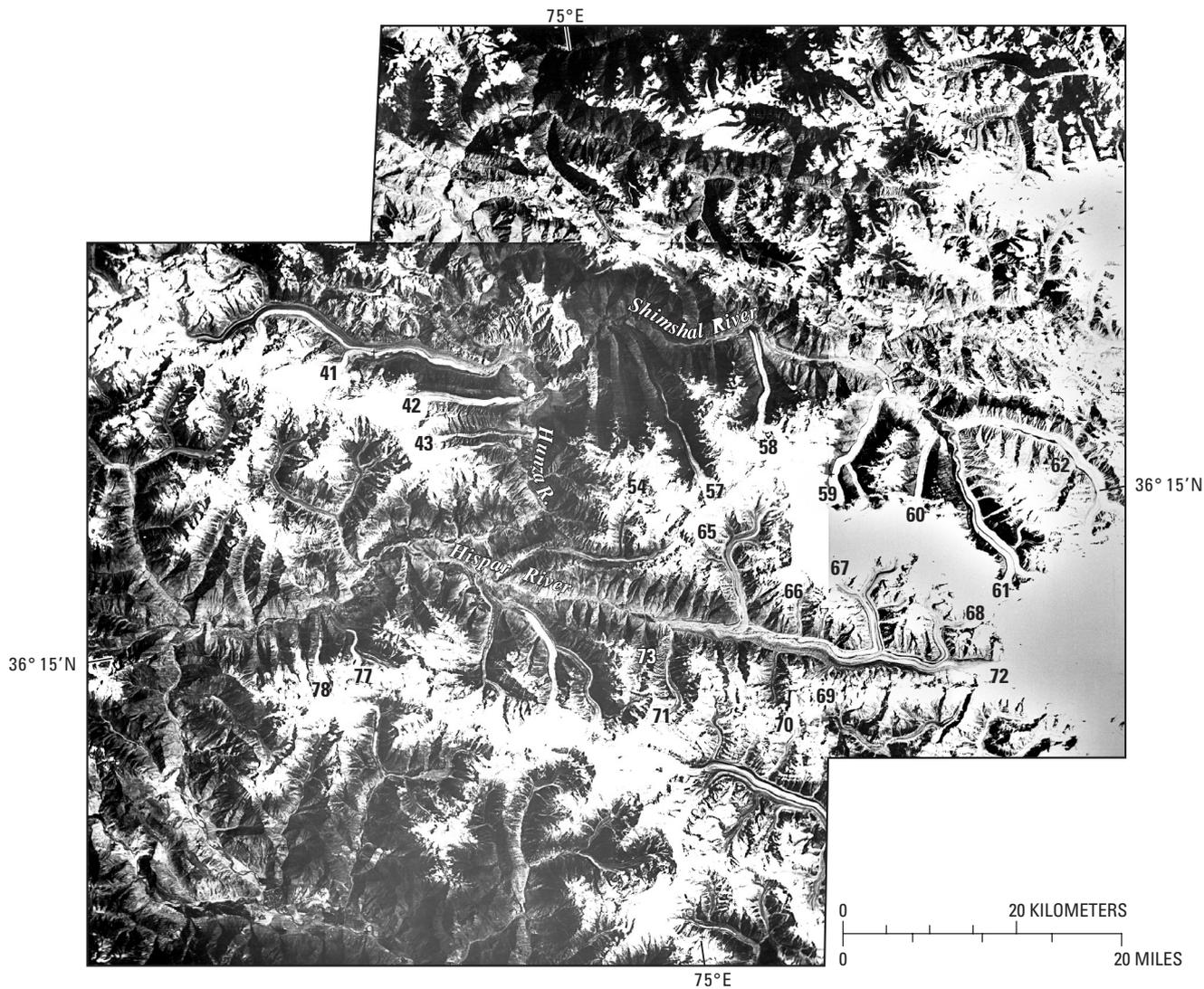
Figure 13.—*Landsat 3 RBV image mosaic showing glaciers in the Hunza region of the Karakoram Range. The main valleys here are the Hunza valley with the Batūra [41],* Pasu *[42], and* Ghulkin *[43] Glaciers, the Shimshal valley with the Momhil [57], Mulungūtti [58], Yāzghil [59],* Yukshin Gardan *[60], Khurdopīn [61], and Vijerab [62] Glaciers, and the Hispar valley with Hispar [72],* Lak-Khiang *[65],* Pumārkish *[66],* Jutmau *[67],* Khanbusa *[68],* Haigatum *[69],* Makrong *[70],* Garumbar *[71], and Yengutz Har [73] Glaciers. The images provide sufficient overlap and can, therefore, be used as a stereoscopic pair. Landsat 3 RBV image nos. 30515–05001, subscene B; 2 August 1979, Path 161–Row 35 (left) and 30532–04542, subscene A; 19 August 1979; Path 160–Row 35 (right) were from the U.S. Geological Survey, EROS Data Center, Sioux Falls, South Dakota 57198, but are now only archived by the authors.*

and its serac field flows downward as a thin white ice stream, and joins an ice flow from the north, which exhibits ogives due to compressive flow from higher elevations. The white ice stream that extends to lower elevations is subject to greater ablation, and the ice undergoes structural changes from ogives to reticulated ice hills. All of these features are clearly visible on SPOT and ASTER imagery.

The remainder of the glacial surface is heavily debris covered and exhibits a variety of supraglacial features. Field measurements and observations show that the debris is granodiorite on the north side of the glacier and black slate on the south side. Satellite imagery also indicates spectral differentiation of granodiorite that is related to weathering. The northern side of the glacier exhibits weathered granodiorite, suggesting that the less weathered debris on the south side results from more active ice flow and sediment redistribution. In general, debris thickness increases toward the terminus and the edges of the glacier.

Figure 14.—Lower part of Batūra Glacier [41] from Yunz, site of a former diffluent valley from Batūra to Pasu Glacier [42]. The white ice surface in the background is particularly noticeable on the imagery (figs. 13, 16) and a useful marker for monitoring future changes. Photograph taken June 1984 by J.F. Shroder, Jr.

Figure 15.—Photograph taken June 1984 showing terminus of Batūra Glacier [41]. The moraine-covered steep slopes directly behind the vegetation in the middle ground were a prominent ice cliff in the late 1970s when investigated by Chinese scientists. The cliff is not obvious on the 1979 imagery, but the vegetation and water-filled kettles produce a strong signature (figs. 13, 16). Photograph by J.F. Shroder, Jr.
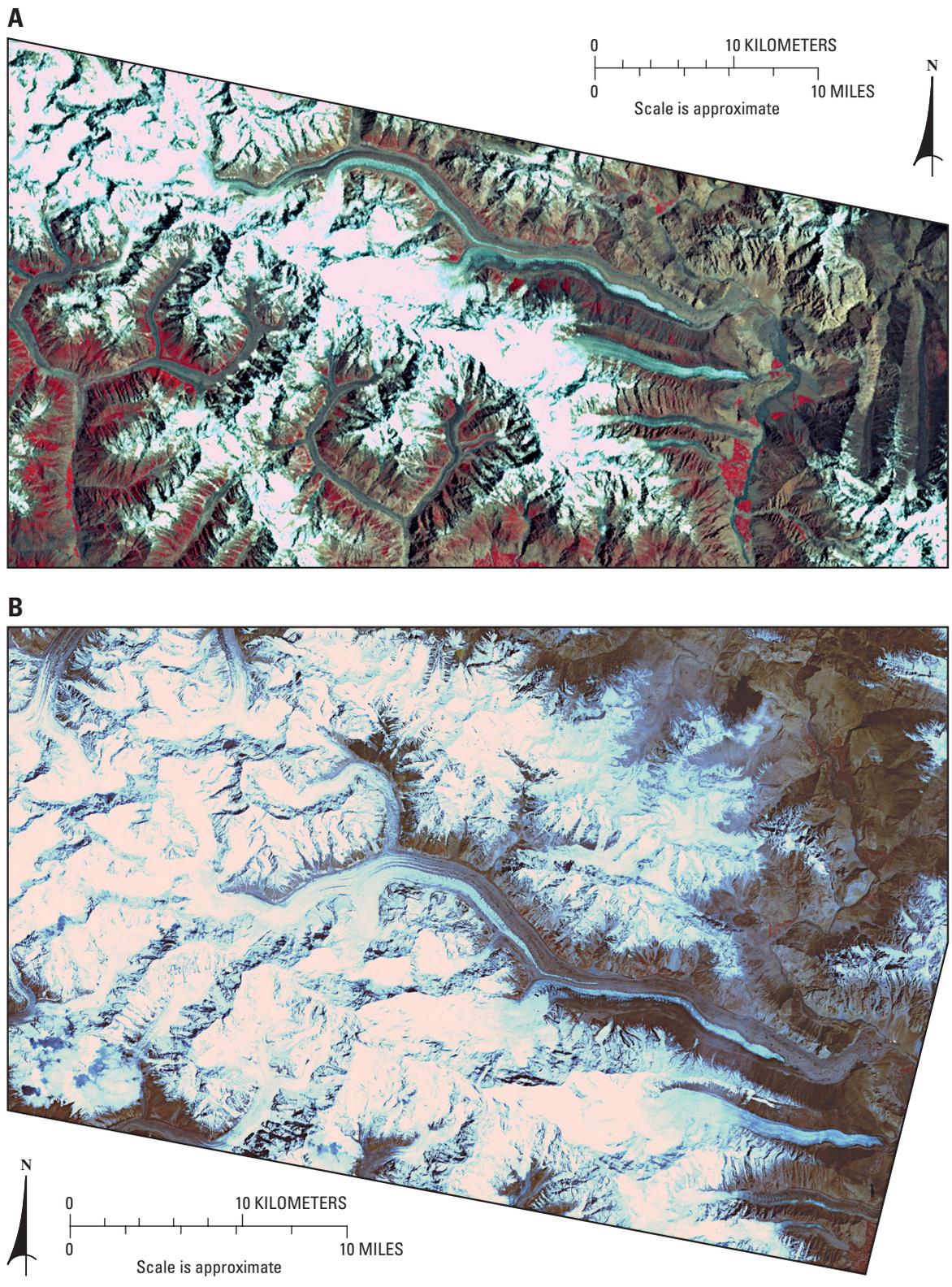
Figure 16.—**A**, Landsat 3 MSS false-color composite image of Batūra Glacier [41] (approximate lat 36°32'N., long 74°40'E.) taken on 15 July 1979, and **B**, ASTER image taken on 30 April 2001. Landsat 3 MSS image no. 3161035007919690, bands 4, 5, 7; 15 July 1979; Path 161–Row 35; and ASTER image no. AST_L1B__003_0 4302001060850_04172002082052_vnir_sub; 30 April 2001 are from the U.S. Geological Survey, EROS Data Center, Sioux Falls, South Dakota 57918.

The Batūra Glacier exhibits a variety of features and characteristics that suggest negative mass balance. From the 19th century until the middle 1940s, the glacier terminus approached the Hunza River (Goudie and others, 1984). Since then, that region has undergone ice flow stagnation and downwasting such that hummocky ground moraine covers a large portion of the proglacial environment (fig. 15). Similarly, the glacier surface has significantly downwasted below the lateral moraines.

Satellite image analysis and change-detection studies support these interpretations, and provide additional evidence. For example, Bishop and others (1995, 1998) conducted a change-detection study and found that the major white-ice stream has been systematically retreating since 1974. Examination of recent ASTER imagery indicates the continuation of this trend (fig. 16B). Differential downwasting of the glacier surface is expected to produce this result; englacial debris can accumulate at the surface and the higher ablation over the exposed ice can generate topographic variation, resulting in the redistribution of nearby supraglacial debris.

Biafo Glacier

At approximately 853 km² in size, 628 km² of which is permanent snow and ice, Biafo Glacier [121] is one of the largest and longest (68 km if uppermost tributaries are included) of the Karakoram glaciers. It differs from many others in the Himalaya because it is mainly nourished by direct snowfall rather than by avalanching (Hewitt and others, 1989). Biafo Glacier's measured annual snow accumulation rate of approximately 0.6 km³, thickness (perhaps 1.4 km at the equilibrium line), and flow rates of 0.8 m d⁻¹ in summer equate to an annual ice flux through the equilibrium line of 0.7 km³ a⁻¹; this matches stake ablation rates equating to 0.7 km³ a⁻¹. The approximate concordance of the three measurements by Hewitt and others (1989) indicates that the ablation zone of Biafo Glacier, whose area covers about 0.09 percent of the whole upper Indus basin, produces approximately 0.09 percent of the total runoff.

The Biafo Glacier has largely linear moraines (fig. 17), and a reported history of considerable fluctuation of its terminus (Mason, 1930; Auden, 1935; Hewitt, 1969; Mayewski and Jeschke, 1979; Hewitt and others, 1989) (fig. 18). Some of this variability may be seasonal, but there has been a general retreat of 0.5 –1 km in the last 120 years. Perhaps of greater significance, however, are the changes on the upper parts of the glacier (fig. 19). During the Shaksgam expedition, Conway's "Snow Lake" consisted of "mostly bare ice" when it was traversed on 20 August 1937 (Shipton, 1938, p. 325). Close-up and panoramic photographs of the same area by Workman and Workman (1911) taken on 16 August 1908 and by Shipton (1940) on 19 August 1939 show extensive snow and white firn fields over clean ice. Shipton (1940, p. 414) noted that travel on the Biafo Glacier was remarkably easy on 19-21 August 1939 "as the smooth white ice extends from its upper reaches almost to the snout." The expedition map (Mott, 1950) also shows extensive clean ice or firn covering much of the upper two-thirds of the glacier. Only thin lateral moraines occurred along the margins, including a narrow strip about 700–800 m wide on the north side of the *Sim Gang* part of "Snow Lake." About forty years later, in 1977 and 1979, (figs. 17, 19, and 20), only a thin band of white ice occurred in the lower third of the glacier, and much of the upper part was dark and debris covered. Even the *Sim Gang* area, at an elevation of about 5,000 m, has a debris-covered surface up to 2 km wide and 8 km long. People who have trekked across this region in recent years have reported that progress in summer months can be most difficult because much of the *Sim Gang* firn has become water saturated, in contrast to prior years of easy travel (Searle, oral comm. to JFS, 1988).
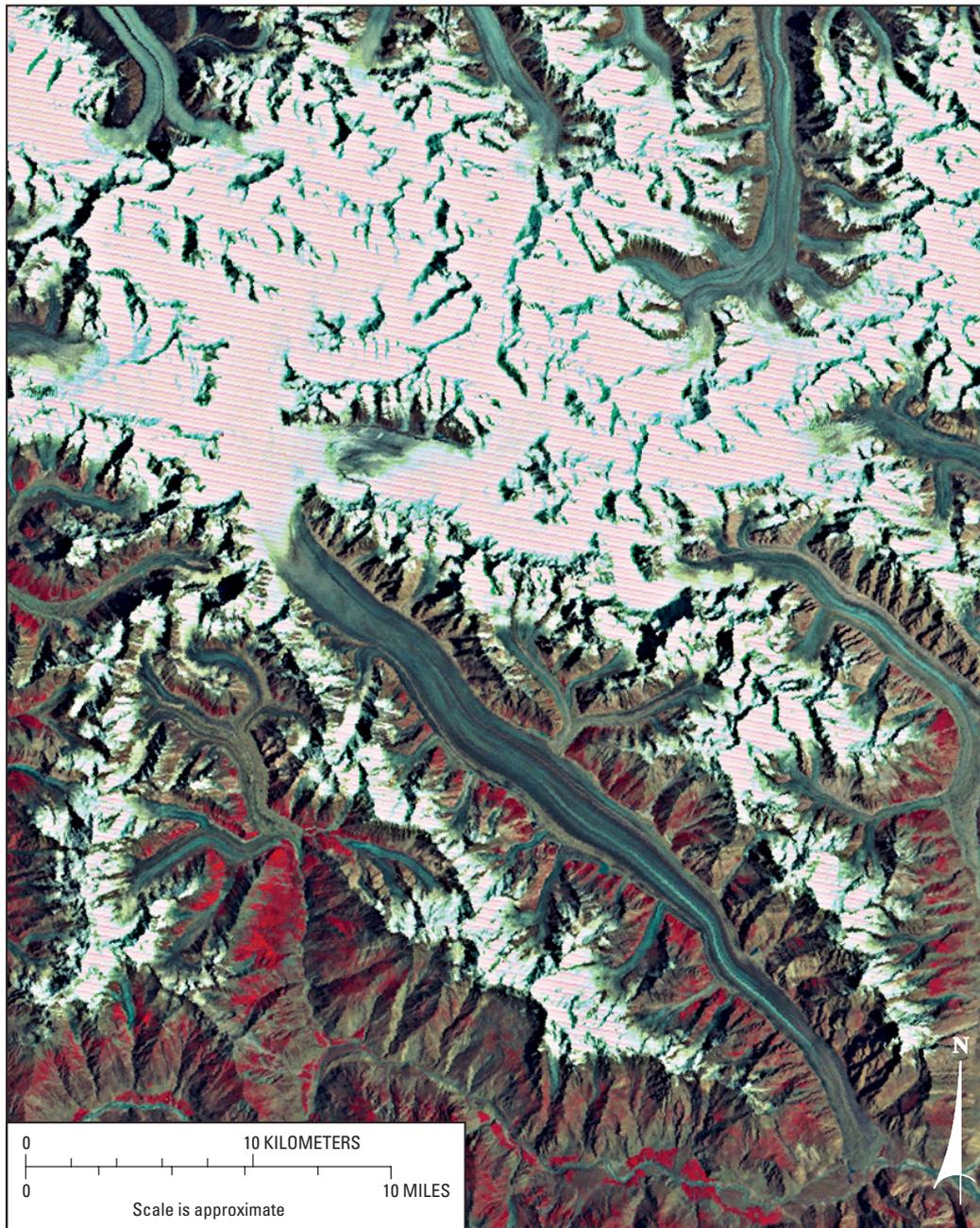
Figure 17.—*Landsat 2 MSS false-color composite image of Biafo Glacier [121] (approximate lat 35°51'N., long 75°45'E.) taken on 2 August 1977, showing linear medial and lateral moraines, together with a complex equilibrium zone in the ice-fall area as well as in the* Sim Gang *("Snow Lake") area (see fig. 19 for locations). The south-facing high peaks on the north side of the east-west trending* Sim Gang *tributary to Biafo provide topographic control of reflected irradiance that strongly affects local ablation, and the location of the transient snowlines. Landsat 2 MSS image no. 2160035007721490, bands 4, 5, 7; 2 August 1977; Path 160–Row 35 is from the U.S. Geological Survey, EROS Data Center, Sioux Falls, South Dakota 57198.*

The ablation region of Biafo Glacier was once characterized by ice standing high above its lateral moraines and the bounding lateral troughs, or 'ablation valleys', but Hewitt and others (1989) have calculated that the glacier has lost at least 2 km³ of its ice mass between 1910 and 1960. Net annual ice losses due to the wastage of the glacier in the 20th century are estimated to be 0.4–0.5 m a⁻¹, which represents 12–15 percent of the annual water yield from ice melt.
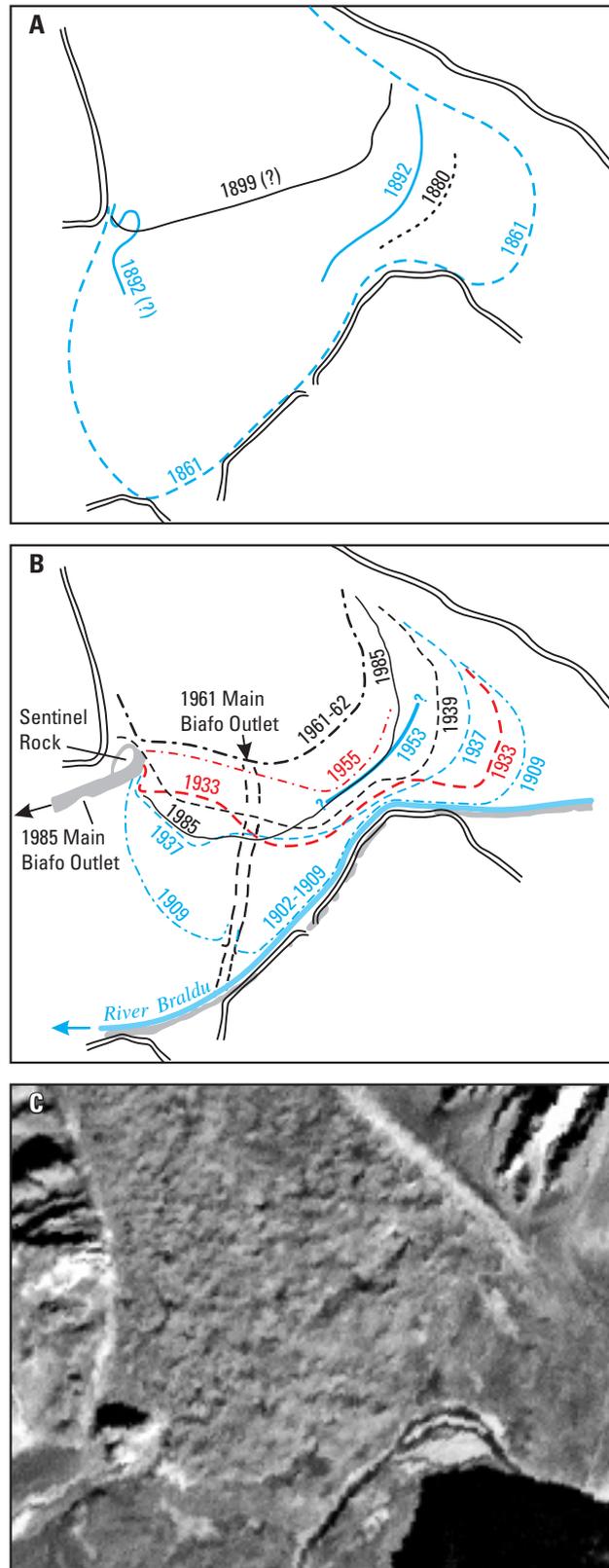
Figure 18.—Terminus, ice portal, and meltwater stream locations of Biafo Glacier [121] (approximate lat 35°51'N., long. 75°45'E.) in the **A**, 19th century map sources; **B**, 20th century map sources, and **C**, 21st century (2004) ASTER image (A and B after Hewitt and others, 1989). Note the existence of the ice portal and melt-water stream discharge in the same position in 2004 as in 1985, as well as the new lake at the terminus. Aster image no. AST_LIA_003_08142004054614_08282004141219, 14 August 2004, is from the U.S. Geological Survey, EROS Data Center, Sioux Falls, South Dakota 57198.
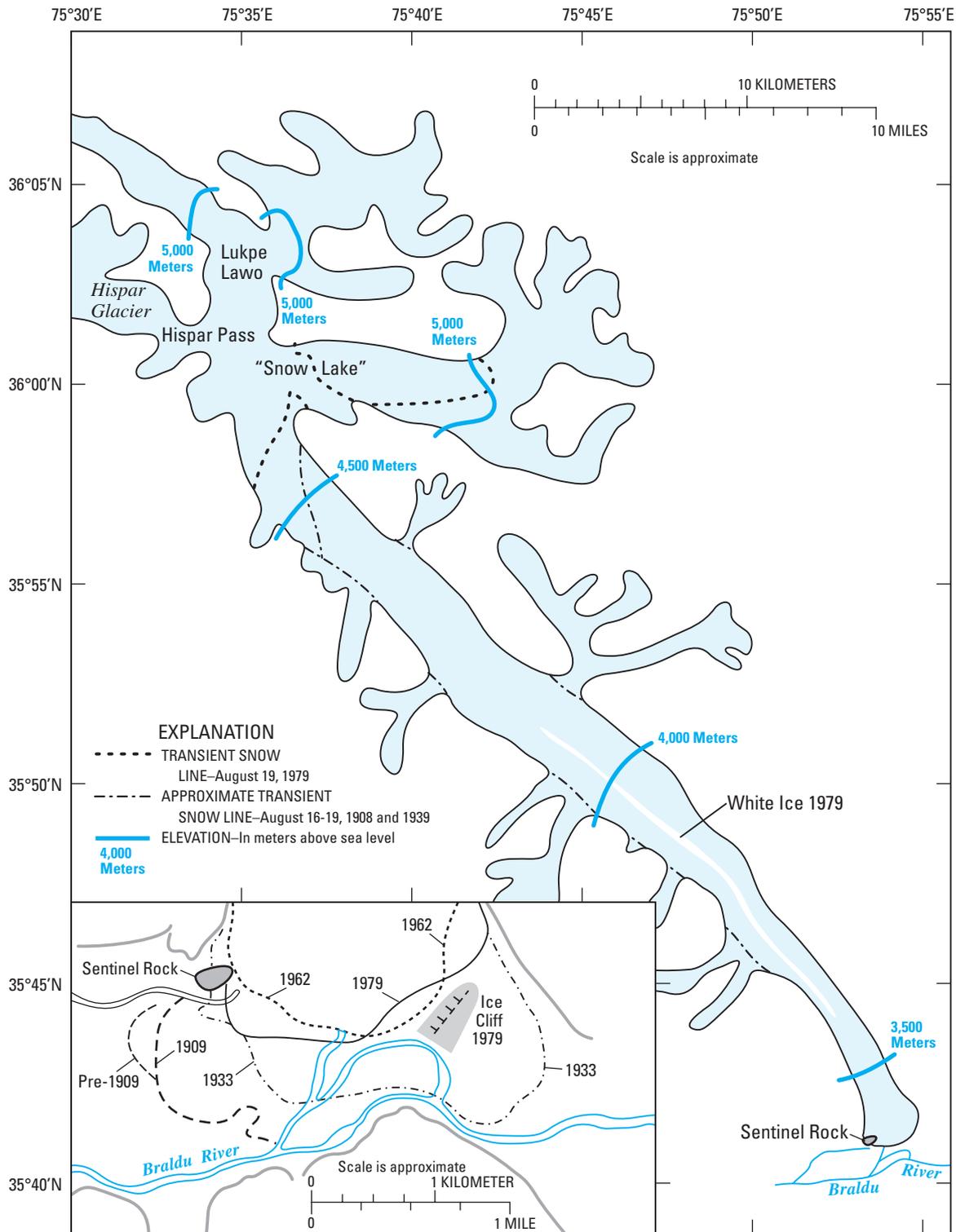
Figure 19.—Sketch map of Biafo Glacier [121] comparing conditions of the overall glacier in August 1908, 1939, and 1979. The transient snow lines of 1908 and 1939 are estimates based on oblique photographs by Workman and Workman (1911) and by Shipton (1940), and on the map by Mott (1950). Mott's map also provided the base for this figure. The terminus positions are from Auden (1935) and Hewitt (1969). All 1979 information is from Landsat 3 RBV image no. 30532–04542, subscene D, 19 August 1979, Path 160, row 35 (fig. 20), with stereo overlap of the "Snow Lake" head area using Landsat 3 RBV image no. 30532–04542, subscene B, 19 August 1979, Path 160–Row 35, and the terminus area using Landsat 3 RBV image no. 30531–04484, subscene C, 18 August 1979, Path 159–Row 35 (fig. 20).
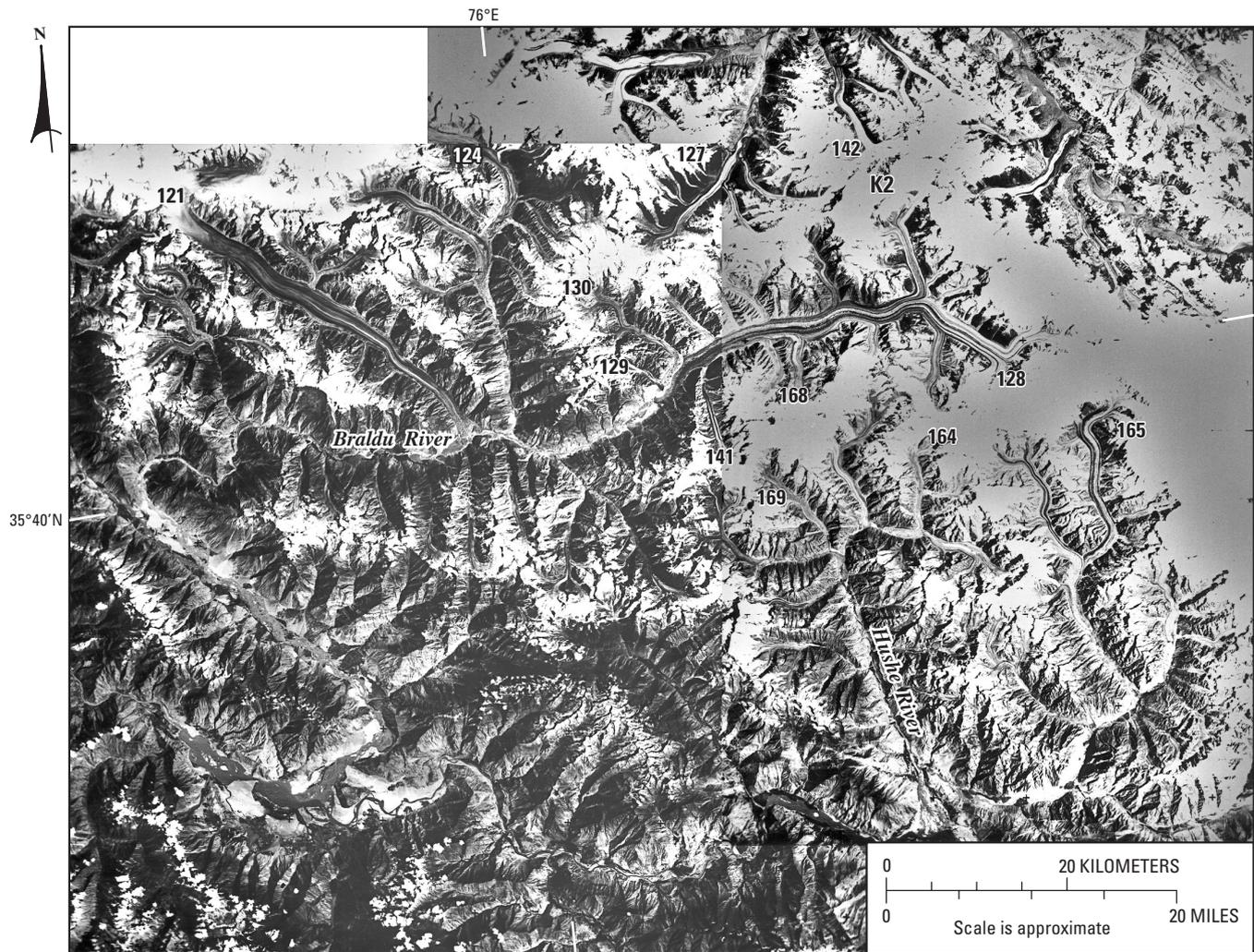
Figure 20.—*Landsat 3 RBV image mosaic showing glaciers in the K2 area of the Karakoram Range. Within the mosaic are part of Biafo [121], Choktoi-Panmah [124], Baltoro [128], Sarpo Laggo [127], Kondus [165], and Kaberi [164] Glaciers. K2 (Qogir Feng) is at the upper right. The images provide sufficient overlap that they can be used as a stereoscopic pair. The Landsat 3 RBV image nos. 30532–04542, subscene D; 19 August 1979; Path 160–Row 35 (left) and 30531–04484, subscene C; 18 August 1979; Path 159–Row 35 (right) were from the U.S. Geological Survey, EROS Data Center, Sioux Falls, South Dakota 57198, but are now only archived by the authors.*

Glaciers Having Unusual or Irregular Flow

The Karakoram and Alaska-Yukon regions account for about 90 percent of the known surging glacier events (Hewitt, 1969). These events are thought to be caused by the buildup of high water pressure in the basal passageway system or in deformable bed sediments (Kamb and others, 1985; Hambrey, 1994; Menzies, 2002). Wang and others (1984) described a breakout flood from the surging *Balt Bare Glacier* in the Karakoram that destroyed part of the KKH. The exceptionally hot (summer temperatures commonly greater than 35 °C) ablation zones in the deep arid valleys of the Karakoram Himalaya contributed meltwater that may have been a factor in surging there.

Unusual or irregular glacier flow was investigated using MSS imagery on western Himalaya glaciers which had histories of advance, retreat, or surge (table 2). Most of these glaciers show no obvious surficial evidence of such movement. The smaller glaciers generally showed the least evidence of movement, in part because the pixel resolution of the MSS imagery did not allow discrimination of diagnostic features on smaller glaciers. Also, many glaciers have a history of rapid movement followed by stagnation and downwasting that produces an extensive debris cover, kettles, and other similar thermokarst phenomena. These surface features are common in the western Himalaya, and limit the potential to differentiate glaciers with irregular rapid movement on MSS imagery.

Using features visible on the older Landsat small-scale imagery, we developed a set of criteria to categorize as many different types of supraglacial features as possible. A few criteria had already been developed to differentiate between surging and nonsurging glaciers using satellite-image interpretation (Krimmel and others, 1976; Meier, 1976; Post and others, 1976; Holdsworth and others, 2002). Kotlyakov (1980) listed surge criteria used in the Soviet Union; Liestøl (1993, table 4, p. E137) listed the names of 86 glaciers in Svalbard which surged between 1838 and 1990; and Elson (1980) listed some general criteria, not all of which are visible on MSS imagery. Elson (1980) also noted that glacial features on Landsat images should be listed as "resolved" if they were identified without prior knowledge, and "detected" if previous information was used to locate them. Major "resolved" surge features include convoluted medial moraines (definitive evidence of surge-type glaciers), unusual pits on the surface of the accumulation area, a stagnant lower part, chaotic crevasses, sheared-off tributary glaciers, the thrust of glacier tongues over other glaciers, large horizontal displacements, and a bulging terminal profile. Goudie and others (1984, p. 413) studied "so-called 'surging' glaciers" in the Karakoram, and noted that major advances and retreats seem to simply reflect the way in which glaciers can respond rapidly as environmental conditions dictate. In other words, they appear to be saying that a sharp distinction between surge-type and non-surge-type glaciers might not exist. Based on these ideas, and using the satellite imagery, we developed a list of resolvable criteria for recognizing the various glacier types in northern Pakistan. The criteria tend to be gradually transitional from one to another, so that a clear distinction between surge-type and non-surge-type glaciers in northern Pakistan may not be possible, if in fact this distinction really exists at all.

Criteria for Recognizing Different Types of Unusual or Rapid Glacier Flow or Retreat

Criteria were developed primarily for use with the older Landsat 3 RBV and MSS imagery, and the numbers of glaciers identified as being of particular types have changed in the intervening decades. The criteria and the numbers of glaciers exhibiting these criteria are:

1. Strongly convoluted medial or lateral moraines (5 glaciers).

2. Medial or lateral moraines convoluted or offset by extensive crevasses or ogives (13 glaciers).

3. Tributary ice overriding or displacing main glacier ice (7 glaciers).

4. Marked depression of ice surface below lateral moraines or tributary glaciers (14 glaciers).

5. Lateral and medial moraines slightly sinuous, or lobate, or offset by crevasses or ogives (76 glaciers).

6. Recent major melting or retreat of ice front leaving light-colored deglacierized terrain (9 glaciers).

TABLE 2.—*Glaciers in northern Pakistan that were directly observed to retreat, advance, or surge sometime in the past*

[Glaciers were selected to test whether or not prior movement or retreat could be detected on Landsat imagery. Glaciers are located in figure 1. Exceptional advances are from Hewitt (1969) and Miller (1984)]

Glacier number	Glacier name and location	Latitude	Longitude	Advance(s)	Features visible on satellite images[1]
34	*Karambar* (Gilgit-*Iskhoman* valley)	36°38′N.	74°10′E.	1930	Slight ogive or crevasse pattern on right (north) lateral moraine; medial moraine not convoluted; end moraine extensively downwasted. Images used for analysis were (2) and (3) as a stereoscopic pair
41	Batūra (Hunza valley)	36°32′N.	74°40′E.	1913–25; 1974–79	Ogives; slightly undulose medial moraine (figs. 14, 15, 16). Images used for analysis were (4) and (5) as a stereoscopic pair
42	*Pasu* (Hunza valley)	36°28′N.	74°45′E.	c.1910–1930	Ogives; ice surface deeply below lateral moraines; snout backwasted. Images used for analysis were (4) and (5) as stereoscopic pair
43	*Ghulkin* (Hunza valley)	36°25′N.	74°50′E.	1913–25, 1966–78	Ogives; ice surface below lateral moraine; snout digitate and far advanced to furthest end moraine above Hunza river. Images used for analysis were (4) and (5) as a stereoscopic pair
45–47	*Hasanabad* and tributaries (Hunza valley)	36°21′N.	74°34′E.	1903–06 surge	Extensive dirty ice; no evidence of rapid movement; two tributary glaciers joined and flow together about 1 km from terminus. Images used for analysis were (1) and (4)
54	*Balt Bare* (Hunza valley)	36°20′N.	74°56′E.	1976 surge	No evidence of rapid movement; light-colored scars of 1974 debris-flow from glacier visible in meltwater channel. Images used for analysis were (4) and (5) as a stereoscopic pair
71	*Garumbar* (Hispar valley)	36°07′N.	75°01′E.	1892–1925?	Prominent recently deglaciated gorge for 4 km to Hispar Glacier with strong downwasted and ice-collapse features nearly to snow-line (fig. 13). Images used for analysis were (4) and (5) as a stereoscopic pair
73	Yengutz Har (Hispar valley)	36°07′N.	74°58′E.	1901–03 surge	Small with dirty ice; no evidence of rapid movement; sizeable alluvial fan at canyon mouth below glacier at Hispar village (fig. 13). Images used for analysis were (4) and (5) as a stereoscopic pair
75	*Hopar* (Hispar valley)	36°10′N.	74°57′E.	1929–30	Dirty ice; no evidence of rapid movement. Images used for analysis were (4) and (5) as a stereoscopic pair
77	Minapin (Hunza valley)	36°11′N.	74°34′E.	1892–93	Moraines not convoluted. Images used for analysis were (1) and (4)
90	*Kutiah* (Stak valley)	35°48′N.	75°00′E.	1953 surge	Some dirty ice; no evidence of rapid movement. Image used for analysis was (1)
108	*Niamul Gans* (tributary of Chogo Lungma, Shigar valley)	35°48′N.	75°15′E.	1902–03	Dark and obscure. Image used for analysis was (6)

[1]Landsat 2 MSS and 3 RBV images used for analysis were (1) 2161035007726990, (2) 30515–04595–C, (3) 30515–05001–A, (4) 30515–05001–B, (5) 30532–04542–A and (6) 30532–04542–C. See table 1 for more information about the images.

7. Extensive area of debris-covered downwasting ice or stagnant ice (106 glaciers).

8. Linear moraines and accordant tributaries (47 glaciers).

Because of difficulty distinguishing different types of motion observed in the field on the MSS imagery, a general study was conducted on northern Pakistan glaciers for which good data existed. Many of the glaciers of the Ghujerab Mountains (Chapchingal and Karun Kuh Groups) north of the main Karakoram, and the small glaciers of the Hindu Kush, Hindu Raj, and Kohistan, were not considered. A few glaciers on the Chinese side were included because of their close proximity to Pakistan and/or because they exhibited some unusual features. The larger glaciers were analyzed preferentially because of the pixel resolution of the MSS imagery, limited ASTER imagery, and because the larger ice masses had more prior information available. Although some smaller glaciers on the periphery of the main Karakoram were included because they had specific characteristics observable on the imagery, most less significant, smaller glaciers in the central Karakoram were excluded. In some cases, tributaries to larger glaciers were treated separately; other tributaries that were unnamed or not particularly different were omitted.

A total of 161 of the larger glaciers of northern Pakistan and 8 in adjacent China were analyzed in this study (listed by number and name in table 3). The longest of these, the Siachen Glacier [155] (Bhutiyana, 1999) in the far northeast corner of Pakistan, is about 67 km long (see fig. 21). The mean length of all glaciers studied is about 15 km. Approximately 75 of the glaciers are between 10–19 km long, 25 between 20–29 km, 4 each from 30–39 km and 40–49 km, 3 between 50–59 km, and only one is 60–70 km in length.

Movement Criteria 1 and 2: Convoluted Medial or Lateral Moraines

A total of 18 glaciers have moraines that are convoluted or strongly convoluted, and these range across northern Pakistan from the mountains on the eastern border to those on the western border. The largest and most prominent examples are in the valleys of Shimshal (fig. 13), Hispar (fig. 13) and Braldu, although several also occur across the border in China, north of the K2 (Qogir Feng) mountain area (fig. 20). In a less prominent but interesting example, the *Selkar Chorten* and *North Terong Glaciers* [153], near the terminus of the Siachen Glacier [155] (fig. 21), have linear moraines and flow together accordantly before turning at right angles into the South Terong river valley. The lowermost 4 km of the terminus was strongly convoluted, suggesting perhaps that meltwater from the *South Terong Glacier* [152] could have been partly responsible. The *South Terong Glacier* was mapped (1938–1946) as connected with *North Terong-Selkar Chorten Glacier* [153], but they were later separated by several kilometers of valley train and meltwater channels (fig. 21).

The glaciers of the Shimshal valley (fig. 13) are well known because of their proclivity to periodically dam the main river (Mason, 1930). The Mulungūtti [58] and Yāzghil [59] Glaciers still extend to the river, essentially the same as they have done since the first maps and descriptions were made in 1892 (Mason, 1930). The Khurdopīn Glacier [61] seems, however, to have undergone some changes due to unusual flow in this same time frame. The glacier is notorious for causing glacier-outburst floods (jökulhlaups), as it periodically blocks meltwater from the Vījerāb Glacier [62]. Mason (1930, p. 248) reported that in about the lower 5 km the "moraine is represented by two dark median lines." Either this is a mistake or some unusual movement has occurred since that time, because high up the glacier there is one linear medial moraine and one wide lateral moraine that continue down the ice to the terminus — a zone of strongly convoluted moraines almost 10 km long (fig. 13, table 3).

Glacier number	Glacier name (general location)	Latitude and longitude	Length (km)	1	2	3	4	5	6	7	8	Satellite images[1]
1	Upper Tirich (Chitrāl)	36°20′N. 75°50′E.	20					X				RBV30553–05112–B; 09 Sep 79
2	Lower Tirich (Chitrāl)	36°19′N. 70°57′E.	8								X	RBV30553–05112–B; 09 Sep 79
3	*Darban-Udren* (Chitrāl)	36°27′N. 72°00′E.	24							X	X	RBV30553–05112–B; 09 Sep 79
4	Hoski-o Shayoz (NW Chitrāl)	36°31′N. 72°10′E.	16				X					RBV30553–05105–D; 09 Sep 79 Stereo30516–05053–C; 03 Aug 79
5	*Shaghordak* (*Hurusko Kuh*, NW Chitrāl)	36°38′N. 72°14′E.	7		X			X				RBV30553–05105–D; 09 Sep 79 Stereo30516–05053–C; 03 Aug 79
6	Chikār (N Chitrāl)	36°38′N. 72°19′E.	9				X	X				RBV30553–05015–D; 09 Sep 79 Stereo30516–05053–C; 03 Aug 79
7	Kotgāz (N Chitrāl)	36°43′N. 72°17′E.	18				X	X				RBV30553–05105–D; 09 Sep 79 Stereo30516–05053–C; 03 Aug 79
8	Chhutidum (N Chitrāl)	36°45′N. 72°25′E.	10		X			X				RBV30553–05105–D; 09 Sep 79 Stereo30516–05053–C; 03 Aug 79
9	Noroghikun (N Chitrāl)	36°44′N. 72°32′E.	15		X			X				RBV30553–05105–D; 09 Sep 79 Stereo30516–05053–C; 03 Aug 79
10	Kach (N Chitrāl)	36°47′N. 72°41′E.	10							X	X	RBV30516–05053–C; 03 Aug 79
11	Madit (*Yarkun*, Hindu Raj)	36°42′N. 73°00′E.	8				X	X				RBV30516–05053–D; 03 Aug 79
12	Risht (*Yarkun*, Hindu Raj)	36°43′N. 73°01′E.	9				X	X				RBV30516–05053–D; 03 Aug 79
13	Shetor (*Yarkun*, Hindu Raj)	36°43′N. 73°05′E.	14				X	X				RBV30516–05053–D; 03 Aug 79
14	Ponārilio (*Yarkun*, Hindu Raj)	36°45′N. 73°09′E.	10							X	X	RBV30516–05053–D; 03 Aug 79
15	Kotalkash (*Yarkun*, Hindu Raj)	36°45′N. 73°12′E.	13				X				X	RBV30516–05053–D; 03 Aug 79
16	Koyo (*Yarkun*, Hindu Raj)	36°45′N. 73°14′E.	5							X	X	RBV30516–05053–D; 03 Aug 79
17	Pechus (*Yarkun*, Hindu Raj)	36°45′N. 73°16′E.	10				X				X	RBV30516–05053–D; 03 Aug 79
18	Chhatiboi (*Yarkun*, Hindu Raj)	36°45′N. 73°19′E.	12				X					RBV30516–05053–D; 03 Aug 79
19	Chikār-Darkot (*Yarkun*, Hindu Raj)	36°46′N. 73°23′E.	10				X	X				RBV30516–05053–D; 03 Aug 79
20	Gazin-Bārbīn (*Yarkun*, Hindu Raj)	36°36′N. 73°02′E.	9					X				RBV30516–05053–D; 03 Aug 79
21	*Mushk Bar* (Thui Gol, Gilgit)	36°33′N. 73°06′E.	10					X				RBV30516–05053–D; 03 Aug 79
22	*Kerun Bar* (Thui Gol, Gilgit)	36°39′N. 73°14′E.	8					X				RBV30516–05053–D; 03 Aug 79
23	*West Gamu Bar* (Thui Gol, Gilgit)	36°37′N. 73°19′E.	7				X					RBV30516–05053–D; 03 Aug 79

[Glacier numbers are cited in the text and plotted on figure 1. Selection based on the following criteria: (1) size large enough to provide resolvable evidence of unusual movement or other resolvable distinguishing landforms; (2) availability of maps or imagery detailed enough to allow discrimination of features. Movement criteria: (1) strongly convoluted medial or lateral moraines (5 glaciers); (2) medial or lateral moraines convoluted or offset by extensive crevasses or ogives (13 glaciers); (3) tributary ice overriding or displacing main glacier ice (7 glaciers); (4) marked depression of ice surface below lateral moraines or tributary glaciers (14 glaciers); (5) lateral and medial moraines slightly sinuous, or lobate, or offset by crevasses or ogives (76 glaciers); (6) recent major melting or retreat of ice front leaving light-colored deglacierized terrain behind (9 glaciers); (7) extensive area of debris-covered downwasting ice or stagnant ice (106 glaciers); and (8) linear moraines and accordant tributaries (47 glaciers). Glacier maps were obtained from many different sources and our field work. In some cases, hyphenated names include tributary names, in others the name itself is a hyphenated phrase. Abbreviations: km, kilometer; ?, glaciers with uncertain names or different spellings]

Glacier number	Glacier name (general location)	Latitude and longitude	Length (km)	Movement criteria								Satellite images[1]
				1	2	3	4	5	6	7	8	
24	*East Ghamu Bar* (Darkot Bar, Gilgit)	36°36′N. 73°22′E.	9					X		X		RBV30516–05053–D; 03 Aug 79
25	Zindikharam (*Yarkun*, Hindu Raj)	36°46′N. 73°27′E.	8		X		X			X		RBV30516–05053–D; 03 Aug 79 Stereo30515–04595–C; 02 Aug 79
26	Chikzar (*Yarkun*, Hindu Raj)	36°45′N. 73°31′E.	7				X					RBV30516–05053–D; 03 Aug 79 Stereo30515–04595–C; 02 Aug 79
27	Chiāntar (*Yarkun*, Hindu Raj)	36°47′N. 73°45′E.	28								X	RBV30516–05053–D; 03 Aug 79 Stereo30515–04595–C; 02 Aug 79
28	Garmush (Chiāntar tributary)	36°45′N. 73°37′E.	14								X	RBV30516–05053–D; 03 Aug 79 Stereo30515–04595–C; 02 Aug 79
29	*Chhateboi* or *Chashboi* (upper Karambar)	36°48′N. 73°52′E.	15		X							RBV30516–05053–D; 03 Aug 79 Stereo30515–04595–C; 02 Aug 79
30	*Sokha Robat* (upper Karambar)	36°47′N. 73°58′E.	9		X					X		RBV30516–05053–D; 03 Aug 79 Stereo30515–04595–C; 02 Aug 79 30515–05001–A; 02 Aug 79
31	*Chillinji* (upper Karambar)	36°46′N. 74°03′E.	8							X		RBV30516–05053–D; 03 Aug 79 Stereo30515–04595–C; 02 Aug 79 30515–05001–A; 02 Aug 79
32	*Wargot* (upper Karambar)	36°44′N. 73°58′E.	8								X	RBV30516–05053–D; 03 Aug 79 Stereo30515–04595–C; 02 Aug 79 30515–05001–A; 02 Aug 79
33	*Pekhin* (upper Karambar)	36°42′N. 73°55′E.	12							X		RBV30516–05053–D; 03 Aug 79 Stereo30515–04595–C; 02 Aug 79 30515–05001–A; 02 Aug 79
34	*Karambar* (upper Karambar)	36°38′N. 74°10′E.	15		X		X	X				RBV30516–05053–D; 03 Aug 79 Stereo30515–04595–C; 02 Aug 79 30515–05001–A; 02 Aug 79
35	*Bohrt* (upper Karambar)	36°33′N. 74°07′E.	10					X				RBV30515–05001–A; 02 Aug 79
36	*Bad Swat* (upper Karambar)	36°01′N. 74°04′E.	10					X				RBV30515–05001–A; 02 Aug 79
37	*Bajgaz* (upper Karambar)	36°23′N. 74°01′E.	15							X		RBV30515–05001–A; 02 Aug 79
38	*Koz Yaz* (upper Hunza)	36°48′N. 74°09′E.	16					X				RBV30515–05001–A; 02 Aug 79 30515–04595–C; 02 Aug 79
39	Yashkūk Yāz (upper Hunza)	36°43′N. 74°18′E.	20					X		X		RBV30515–05001–A; 02 Aug 79 30515–04595–C; 02 Aug 79
40	*Ku-ki-jerab* (upper Hunza)	36°45′N. 74°25′E.	17		X							RBV30515–05001–A; 02 Aug 79 30515–04595–C; 02 Aug 79
41	Batūra (Hunza)	36°32′N. 74°40′E.	55					X		X		RBV30515–05001–B; 02 Aug 79 30532–04542–A; 19 Aug 79
42	*Pasu* (Hunza)	36°28′N. 74°45′E.	26				X	X				RBV30515–05001–B; 02 Aug 79 30532–04542–A; 19 Aug 79
43	*Ghulkin* (Hunza)	36°25′N. 74°50′E.	15					X		X		RBV30515–05001–B; 02 Aug 79 30532–04542–A; 19 Aug 79

[Glacier numbers are cited in the text and plotted on figure 1. Selection based on the following criteria: (1) size large enough to provide resolvable evidence of unusual movement or other resolvable distinguishing landforms; (2) availability of maps or imagery detailed enough to allow discrimination of features. Movement criteria: (1) strongly convoluted medial or lateral moraines (5 glaciers); (2) medial or lateral moraines convoluted or offset by extensive crevasses or ogives (13 glaciers); (3) tributary ice overriding or displacing main glacier ice (7 glaciers); (4) marked depression of ice surface below lateral moraines or tributary glaciers (14 glaciers); (5) lateral and medial moraines slightly sinuous, or lobate, or offset by crevasses or ogives (76 glaciers); (6) recent major melting or retreat of ice front leaving light-colored deglacierized terrain behind (9 glaciers); (7) extensive area of debris-covered downwasting ice or stagnant ice (106 glaciers); and (8) linear moraines and accordant tributaries (47 glaciers). Glacier maps were obtained from many different sources and our field work. In some cases, hyphenated names include tributary names, in others the name itself is a hyphenated phrase. Abbreviations: km, kilometer; ?, glaciers with uncertain names or different spellings]

Glacier number	Glacier name (general location)	Latitude and longitude	Length (km)	Movement criteria								Satellite images[1]
				1	2	3	4	5	6	7	8	
44	*Gulmit* (Hunza)	36°24′N. 74°45′E.	12					X		X		RBV30515–05001–B; 02 Aug 79 30532–04542–A; 19 Aug 79
45	*Shispar* (*Hasanābād* tributary)	36°24′N. 74°36′E.	14							X		RBV30515–05001–B; 02 Aug 79
46	*Mutschual* (*Hasanābād* tributary)	36°23′N. 74°31′E.	21							X		RBV30515–05001–B; 02 Aug 79
47	*Hasanābād* (Hunza)	36°21′N. 74°34′E.	1							X		RBV30515–05001–B; 02 Aug 79
48	*Shittinbar* (Chalt, Hunza)	36°22′N. 74°24′E.	7					X		X		RBV30515–05001–B; 02 Aug 79
49	*Baltar* (Hunza)	36°27′N. 74°24′E.	17					X	X	X		RBV30515–05001–B; 02 Aug 79
50	*Sat Maro-Kukuar* (Hunza)	36°29′N. 74°15′E.	20					X	X	X		RBV30515–05001–A; 02 Aug 79
51	*Aldar Kush* (Hunza)	36°24′N. 74°12′E.	6					X		X		RBV30515–05001–A; 02 Aug 79
52	*Diantar* (Hunza)	36°24′N. 74°08′E.	8					X		X		RBV30515–05001–A; 02 Aug 79
53	*Gharesha-Trivor* (Nagir, Hunza)	36°14′N. 75°00′E.	21					X		X		RBV30515–05001–B; 02 Aug 79 Stereo30532–04542–A; 19 Aug 79
54	*Balt Bare* (Hunza)	36°20′N. 74°56′E.	6					X		X		RBV30515–05001–B; 02 Aug 79 Stereo30532–04542–A; 19 Aug 79
55	*Ghutulji* (Shimshāl)	36°24′N. 74°58′E.	7					X		X		RBV30515–05001–B; 02 Aug 79 Stereo30532–04542–A; 19 Aug 79
56	*Lupghar* (Shimshāl)	36°16′N. 75°24′E.	17					X		X		RBV30515–05001–B; 02 Aug 79 Stereo30532–04542–A; 19 Aug 79
57	Momhil (Shimshāl)	36°21′N. 75°06′E.	22					X		X		RBV30515–05001–B; 02 Aug 79 Stereo30532–04542–A; 19 Aug 79
58	*Mulunqūtti* (Shimshāl)	36°27′N. 75°13′E.	15				X	X				RBV30515–05001–B; 02 Aug 79 Stereo30532–04542–A; 19 Aug 79
59	*Yāzghil* (Shimshāl)	36°20′N. 75°20′E.	25					X				RBV30532–04542–A; 19 Aug 79
60	*Yukshin Gardan* (Shimshāl)	36°15′N. 75°25′E.	17					X				RBV30532–04542–A; 19 Aug 79
61	Khurdopīn (Shimshāl)	36°13′N. 75°30′E.	32	X							X	RBV30532–04542–A; 19 Aug 79 RBV30532–04542–B; 19 Aug 79
62	*Vīrjerāb* (Shimshāl)	36°15′N. 75°40′E.	40	X							X	RBV30532–04542–A; 19 Aug 79 RBV30532–04542–B; 19 Aug 79
63	Braldu	36°10′N. 75°52′E.	35		X						X	RBV30532–04542–B; 19 Aug 79
64	*Skamri* (China)	36°03′N. 76°15′E.	36	X				X		X		RBV30532–04542–B; 19 Aug 79 Stereo30531–04484–A; 18 Aug 79 30531–04484–B; 18 Aug 79
65	*Lak-Khiang* (Hispar tributary)	36°10′N. 75°08′E.	19					X		X		RBV30515–05001–B; 02 Aug 79 Stereo30532–04542–A; 19 Aug 79

[Glacier numbers are cited in the text and plotted on figure 1. Selection based on the following criteria: (1) size large enough to provide resolvable evidence of unusual movement or other resolvable distinguishing landforms; (2) availability of maps or imagery detailed enough to allow discrimination of features. Movement criteria: (1) strongly convoluted medial or lateral moraines (5 glaciers); (2) medial or lateral moraines convoluted or offset by extensive crevasses or ogives (13 glaciers); (3) tributary ice overriding or displacing main glacier ice (7 glaciers); (4) marked depression of ice surface below lateral moraines or tributary glaciers (14 glaciers); (5) lateral and medial moraines slightly sinuous, or lobate, or offset by crevasses or ogives (76 glaciers); (6) recent major melting or retreat of ice front leaving light-colored deglacierized terrain behind (9 glaciers); (7) extensive area of debris-covered downwasting ice or stagnant ice (106 glaciers); and (8) linear moraines and accordant tributaries (47 glaciers). Glacier maps were obtained from many different sources and our field work. In some cases, hyphenated names include tributary names, in others the name itself is a hyphenated phrase. Abbreviations: km, kilometer; ?, glaciers with uncertain names or different spellings]

Glacier number	Glacier name (general location)	Latitude and longitude	Length (km)	Movement criteria								Satellite images[1]
				1	2	3	4	5	6	7	8	
66	Pumārikish (Hispar tributary)	36°08′N. 75°12′E.	8					X		X		RBV30515–05001–B; 02 Aug 79 Stereo30532–04542–A; 19 Aug 79
67	Jutmau (Hispar tributary)	36°08′N. 75°19′E.	20							X	X	RBV30532–04542–A; 19 Aug 79
68	Khanbasa (Hispar tributary)	36°07′N. 75°24′E.	19							X	X	RBV30532–04542–A; 19 Aug 79
69	Haigatum (Hispar tributary)	36°04′N. 75°13′E.	5					X		X		RBV30515–05001–B; 02 Aug 79 Stereo30532–04542–A; 19 Aug 79 30532–04542–C; 19 Aug 79
70	Makrong (Hispar tributary)	36°04′N. 75°09′E.	8					X		X		RBV30515–05001–B; 02 Aug 79 Stereo30532–04542–A; 19 Aug 79 30532–04542–C; 19 Aug 79
71	Garumbar (Hispar)	36°07′N. 75°01′E.	12					X	X			RBV30515–05001–B; 02 Aug 79 Stereo30532–04542–A; 19 Aug 79 30532–04542–C; 19 Aug 79
72	Hispar	36°05′N. 75°15′E.	48	X		X				X		RBV30515–05001–B; 02 Aug 79 Stereo30532–04542–A; 19 Aug 79 30532–04542–C; 19 Aug 79
73	Yengutz Har (Hispar)	36°07′N. 74°58′E.	5					X		X		RBV30515–05001–B; 02 Aug 79 Stereo30532–04542–A; 19 Aug 79 30532–04542–C; 19 Aug 79
74	Miar or Shalhubu Sumaiyar Bar-Barpu (Nagir, Hispar)	36°10′N. 74°50′E.	23				X	X				RBV30515–05001–B; 02 Aug 79 Stereo30532–04542–A; 19 Aug 79 30532–04542–C; 19 Aug 79
75	Buāltar or Hopar (Nagir, Hispar)	36°10′N. 74°45′E.	20				X	X		X		RBV30515–05001–B; 02 Aug 79 Stereo30532–04542–A; 19 Aug 79 30532–04542–C; 19 Aug 79
76	Sumaiyar or Silkiang (Rakaposhi, Hunza)	36°12′N. 74°39′E.	7					X		X		RBV30515–05001–B; 02 Aug 79
77	Minapin (Rakaposhi, Hunza)	36°11′N. 74°34′E.	10					X				RBV30515–05001–B; 02 Aug 79
78	Pisan (Rakaposhi, Hunza)	36°11′N. 74°30′E.	9					X				RBV30515–05001–B; 02 Aug 79
79	Ghulmet (Rakaposhi, Hunza)	36°11′N. 74°28′E.	6								X	RBV30515–05001–B; 02 Aug 79
80	Jaglot? (Rakaposhi, Hunza)	36°05′N. 74°24′E.	6							X		RBV30515–05001–B; 02 Aug 79
81	Surgin (Rakaposhi, Gilgit)	36°06′N. 74°29′E.	7							X		RBV30515–05001–B; 02 Aug 79
82	Hinarche (Rakaposhi, Gilgit)	36°05′N. 74°34′E.	14					X		X		RBV30515–05001–B; 02 Aug 79
83	Yuna (Rakaposhi, Gilgit)	36°04′N. 74°39′E.	6							X		RBV30515–05001–B; 02 Aug 79
84	Burcha (Rakaposhi, Gilgit)	36°03′N. 74°40′E.	15							X		RBV30515–05001–B; 02 Aug 79
85	Saltli (Haramosh)	36°02′N. 74°45′E.	4							X		RBV30515–05001–B; 02 Aug 79

[Glacier numbers are cited in the text and plotted on figure 1. Selection based on the following criteria: (1) size large enough to provide resolvable evidence of unusual movement or other resolvable distinguishing landforms; (2) availability of maps or imagery detailed enough to allow discrimination of features. Movement criteria: (1) strongly convoluted medial or lateral moraines (5 glaciers); (2) medial or lateral moraines convoluted or offset by extensive crevasses or ogives (13 glaciers); (3) tributary ice overriding or displacing main glacier ice (7 glaciers); (4) marked depression of ice surface below lateral moraines or tributary glaciers (14 glaciers); (5) lateral and medial moraines slightly sinuous, or lobate, or offset by crevasses or ogives (76 glaciers); (6) recent major melting or retreat of ice front leaving light-colored deglacierized terrain behind (9 glaciers); (7) extensive area of debris-covered downwasting ice or stagnant ice (106 glaciers); and (8) linear moraines and accordant tributaries (47 glaciers). Glacier maps were obtained from many different sources and our field work. In some cases, hyphenated names include tributary names, in others the name itself is a hyphenated phrase. Abbreviations: km, kilometer; ?, glaciers with uncertain names or different spellings]

Glacier number	Glacier name (general location)	Latitude and longitude	Length (km)	Movement criteria								Satellite images[1]
				1	2	3	4	5	6	7	8	
86	*Kaltaro* (Haramosh)	36°06′N. 74°47′E.	10							X		RBV30515–05001–B; 02 Aug 79
87	*Baskai* (Haramosh)	35°56′N. 74°52′E.	9							X		RBV30515–05001–B; 02 Aug 79
88	*Mani* (Haramosh)	35°53′N. 74°53′E.	12							X		RBV30515–05001–B; 02 Aug 79 Stereo30515–05001–D; 02 Aug 79
89	*Ishkapal* (Haramosh)	35°49′N. 74°50′E.	7							X		RBV30515–05001–B; 02 Aug 79 Stereo30515–05001–D; 02 Aug 79
90	*Kutiah* (Haramosh)	35°48′N. 75°00′E.	16				X	X		X		RBV30515–05001–B; 02 Aug 79 Stereo30515–05001–D; 02 Aug 79
91	*Stak* (Haramosh)	35°48′N. 75°04′E.	9					X		X		RBV30515–05001–B; 02 Aug 79 Stereo30515–05001–D; 02 Aug 79
92	*Rākhiot* (Nanga Parbat)	35°20′N. 74°35′E.	13				X	X				RBV30515–05001–D; 02 Aug 79 Stereo30532–04542–C; 19 Aug 79
93	*Buldar* (Nanga Parbat)	35°22′N. 74°42′E.	7							X		RBV30515–05001–D; 02 Aug 79
94	*Lotang* (Nanga Parbat)	35°22′N. 74°45′E.	5							X		RBV30515–05001–D; 02 Aug 79
95	*Sachen* (Nanga Parbat)	35°20′N. 74°45′E.	9							X		RBV30515–05001–D; 02 Aug 79
96	*Tsongra-Chungpar* (Nanga Parbat)	35°16′N. 74°42′E.	10							X		RBV30515–05001–D; 02 Aug 79
97	*Bizin* (Nanga Parbat)	35°12′N. 74°38′E.	11							X		RBV30515–05001–D; 02 Aug 79
98	*Tap* (Nanga Parbat)	35°13′N. 74°35′E.	5							X		RBV30515–05001–D; 02 Aug 79
99	*Sheigri* (Nanga Parbat)	35°11′N. 74°34′E.	6							X		RBV30515–05001–D; 02 Aug 79
100	*Toshain* or *Rupal* (Nanga Parbat)	35°10′N. 74°31′E.	15								X	RBV30515–05001–D; 02 Aug 79
101	*Diamir* (Nanga Parbat)	35°16′N. 74°32′E.	15							X		RBV30515–05001–D; 02 Aug 79
102	*Patro* (Nanga Parbat)	35°18′N. 74°31′E.	4							X		RBV30515–05001–D; 02 Aug 79
103	Chogo Lungma (Haramosh, *Basna*)	36°00′N. 75°00′E.	40							X	X	RBV30515–05001–B; 02 Aug 79 Stereo30532–04542–C; 19 Aug 79
104	*Haramosh* (Chogo Lungma tributary)	35°57′N. 75°00′E.	16					X				RBV30515–05001–B; 02 Aug 79 Stereo30532–04542–C; 19 Aug 79
105	*West Kupultung-Kung?* (Chogo Lungma tributary)	35°55′N. 75°05′E.	15					X			X	RBV30515–05001–B; 02 Aug 79 Stereo30532–04542–C; 19 Aug 79
106	*East Kupultung-Kung?* (Chogo Lungma tributary)	35°54′N. 75°08′E.	13					X				RBV30515–05001–B; 02 Aug 79 Stereo30532–04542–C; 19 Aug 79
107	*Marpah-Remendok* (Chogo Lungma valley)	35°53′N. 75°11′E.	15				X	X		X		RBV30515–05001–B; 02 Aug 79 Stereo30532–04542–C; 19 Aug 79

[Glacier numbers are cited in the text and plotted on figure 1. Selection based on the following criteria: (1) size large enough to provide resolvable evidence of unusual movement or other resolvable distinguishing landforms; (2) availability of maps or imagery detailed enough to allow discrimination of features. Movement criteria: (1) strongly convoluted medial or lateral moraines (5 glaciers); (2) medial or lateral moraines convoluted or offset by extensive crevasses or ogives (13 glaciers); (3) tributary ice overriding or displacing main glacier ice (7 glaciers); (4) marked depression of ice surface below lateral moraines or tributary glaciers (14 glaciers); (5) lateral and medial moraines slightly sinuous, or lobate, or offset by crevasses or ogives (76 glaciers); (6) recent major melting or retreat of ice front leaving light-colored deglacierized terrain behind (9 glaciers); (7) extensive area of debris-covered downwasting ice or stagnant ice (106 glaciers); and (8) linear moraines and accordant tributaries (47 glaciers). Glacier maps were obtained from many different sources and our field work. In some cases, hyphenated names include tributary names, in others the name itself is a hyphenated phrase. Abbreviations: km, kilometer; ?, glaciers with uncertain names or different spellings]

Glacier number	Glacier name (general location)	Latitude and longitude	Length (km)	Movement criteria								Satellite images[1]
				1	2	3	4	5	6	7	8	
108	*Niamul Gans* (Chogo Lungma valley)	35°48′N. 75°15′E.	14						X	X		RBV30532–04542–C; 19 Aug 79
109	*Tippur Gans* (upper Basna valley)	35°51′N. 75°20′E.	7							X		RBV30532–04542–C; 19 Aug 79
110	*Sgari-bian* (Chogo Lungma tributary)	35°04′N. 75°00′E.	9								X	RBV30515–05001–B; 02 Aug 79 30532–04542–C; 19 Aug 79
111	*Bolucho* (Chogo Lungma tributary)	36°08′N. 75°00′E.	5					X	X			RBV30515–05001–B; 02 Aug 79 30532–04542–C; 19 Aug 79
112	*Arincu* (Chogo Lungma tributary)	36°00′N. 75°11′E.	8					X				RBV30515–05001–B; 02 Aug 79 30532–04542–C; 19 Aug 79
113	*Kero Lungma* (upper Basna valley)	36°00′N. 75°15′E.	15					X		X		RBV30532–04542–A; 19 Aug 79 Stereo30532–04542–C; 19 Aug 79
114	*Hucho Alchori* (upper Basna valley)	35°59′N. 75°23′E.	13					X		X		RBV30532–04542–A; 19 Aug 79 Stereo30532–04542–C; 19 Aug 79
115	*Niaro Gans* (upper *Basna* valley)	35°55′N. 75°17′E.	5							X		RBV30532–04542–C; 19 Aug 79
116	*Solu-Sokha* (upper *Basna* valley)	35°59′N. 75°30′E.	15					X		X		RBV30532–04542–C; 19 Aug 79
117	*Sosbun* (Braldu)	35°52′N. 75°34′E.	16					X		X		RBV30532–04542–D; 19 Aug 79
118	*Tsilbu-Hoh Lungma* (Braldu)	35°50′N. 75°33′E.	9							X		RBV30532–04542–D; 19 Aug 79
119	*Chongahanmong* (Braldu)	35°48′N. 75°33′E.	5					X		X		RBV30532–04542–D; 19 Aug 79
120	*West Tongo?* (Braldu)	35°48′N. 75°39′E.	5					X		X		RBV30532–04542–D; 19 Aug 79
121	Biafo (Braldu)	35°50′N. 75°45′E.	54					X		X	X	RBV30531–04484–C; 18 Aug 79 Stereo30532–04542–B; 19 Aug 79 30532–04542–D; 19 Aug 79
122	*Sim Gang* (Biafo tributary)	36°00′N. 75° 35′E.	15					X		X		RBV30531–04484–C; 18 Aug 79 Stereo30532–04542–B; 19 Aug 79 30532–04542–D; 19 Aug 79
123	*Uzun Blakk Baintha Lukpar* (Biafo tributary)	35°53′N. 75°45′E.	10					X		X		RBV30531–04484–C; 18 Aug 79 Stereo30532–04542–B; 19 Aug 79 30532–04542–D; 19 Aug 79
124	*Choktoi-Panmah* (*Dumordo*-Braldu)	35°53′N. 75°58′E.	30	X	X	X	X	X	X	X	X	RBV30531–04484–C; 18 Aug 79 Stereo30532–04542–B; 19 Aug 79 30532–04542–D; 19 Aug 79
125	*Drenmang* (Panmah tributary)	35°59N. 76°03.E.	8		X			X				RBV30531–04484–C; 18 Aug 79 Stereo30532–04542–B; 19 Aug 79 30532–04542–D; 19 Aug 79
126	*Chiring* (Panmah tributary)	35°55′N. 76°04′E.	16		X			X	X			RBV30531–04484–C; 18 Aug 79 Stereo30532–04542–B; 19 Aug 79 30532–04542–D; 19 Aug 79

[Glacier numbers are cited in the text and plotted on figure 1. Selection based on the following criteria: (1) size large enough to provide resolvable evidence of unusual movement or other resolvable distinguishing landforms; (2) availability of maps or imagery detailed enough to allow discrimination of features. Movement criteria: (1) strongly convoluted medial or lateral moraines (5 glaciers); (2) medial or lateral moraines convoluted or offset by extensive crevasses or ogives (13 glaciers); (3) tributary ice overriding or displacing main glacier ice (7 glaciers); (4) marked depression of ice surface below lateral moraines or tributary glaciers (14 glaciers); (5) lateral and medial moraines slightly sinuous, or lobate, or offset by crevasses or ogives (76 glaciers); (6) recent major melting or retreat of ice front leaving light-colored deglacierized terrain behind (9 glaciers); (7) extensive area of debris-covered downwasting ice or stagnant ice (106 glaciers); and (8) linear moraines and accordant tributaries (47 glaciers). Glacier maps were obtained from many different sources and our field work. In some cases, hyphenated names include tributary names, in others the name itself is a hyphenated phrase. Abbreviations: km, kilometer; ?, glaciers with uncertain names or different spellings]

Glacier number	Glacier name (general location)	Latitude and longitude	Length (km)	Movement criteria								Satellite images[1]
				1	2	3	4	5	6	7	8	
127	*Sarpo Lago* (Baltoro Mutagh)	36°00′N. 76° 22′ E.	29		X			X		X		RBV30531–04484–A; 18 Aug 79 Stereo30532–04542–B; 19 Aug 79 30532–04542–D; 19 Aug 79
128	Baltoro (Biaho Lungma, Braldu)	35°46′N. 76°15′E.	52							X	X	RBV30531–04484–C; 18 Aug 79 Stereo30532–04542–D; 19 Aug 79
129	*Uli Biaho* (Baltoro tributary)	35°13′N. 76°09′E.	8			X						RBV30531–04484–C; 18 Aug 79 Stereo30532–04542–D; 19 Aug 79
130	*Trango* (Baltoro tributary)	35°45′N. 76°10′E.	16			X				X		RBV30531–04484–C; 18 Aug 79 Stereo30532–04542–D; 19 Aug 79
131	*Dunge* (Baltoro tributary)	35°45′N. 76°14′E.	10				X					RBV30531–04484–C; 18 Aug 79 Stereo30532–04542–D; 19 Aug 79
132	*Biaie* (Baltoro tributary)	35°46′N. 76°16′E.	6							X		RBV30531–04484–C; 18 Aug 79 Stereo30532–04542–D; 19 Aug 79
133	*Mutagh* (Baltoro tributary)	35°47′N. 76°18′E.	11				X					RBV30531–04484–C; 18 Aug 79 Stereo30532–04542–D; 19 Aug 79
134	Biange-*Younghusband* (Baltoro tributary)	35°48′N. 76°24′E.	12							X		RBV30531–04484–C; 18 Aug 79 Stereo30532–04542–D; 19 Aug 79
135	K2-Godwin Austen (Baltoro tributary)	35°50′N. 76°31′E.	18							X		RBV30531–04484–C; 18 Aug 79 Stereo30532–04542–B; 19 Aug 79
136	*South Gasherbrum* (Baltoro tributary)	35°52′N. 76°40′E.	6							X		RBV30531–04484–C; 18 Aug 79
137	*Upper Baltoro* (Baltoro tributary)	35°43′N. 76°31′E.	14							X		RBV30531–04484–C; 18 Aug 79
138	*Vigne* (Baltoro tributary)	35°43′N. 76°26′E.	5							X		RBV30531–04484–C; 18 Aug 79 Stereo30532–04542–B; 19 Aug 79
139	*Yermanendu* (Baltoro tributary)	35°38′N. 76°17′E.	10							X		RBV30531–04484–C; 18 Aug 79 Stereo30532–04542–B; 19 Aug 79
140	Mundu (Baltoro tributary)	35°40′N. 76°17′E.	8							X		RBV30531–04484–C; 18 Aug 79 Stereo30532–04542–B; 19 Aug 79
141	*Liligo* (Baltoro tributary)	35°40′N. 76°13′E.	6						X			RBV30531–04484–C; 18 Aug 79 Stereo30532–04542–B; 19 Aug 79
142	K2 North (Baltoro Mutagh, China)	36°00′N. 76°28′E.	16		X				X			RBV30531–04484–C; 18 Aug 79 Stereo30532–04542–B; 19 Aug 79
143	*Skyang Lungpa* (Baltoro Mutagh, China)	35°54′N. 76°40′E.	11							X		RBV30531–04484–C; 18 Aug 79 Stereo30532–04542–B; 19 Aug 79
144	*Gasherbrum-Chagharlung* (Baltoro Mutagh, China)	35°51′N. 76°42′E.	15					X				RBV30531–04484–C; 18 Aug 79 Stereo30532–04542–B; 19 Aug 79
145	*Urdok* (Baltoro Mutagh, China)	35°47′N. 76°45′E.	24					X		X		RBV30531–04484–C; 18 Aug 79 Stereo30532–04542–B; 19 Aug 79
146	*Staghar* (Siachen Mutagh, China)	35°45′N. 76°48′E.	18							X		RBV30531–04484–C; 18 Aug 79 Stereo30532–04542–B; 19 Aug 79
147	*Singhi* (Siachen Mutagh, China)	35°41′N. 77°00′E.	24							X		RBV30531–04484–D; 18 Aug 79
148	*Kyagar* (Siachen Mutagh, China)	35°38′N. 77°11′E.	19							X		RBV30531–04484–D; 18 Aug 79

[Glacier numbers are cited in the text and plotted on figure 1. Selection based on the following criteria: (1) size large enough to provide resolvable evidence of unusual movement or other resolvable distinguishing landforms; (2) availability of maps or imagery detailed enough to allow discrimination of features. Movement criteria: (1) strongly convoluted medial or lateral moraines (5 glaciers); (2) medial or lateral moraines convoluted or offset by extensive crevasses or ogives (13 glaciers); (3) tributary ice overriding or displacing main glacier ice (7 glaciers); (4) marked depression of ice surface below lateral moraines or tributary glaciers (14 glaciers); (5) lateral and medial moraines slightly sinuous, or lobate, or offset by crevasses or ogives (76 glaciers); (6) recent major melting or retreat of ice front leaving light-colored deglacierized terrain behind (9 glaciers); (7) extensive area of debris-covered downwasting ice or stagnant ice (106 glaciers); and (8) linear moraines and accordant tributaries (47 glaciers). Glacier maps were obtained from many different sources and our field work. In some cases, hyphenated names include tributary names, in others the name itself is a hyphenated phrase. Abbreviations: km, kilometer; ?, glaciers with uncertain names or different spellings]

Glacier number	Glacier name (general location)	Latitude and longitude	Length (km)	Movement criteria								Satellite images[1]
				1	2	3	4	5	6	7	8	
149	*North Rimo* (*Rimo Mutagh*, China)	35°29′N. 77°30′E.	20	X								RBV30531–04484–D; 18 Aug 79
150	*Central Rimo* (*Rimo Mutagh*)	35°27′N. 77°30′E.	40				X		X			RBV30531–04484–D; 18 Aug 79
151	*South Rimo* (*Rimo Mutagh*)	35°20′N. 77°30′E.	22				X		X			RBV30531–04484–D; 18 Aug 79
152	*South Terong* (upper Nubra valley)	35°12′N. 77°24′E.	21							X	X	RBV30531–04484–D; 18 Aug 79
153	*Selkar Chorten-North Terong* (upper Nubra valley)	35°15′N. 77°20′E.	24	X						X	X	RBV30531–04484–D; 18 Aug 79
154	*Dzingrulma* (upper Nubra valley)	35°10′N. 77°10′E.	5					X				RBV30531–04484–D; 18 Aug 79
155	Siachen (upper Nubra valley)	35°30′N. 77°00′E.	67							X		RBV30531–04484–D; 18 Aug 79
156	*Chumick Saltoro I* ? (Siachen tributary)	35°13′N. 77°08′E.	11							X	X	RBV30531–04484–D; 18 Aug 79
157	*Chumick Saltoro II* ? (Siachen tributary)	35°21′N. 77°07′E.	15							X		RBV30531–04484–D; 18 Aug 79
158	Lolofong (Siachen tributary)	35° 26′N. 77°00′E.	12							X		RBV30531–04484–D; 18 Aug 79
159	*Saltoro* (Siachen tributary)	35°30′N. 76°56′E.	18							X		RBV30531–04484–D; 18 Aug 79
160	*Teram Shehr* (Siachen tributary)	35°30′N. 77°05′E.	28							X		RBV30531–04484–D; 18 Aug 79
161	*Gyong* (upper Saltoro valley)	35°07′N. 77°00′E.	12						X			RBV30531–04484–D; 18 Aug 79
162	Chūmik-Bilafond (upper Saltoro valley)	35°15′N. 76°52′E.	21							X	X	RBV30531–04484–D; 18 Aug 79
163	*Sherpi Kang* (*Kondus,* Saltoro valley)	35°22′N. 76°47′E.	19				X	X	X			RBV30531–04484–D; 18 Aug 79
164	Kaberi (*Kondus,* Saltoro valley)	35°30′N. 76°38′E.	23				X		X	X		RBV30531–04484–C; 18 Aug 79
165	*Kondus* (*Kondus,* Saltoro valley)	35°30′N. 76°41′E.	25				X		X	X	X	RBV30531–04484–C; 18 Aug 79
166	*Chogolisa* (Hushe valley)	35°30′N. 76°30′E.	21				X		X			RBV30531–04484–C; 18 Aug 79
167	*Chundugaro* (Hushe valley)	35°32′N. 76°24′E.	13							X	X	RBV30531–04484–C; 18 Aug 79 Stereo30532–04542–D; 19 Aug 79
168	Masherbrum (Hushe valley)	35°34′N. 76°19′E.	12							X		RBV30531–04484–C; 18 Aug 79 Stereo30532–04542–D; 19 Aug 79
169	*Aling* (Hushe valley)	35°29′N. 76°15′E.	12				X	X		X		RBV30531–04484–C; 18 Aug 79 Stereo30532–04542–D; 19 Aug 79

[1] Landsat 3 return beam vidicon (RBV) subscenes; see footnote 2 in table 1.
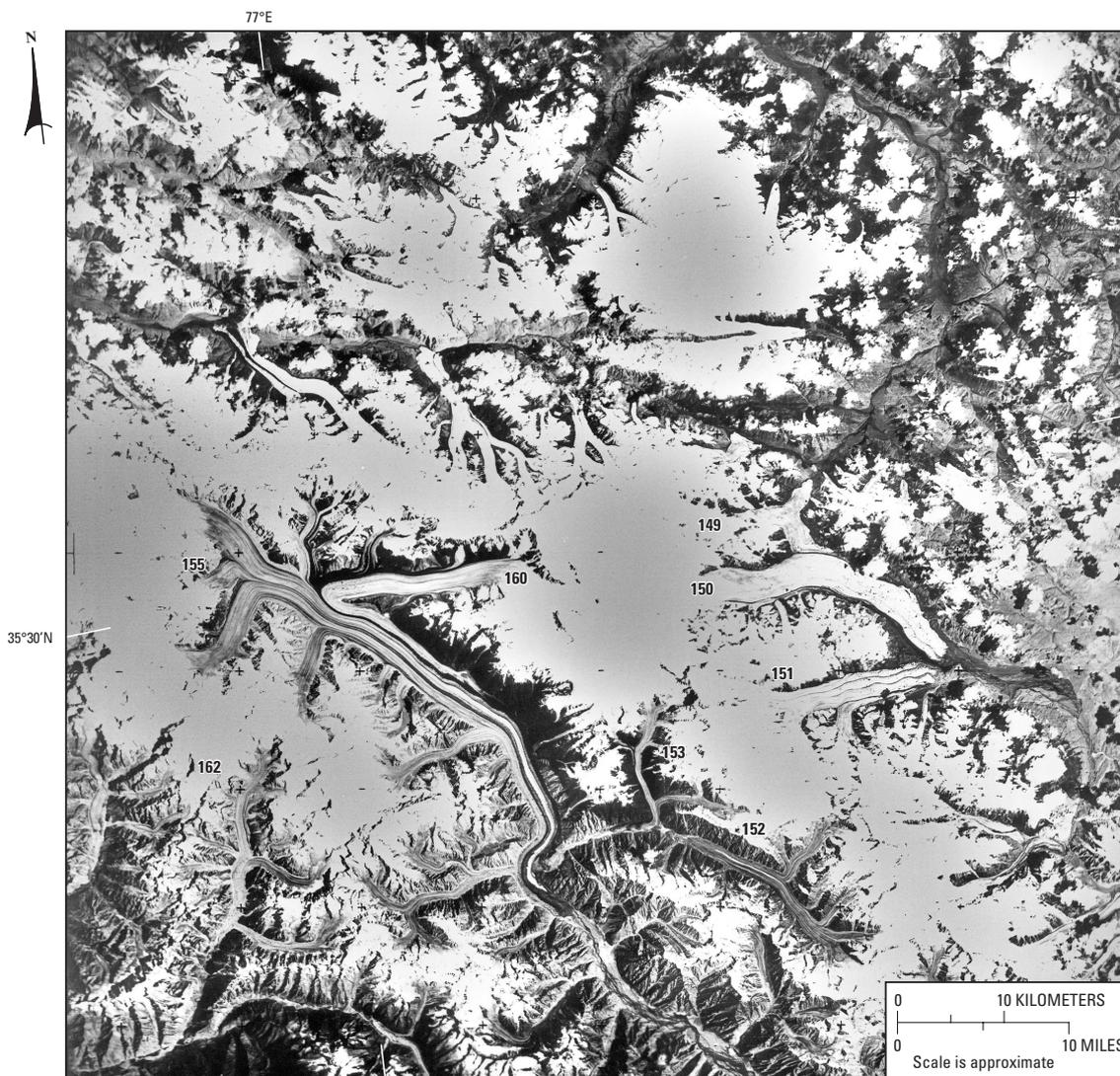
Figure 21.—*Landsat 3 RBV image of Siachen [155],* Teram Shehr [160], north [149], central [150], and south Rimo [151], North Terong-Selkar Chorten *[153],* South Terong *[152], and Bilafond [162] Glaciers. Especially prominent are the abrupt bend of the* Teram Shehr Glacier *to join the Siachen Glacier, and the seeming failure of the diffluent north Rimo Glacier to join the clean white ice of the central Rimo Glacier. Also obvious are plentiful supraglacier meltwater lakes on central Rimo Glacier and slightly sinuous medial moraines on south Rimo Glacier. The Landsat 3 RBV image no. 30531–04484, subscene D; 18 August 1979; Path 159–Row 35, is from the U.S. Geological Survey, EROS Data Center, Sioux Falls, South Dakota 57198, but is now only archived by the authors.*

Movement Criteria 3: Tributary Ice Overriding or Displacing Main Glacier Ice

Tributary ice overrode or displaced the main glacier ice in seven obvious examples, notably on Hispar [72] (figs. 13, 22), *Panmah* [124] (fig. 20), and Baltoro [128] (fig. 20) Glaciers. Odell (1937), and Visser and Visser-Hooft (1938; as reported by Washburn, 1939), noted that one glacier overriding another might be caused by differences in elevation of their floors and by their differences in volume, density, degree of compactness, texture, temperature, meltwater, and rate of flow. Because the Hispar Glacier has both convoluted and overridden or displaced moraine, and because of reasonable accessibility, it was selected for field verification, and was visited in 1984.

A

B

65

HV

66

73

72

71

N 0   5 KILOMETERS

0   5 MILES

Scale is approximate
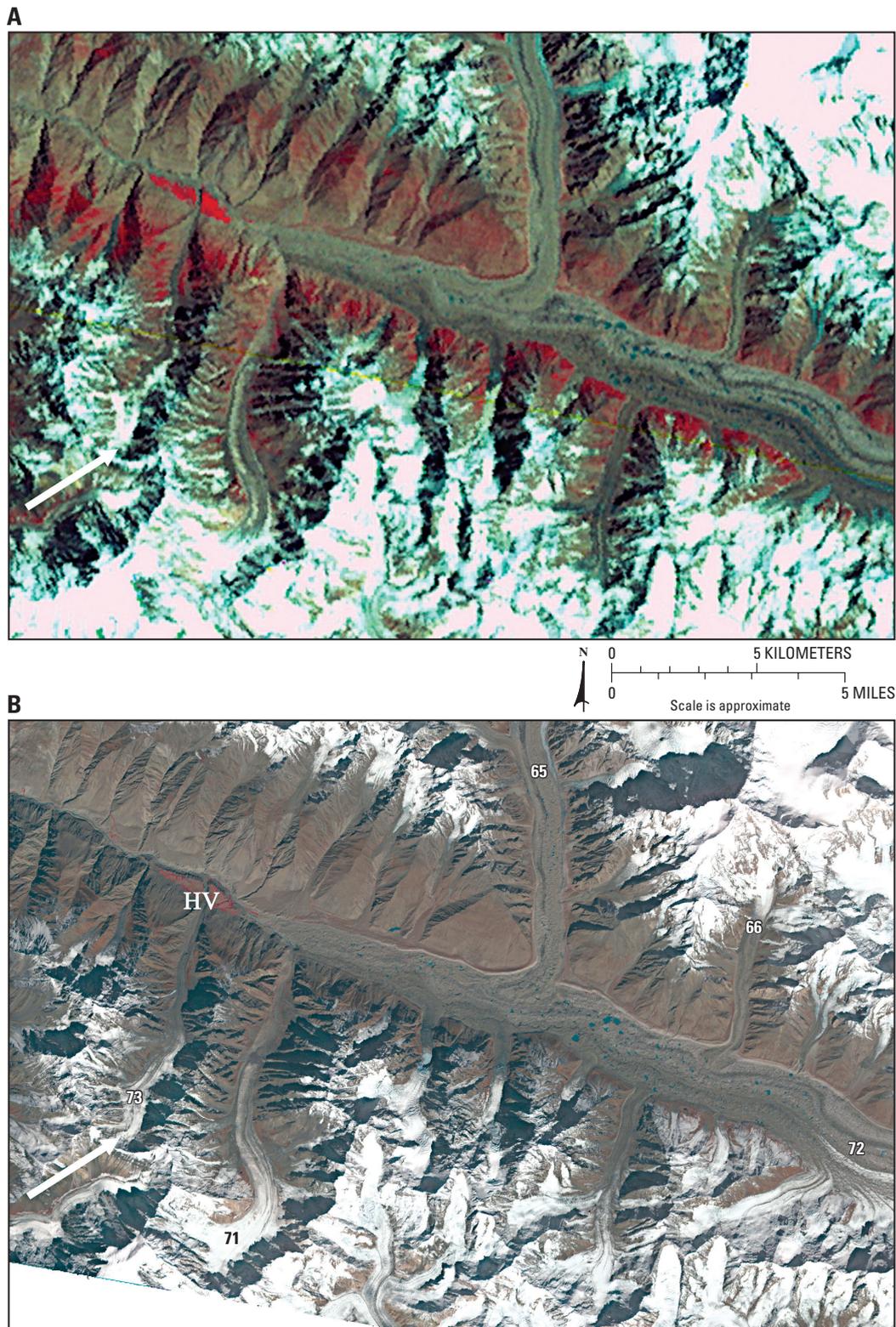
Figure 22.—**A**, *Landsat 3 MSS false-color composite image taken on 15 July 1979, and* **B**, *ASTER image taken on 30 September 2001, showing the terminus of Hispar Glacier [72] (approximate lat 36°05'N., long 75°15'E.) above which are various flow discontinuities expressed as overridden or displaced ice from tributary glaciers, such as* Lak-Khiang [65] *and Pumārikish [66] Glaciers. HV is Hispar Village. The white arrows indicate Yengutz Har Glacier [73] that advanced rapidly between 1892 and 1901. Historic debris flows from this glacier created the large fan where Hispar Village is located. Landsat 3 MSS image no. 3161035007919690, bands 4, 5, 7; 15 July 1979; Path 161– Row 35, and ASTER image no. AST_L1B-003_09302001055833_04172002120543 are from the U.S. Geological Survey, EROS Data Center, Sioux Falls, South Dakota 57198.*

The east-to-west flowing Hispar Glacier was described by Workman and Workman (1911) as being forced against its south wall by its four large tributaries, (*Lak-Khiang* [65], Pumārikish [66], *Jutmaru* [67], and *Khanbasa* [68] Glaciers and several smaller tributaries that flow in from the north (fig. 13). The terminus of the Hispar Glacier has reportedly changed little in more than 70 years of record during the early to middle 20th century (Mercer, 1963); general downwasting of just a few tens of meters and backwasting of less than a kilometer has been observed since the photographs of Hayden (1907) in 1906 and Workman and Workman (1911) in 1908 (fig. 23). The *Lak-Khiang Glacier*, furthest downstream of the tributaries entering from the north, still enters the Hispar valley with a "huge west lateral moraine sweeping around in a splendid curve" (Workman and Workman, 1911, p. 51 and photo), and we observed that the tributary glacier has displaced the entire lower Hispar Glacier to its terminus, 8 km below. The lighter colored Lak moraine is dominantly granite and marble, whereas the darker, narrower, and more compressed moraine on the southern margin is composed of weathered, iron-stained schist and gneiss. Up ice from the *Lak Glacier* tributary is an area about 10 km long, that has extensive kettles and convoluted moraines from the *Jutmaru (Jutmau) Glacier* [67] tributary on the north side. Some of these convolutions seem to be also influenced by other smaller side glaciers — Pumārikish [*Pumari Chhish*] Glacier [66] and *Khatumburumbun Glacier*.

Figure 23.—*Terminus of the Hispar Glacier* [72] *in late July 1984. The dark ice cliff above the river has a strong signature on the satellite imagery (figs. 13, 22). The small dark ice cliff directly right (south) of the river is a former ice portal of the Hispar river, now cut off by retreat of the new portal to its present position further back into the glacier terminus. A collapse zone above the subglacial Hispar river is barely visible to the right (south) side of the terminus. Photograph by J.F. Shroder, Jr.*

Searle (1991) and Wake and Searle (1993) noted that the Pumārikish Glacier [66] (figs. 13, 22) is the smallest of the four major tributaries on the north side of the Hispar Glacier, and has produced the most impressive surge in the Karakoram in recent years. In 1988, the surface of the glacier had risen somewhat, but in 1989, the glacier had surged about 1.5 km out and over the Hispar Glacier. The ice had grown dramatically higher, by more than 50 m, with ice towers and seracs looming 20 m or more above the lateral moraines. Searle (1991) was at a loss to explain the surge, beyond speculation of an overall rock uplift of the source region, and did not recognize the far more likely possibility of increased meltwater.

Workman and Workman (1911) reported that about 25 km above the Hispar terminus, white ice occurred near the merger of the small *Haigatum Glacier* [69], a tributary on the south side. Shipton's map of 1939 also shows this (the preparation and planning for the map is described in Shipton, 1938), but the satellite imagery of 1979 shows only a thin strip of light debris. Instead, white ice is prominent 15 km further up the glacier. Additional evidence for downwasting is the position of the Hispar Glacier, several tens of meters below and now partly cut off from the Pumārikish Glacier and *Khatumburumbun Glacier* tributaries.

Finally, the *Garumbar Glacier's* [71] snout, on the south side of the Hispar valley near the terminus, was about 2.5 km from the Hispar when Workman and Workman (1911) were there in 1908. Mason (1930) reported that it had joined the Hispar Glacier by 1925, but in 1984 it was about 4 km away. Its meltwater river passed beneath the Hispar Glacier and joined the main subglacier river in a zone of general roof collapse that is 100–200 m deep between the *Garumbar Glacier* and the main terminus. The Hispar river abandoned one ice portal on the south side several years ago and moved up ice about 100 m toward the Garumbar valley, close to its present position (fig. 23). The ice portal of the Hispar river was a black cliff of dirty ice that is prominent on the imagery (figs. 13, 22).

In order to make field observations of a small glacier with a known history of rapid flow, we visited the Yengutz Har Glacier [73] (figs. 13, 22) in Hispar valley. In 1892, Conway (1894) noted that the glacier was about 3.5 km from the Hispar river, but by 1901 it had advanced to a position only about 900 m from the river, where it buried several water mills. It was adjacent to Hispar village through at least 1906–1908, when Hayden (1907) and Workman and Workman (1910, 1911) were there. In 1984, it had retreated to close to its position in 1892 (fig. 24). Neither evidence from the original surge, nor signs of the subsequent melting and retreat, are apparent on the satellite imagery (figs. 13, 22).

On the Baltoro Glacier [128] (figs. 20, 25), the debris-covered and kettle-pocked *Trango Glacier* [130] tributary has overridden and displaced the main glacier, and was overridden and displaced in turn by the *Uli Biaho Glacier* [129]. Similarly, the lowermost of the southern tributaries to the *Aling Glacier* [169], at the northwest head of Hushe valley below Masherbrum, has over-ridden the downwasting or stagnant debris-covered ice of the main glacier. This tributary glacier has lobate moraines and a depressed ice surface.

Several glaciers have tributaries with convoluted moraines that terminate against another ice stream. For example, the *Kondus Glacier* [165] is tributary to the Kaberi Glacier [164], which has an extensive area of debris-covered ice over its lower third (fig. 20). The *Kondus Glacier* apparently has piled up against the Kaberi Glacier, causing the moraine of the *Kondus Glacier* to back up in a sinuous pattern. Similarly, the *Panmah Glacier* [124] has convoluted moraines pushed up against the *Choktoi Glacier*, which itself is somewhat convoluted and has a terminus of extensive debris-covered ice (fig. 20). A case might be made that both the *Panmah* and *Kondus Glaciers* surged forward to produce

Figure 24.—*The valley of Yengutz Har Glacier [73] above Hispar village; view from right lateral moraine with glacier terminus out of picture to left. This valley was filled with ice down to the fields in the valley bottom below, after a surge in about 1901. July 1984 photograph by J.F. Shroder, Jr.*
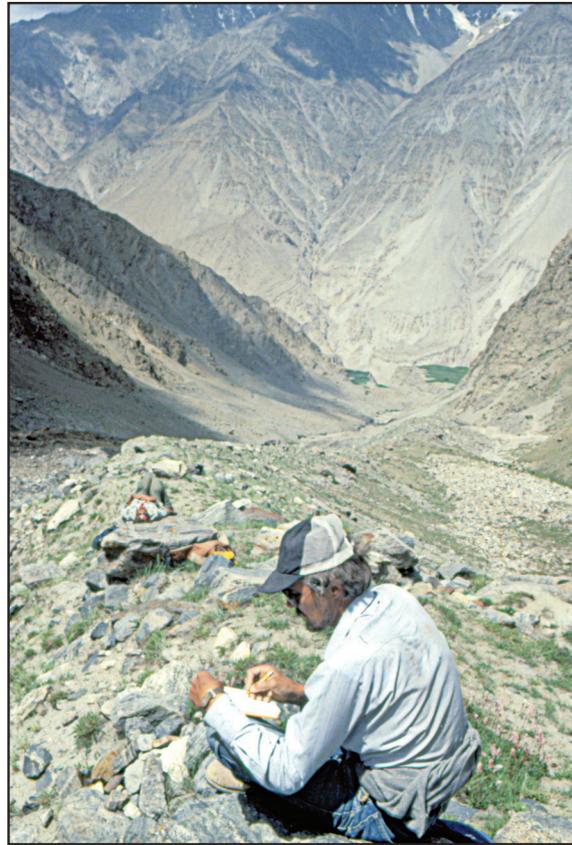
convoluted moraines, overriding or displacing the other glaciers. Subsequent stagnation of the *Panmah* or *Kondus Glaciers* would then allow the Kaberi Glacier or *Choktoi Glacier* to reassert flow dominance and cut off the lower convoluted part of the other glaciers. Close scrutiny of the confluence areas does not show an abrupt truncation of the *Kondus Glacier*, nor is there evidence of interference with the *Choktoi Glacier* by the *Panmah Glacier*. In another case, the clean ice stream of the north Rimo Glacier [149] (fig. 21) was diffluent; the south ice lobe flowed directly up against the clean ice of the central Rimo Glacier [150]. At the confluence, the ice foliation of the north Rimo Glacier lobe was extensively convoluted and did not penetrate through the lateral moraine of the central Rimo Glacier (fig. 21). This moraine between the central and north Rimo Glaciers dominated these glaciers in about 1914, but was "smothered in ice" in 1930 (Dainelli, 1932, p. 398; Mercer, 1963, p. 21). Thus, it appears that tributary glaciers, in some cases, may override or displace the main glacier, and then be overridden, displaced, or completely incorporated themselves. In other cases, the tributary glaciers may run up against another glacier and the forward motion of the tributary glacier is slowed. Reasons for these differences are not clear, but may be controlled in part by spatially and temporally different velocity gradients.
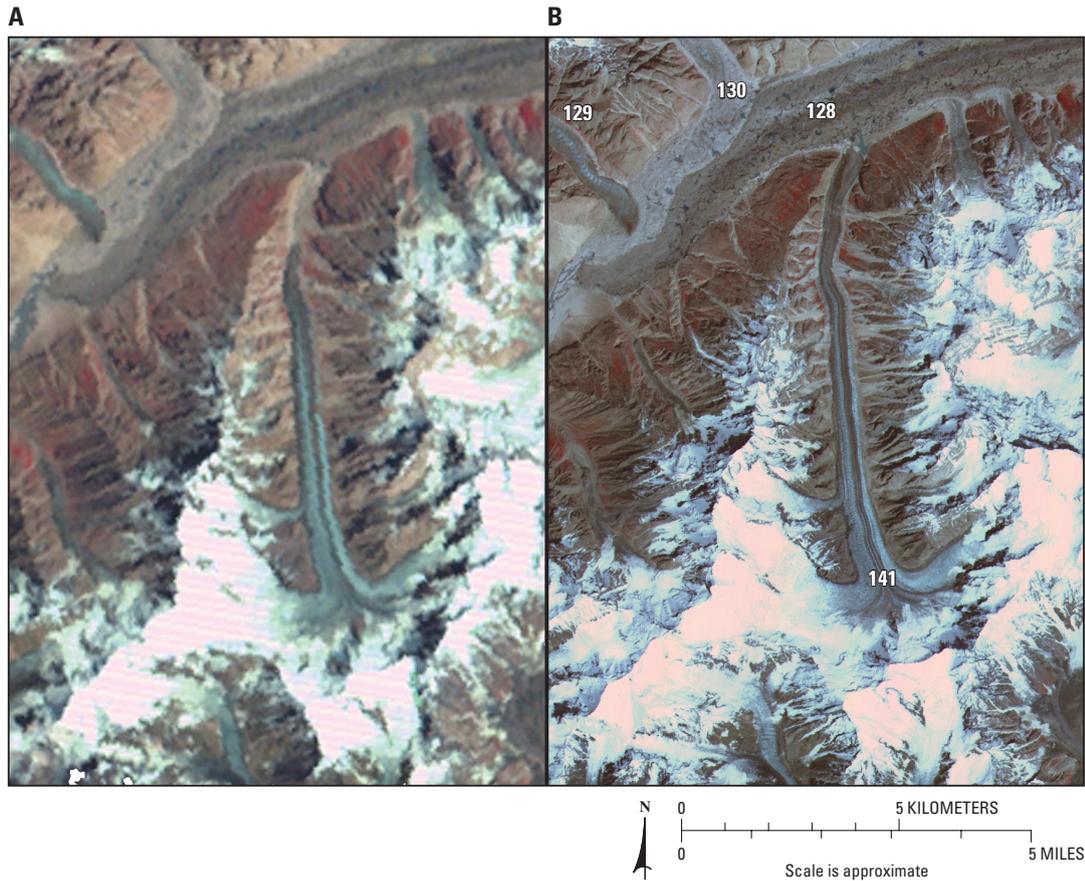
Figure 25.—**A**, *Landsat 3 MSS image taken on 18 July 1978, and* **B**, *ASTER image taken on 14 August 2004, showing terminus of Baltoro Glacier [128] in upper left and* Liligo Glacier [141] *(lat 35°40'N., long 76°13'E.) in center middle. The light-colored, granitic-debris covered* Trango Glacier [130] *overrides and displaces much of the northwestern portion of the Baltoro terminus, and is itself overridden by the dark-colored metasediment debris cover of the* Uli Biaho Glacier [129]. *The* Liligo Glacier *shows a rapid advance or surge in the interim between the two scenes. At present the terminus of* Liligo Glacier *exists in close proximity to the Baltoro terminus, with a small proglacial lake between the two. Landsat 3 MSS image no. 3159036007819990, bands 4, 5, 7; 18 July 1978; Path 159–Row 36, and ASTER image no. AST_L1A_003_08142004054614_08282004141219, 14 August 2004, are from the U.S. Geological Survey, EROS Data Center, Sioux Falls, South Dakota 57198.*

Movement Criteria 4: Marked Depression of Ice Surface Below Lateral Moraines or Tributary Glaciers

This criterion indicates past changes in mass balance or possible surges. Only 14 glaciers were observed with what appeared on the RBV stereo imagery to be unusually depressed or down-wasted surfaces below prominent lateral moraines or tributary glaciers. Based on extensive field observations and subsequent imagery, we now know that if more such RBV stereo imagery had been available, then the number would have been much larger.

Movement Criteria 5: Lateral and Medial Moraines That Are Slightly Sinuous, Lobate, or Offset by Crevasses or Ogives

More than 76 glaciers have slightly sinuous or lobate moraines that primarily reflect nonlinear flow regimes or shear and variable melting near crevasses and ogives. In one prominent example, the *Teram Shehr Glacier* [160] (fig. 21) turns 140° from its due west flow to flow southeast as it joins the Siachen Glacier [155]. The sharp bend is marked by numerous crevasses and large melt ponds on the tensional outside margin of the bend (fig. 21).

Movement Criteria 6: Recent Major Melting or Retreat of Icefront, Leaving Light-Colored Scars

Several glaciers showed recent major melting or retreat of the ice front, and nine of them left light-colored deglacierized areas behind. The *Liligo Glacier* [141], on the south side of Baltoro Glacier [128] near its terminus, has been observed for more than a century by a succession of climbing expeditions to the peak of K2 (Pecci and Smiraglia, 2000). The *Liligo Glacier* was about 0.5 km from the Baltoro Glacier in 1909 (De Filippi, 1912, p. 186–187), 0.75 km away in 1953 (Desio and others, 1961), and 1.75 km away in the 1970s, with a prominent light-colored deglacierized zone between the two. Then in the late 1990s the *Liligo Glacier* advanced partly over the Baltoro, and in 2004 it was still in close proximity to the Baltoro terminus (figs. 20 and 25); in late summer, there was a large lake between the two that drained away into a crevasse. Pecci and Smiraglia (2000) suspected a surge of the *Liligo Glacier*, but noted that the absence of seemingly surge-definitive convoluted medial moraines precluded them from making a definite determination.

In another important example, prior to about 1974 the terminus of the *Balt Bare Glacier* [54] in the upper Hunza Valley had been at about 3,800 m altitude at the base of the main ice fall. In the spring of that year, an extensive mud-rock (rapid, wet debris) flow burst out from the glacier, reaching a maximum discharge of approximately 63 m^3 sec^{-1} and pouring out more than 5×10^6 m^3 of material into the river valley (fig. 26). The flood destroyed part of the KKH, a 120-m long bridge, as well as numerous dwellings and fields, and killed one pedestrian (fig. 27). For a while, the Hunza River was backed up into a lake, behind the debris dam. Then, primarily in 1976, the glacier surged forward more than 2 km (Wang and others, 1984). Interestingly, the 1–3 km-sized fan upon which the nearby *Shash Kat* (*Shishket*) village rests is one of the most well-developed fans in the area; it occurs at the base of a small drainage basin, suggesting that other similar depositional events may have occurred there in the past.
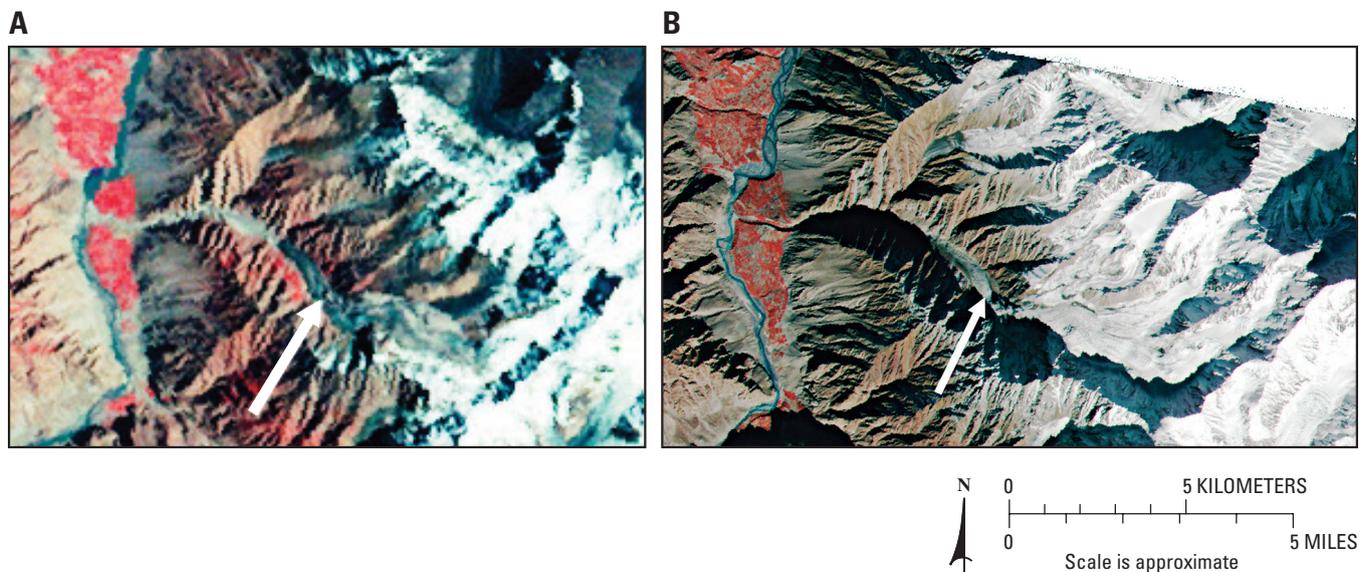
A

B

Figure 26.—Landsat 2 MSS false-color composite and ASTER satellite images of the Balt Bare Glacier *[54] (approximate lat 36°20'N., long 74°56'E.) and its breakout flood of 1974 as it appeared in 1977, and the appearance of the same features in 2003.* **A***. Landsat 2 MSS false-color image obtained on 2 August 1977 immediately after the surge. The arrow indicates the original pre-surge terminus at the base of the ice fall, below which occurs the dark, debris-covered surge mass of glacial ice, the scar of the flood across the fan, as well as the impoundment of the Hunza River.* **B***. The ASTER image of 2003 shows that the* Balt Bare Glacier *has maintained its surge length, the flood scar has been revegetated, and the river has aggraded its channel. Landsat 2 MSS image no. 2160035007721490, bands 4, 5, 7; 2 August 1977; Path 160–Row 35, and ASTER image no. AST_LIA_00310292003055903_11122003124818, 29 October 2003, are from the U.S. Geological Survey, EROS Data Center, Sioux Falls, South Dakota 57198.*

Figure 27.—Photograph of the Balt Bare *fan in July 1992 near the village of* Shash Kat *taken from the Karakoram Highway (KKH) on the west side of the Hunza River valley. The flood of 1974 destroyed the original KKH, part of which can be seen preserved on the river bank on the right side of the photograph. The large size of the fan at the mouth of the small* Balt Bare *valley may indicate past surge-sedimentation events as well. Photograph by J.F. Shroder, Jr*

In addition, the previously mentioned Yengutz Har Glacier [73], which advanced rapidly in the early 1900s and subsequently melted back about 3.5 km, presently appears on the MSS and ASTER imagery only as an insignificant small dark mass with an equally obscure retreat zone (fig. 22). However, it appears to be the source of the large fan on which Hispar village was constructed, in the otherwise rather inhospitable Hispar Valley. Perhaps repeated surges or related outburst floods from such small valleys produce sufficiently large debris fans to enable agriculture in otherwise difficult mountain environments.

Movement Criteria 7: Extensive Area of Debris-Covered Downwasting or Stagnant Ice

Debris-covered termini are exceptionally common in this area and reflect the plentiful mass-wasting and snow-avalanche origin of much of the debris. In some cases, the termini are covered with a chaotic mass of debris simply because so much is in transport; in other cases, the debris is the result of a period of rapid movement followed by slowing or stagnation. It is generally impossible to differentiate between types of debris masses unless collateral information is available. Also, using only imagery, it is impossible to determine if the debris covers clean ice or debris-laden ice. The Hispar [72] and

Yengutz Har [73] Glaciers, for example, have extensive dark-debris cover with debris-laden ice beneath (figs. 13, 22). The K2 North Glacier [142] also is depicted on the imagery as having a dark debris-covered terminus (fig. 20), but on Chinese photographs (Chi and Ren, 1980) the terminus appears as clean white ice overlain by a thin debris cover.

Movement Criteria 8: Linear Moraines and Accordant Tributaries

Finally, large numbers of glaciers in northern Pakistan have linear lateral and medial moraines and accordant tributaries that show dominantly linear flow. Many of these were not designated as exhibiting these characteristics in table 3, because other features seemed more important.

Mountain Geomorphology

Globally significant interactions between climate, surface processes, and tectonics have recently been proposed to explain mountain building and climate change (Raymo and others, 1988; Molnar and England, 1990; Koons 1995; Avouac and Burov, 1996). Much research has focused on climatic versus tectonic forcing (Raymo and others, 1988; Molnar and England, 1990) and the dominant surface processes responsible for relief production and topographic evolution (Montgomery, 1994; Burbank and others, 1996; Brozovik and others, 1997; Whipple and Tucker, 1999).

Research indicates that climate-driven surface processes are capable of reducing lithospheric mass, thereby inducing isostatic uplift or accelerating tectonic uplift, collectively resulting in relief production and complex topography (Gilchrist and others, 1994; Montgomery, 1994; Shroder and Bishop, 2000). The linkages between global climate and topography, however, are controversial, and the operational scale-dependencies of surface processes that govern the geomorphometry of topography and geodynamics are not well understood (Shroder and Bishop, 1998; Bishop and others, 1998a, b; 2002; Bishop and Shroder, 2000).

Multidisciplinary research has provided strong evidence of climate-induced geomorphic change in high-mountain environments (Brozovik and others, 1997; Bishop and others, 1998b; Bush, 2002; Phillips and others, 2000), although there is considerable controversy regarding the role of glaciation (Harbor and Warburton, 1992; Whipple and Tucker, 1999; Whipple and others, 1999). Complex feedback mechanisms within and between climatic, glacial, and lithospheric systems are suspected, although it is difficult to study these interactions because of the need to account for the scale-dependencies of numerous processes and polygenetic topographic evolution in modeling efforts (Koons, 1995; Bishop and others, 2002).

The influence of glaciation on the unloading history of mountain massifs, however, is still relatively unknown. We know that many major valleys in Pakistan, including the Indus, have undergone extensive and periodic glaciation (Shroder and others, 1989). Similarly, glacier-related, catastrophic geomorphic events are also responsible for the denudational unloading. Therefore, because of climate fluctuations and geomorphic temporal overprinting, modern-day river or glacier incision rates alone cannot be applied over millions of years to characterize denudational unloading.

The influence of glacial erosion on the relief structure of the mountains in Pakistan is an important issue. Bishop and others (2002, 2003) concur with Brozovik and others (1997) that, for intermediate altitudes, glaciation can limit relief up to some altitude approaching the equilibrium-line altitude (ELA).

Bishop and others (2003) also suggested that glaciation can produce greater mesoscale relief than river incision because glaciation, in concert with uplift, may be primarily responsible for relief production at high altitudes. Remote sensing of glaciers is expected to provide new insights into the role of glaciation in denudation and relief production, as spatial information on glacierization and estimates of glaciological parameters are needed for erosional and landscape-evolution modeling.

Glacier mapping supports glacial reconstructions and the assessment of glacial geomorphic features. Such studies in Pakistan have revealed the presence of high-altitude glacier erosion surfaces throughout the Hindu Kush, Karakoram, and Nanga Parbat Himalaya. Cosmogenic exposure-age dating of these surfaces and moraines in various locations have revealed glacier advances that likely represent monsoon-enhanced glaciation caused by orbital forcing (Phillips and others, 2000; Owen and others, 2002). Paleoclimatic conditions were significantly different from the climatic conditions of today, which strongly suggests that the landscape is not in topographic equilibrium (for example, it has unequal erosion and uplift rates). This explains the highly differential denudation rates reported by Shroder and Bishop (2000).

The issue of glacier erosion and relief production is at the heart of the climate-forcing hypothesis. It is notoriously difficult to estimate the magnitude of glacial erosion, because observations and measurements cannot be adequately obtained, and glacial processes such as plucking cannot be easily measured. This makes it difficult to account for various processes in models and constrain simulations using observational data. Nevertheless, remote sensing studies facilitate modeling efforts that provide new insights into the role of glaciation in landscape evolution. Preliminary one-dimensional, glacier-erosion simulations, with input parameter estimates obtained from ASTER imagery and digital elevation models (DEMs), depict nonlinear variation in glacial incision rates caused by valley evolution. These simulations also indicate that the spatially averaged rate of incision for a glacier with 300 m of ice thickness is likely to exceed 5 mm a^{-1}. These findings support empirical work indicating that glaciers in Pakistan can produce significant relief over time (Bishop and others, 2003). Collectively, results from remote sensing and geomorphological research suggest that glaciers may play a more significant role in landscape evolution than previously thought.

Another new insight into the role of glaciers in landscape evolution has come from assessing glacier ice velocity fields over mountain ranges. Kääb (2005) addressed the issue of satellite-derived DEM generation and derivation of ice velocity estimates in the Bhutan Himalaya. His results demonstrate the significant spatial variability in glacier flow, such that the glacier velocities in the terminus zones on the south side of the mountain range exhibit significantly lower velocities (10–20 m a^{-1}) than on the north side (20–200 m a^{-1}). We suspect similar, if not more spatial variation in ice flow characteristics in Pakistan. This has implications for glacier erosion, as it is generally assumed that glacial abrasion scales with basal sliding velocity (MacGregor and others, 2000; Tomkin and Braun, 2002). Although relief production via glacial erosion involves numerous factors and processes such as glacial plucking, glacial meltwater production and subglacial fluvial erosion, and cold-based ice at higher altitudes with no basal slip or erosion, we might expect higher glacier denudation rates in those areas in Pakistan that have fast-moving glaciers (other controlling factors being constant). We lack, however, adequate knowledge about numerous climate and lithospheric feedback mechanisms that influence glacier erosion, although glacier erosion and landscape evolution studies reveal that glacier processes are governed by a variety of internal and external factors. The spatial variability in flow velocities suggests the potential for significant variations in glacier erosion with altitude and geographic location,

as well as with time during glacial/interglacial cycles. This may place limits on the magnitude of glacial erosion and relief production as a function of local topographic conditions, cold-based ice (at higher altitudes), and radiative and atmospheric forcing (Bishop and others 2001, 2003).

To understand the role of glaciers in mountain geodynamics, topographic information, glacier boundaries, ice-velocity fields, and land-cover information must be incorporated into glacier flow and mass balance models which consider various glacial dynamics (for example, MacGregor and others, 2000). In this way, the spatial variability of glacier geometry and ice flow are taken into account, and paleo-simulations can be constrained by glacier surface topography and variations in width and surface velocity. Similarly, supraglacial conditions can be assessed from satellite imagery (Bishop and others, 1995, Bishop and others, 2004). Using these tools, earth scientists can better investigate the complex interdependencies associated with climatic, tectonic, and surface processes that are responsible for polygenetic topographic evolution.

Conclusions

Glaciers of the Hindu Kush, Nanga Parbat, and the Karakoram Himalaya of Pakistan have diverse characteristics resulting from complex topography, spatial and temporal differences in snow and rock-debris supply, differences of flow, and variability of ablation. Remote-sensing assessments using older Landsat MSS, RBV, and newer ASTER imagery provide a new means of characterizing various aspects of glaciers and detecting perimeter changes.

In general, glaciers on the south sides of the ranges or in the deeper valleys tend to be more debris covered than those in higher locations or further into the interior. This may be because there is greater exposure to monsoon-generated deep snows and erosive avalanches on the south sides, greater debris generation from slopes in deep valleys of exceptional relief, and greater ablation in the lower altitude valleys tributary to the Indus River. Flow behavior and flow history appear to have no regional control, but instead vary throughout the ranges. From a regional perspective, many glaciers of northern Pakistan are in a general state of down wasting and back wasting. Rapid advances or surges are reasonably common and may relate to meltwater increases. Although initially catastrophic and devastating, surge events in several places have been accompanied by strong water-deposited sediment that adds to potentially arable land for later use by mountain villagers.

More sophisticated analysis and modeling of glaciers utilizing ASTER imagery and DEMs, such as those in the ongoing GLIMS research effort, promise to greatly improve our understanding of glacial fluctuation in the western Himalaya and Hindu Kush. These studies will result in the first quantitative assessments of regional mass balance and elucidation of the role of glaciation in relief production and landscape evolution in Pakistan.

References Cited

Aizen, V.B., Aizen, E.M., Dozier, J., Melack, J.M., Sexton, D.D., and Nesterov, V.N., 1997, Glacial regime of the highest Tien Shan Mountains, Pobeda-Khan Tengry Massif: Journal of Glaciology, v. 33, no. 145, p. 503–512.

Aniya, M., Sato, H., Naruse, R., Skvarca, P., and Casassa, G.,1996, The use of satellite and airborne imagery to inventory outlet glaciers of the Southern Patagonia Icefield, South America: Photogrammetric Engineering and Remote Sensing, v. 62, no. 12, p. 1361–1369.

Auden, J.B., 1935, The snout of the Biafo Glacier in Baltistan: Geological Survey of India, Records, v. 68, pt. 4, p. 400–413.

Avouac, J.P., and Burov, E.B., 1996, Erosion as a driving mechanism of intracontinental mountain growth: Journal of Geophysical Research, v.101, p. 747–769.

Bateson, S., and Bateson, R., translators, 1952, Tirich Mir — The Norwegian Himalayan Expedition: London, Hodder and Stoughton, 192 p.

Batūra Glacier Investigation Group (BGIG), 1979, The Batūra Glacier in the Karakoram Mountains and its variations: Scientia Sinica, v. 22, no. 8, p. 958–974.

Batūra Glacier Investigation Group (BGIG), 1980, Professional papers on the Batūra Glacier, Karakoram Mountains: Beijing, Science Press, 271 p. (In Chinese with English abstracts)

Beniston, M., 1994, Mountain environments in changing climates: Routledge, London, 496 p.

Berthier, E., Arnaud, Y., Kumar, R., Ahmad, S., Wagnon, P., and Chevallier, P., 2007, Remote sensing estimates of glacier mass balance in the Himachal Pradesh (western Himalaya, India): Remote Sensing of Environment, v. 108, issue. 3, p. 327–338. doi:10.1016/j.rse.2006.11.017

Bhutiyana, M.R., 1999, Mass-balance studies on Siachen Glacier in the Nubra Valley, Karakoram Himalaya, India: Journal of Glaciology, v. 45, no. 149, p. 112–118.

Bishop, M.P., Barry, R.G., Bush, A.B.G., Copland, L., and others, 2004, Global land-ice measurements from space (GLIMS) — Remote sensing and GIS investigations of the Earth's cryosphere: Geocarto International, v. 19, no. 2, p. 57–84.

Bishop, M.P., Bonk, R., Kamp, U., Jr., and Shroder, J.F., Jr., 2001, Terrain analysis and data modeling for alpine glacier mapping: Polar Geography, v. 24, no. 4, p. 257–276.

Bishop, M.P., Kargel, J.S., Kieffer, H.H., MacKinnon, D.J., Raup, B.H., and Shroder, J.F., Jr., 2000, Remote-sensing science and technology for studying glacier processes in high Asia: Annals of Glaciology, v. 31, p. 164–170.

Bishop, M.P., and Shroder, J.F., Jr., 2000, Remote sensing and geomorphometric analysis for assessing topographic complexity and erosion dynamics in the Nanga Parbat Himalaya, in Khan, M.A., Treloar, P.J., Searle, M.P., and J.M. Qasim, eds., Tectonics of the Nanga Parbat Syntaxis and Western Himalaya: Geological Society of London Special Publication 170, p. 181–200.

Bishop, M.P., and Shroder, J.F., Jr., eds., 2004, Geographic Information Science and Mountain Geomorphology: Springer-Praxis, Chichester, U.K., 486 p.

Bishop, M.P., Shroder, J.F., Jr., Bonk, R., and Olsenholler, J., 2002, Geomorphic change in high mountains: A western Himalayan perspective: Global and Planetary Change, v. 32, p. 311–329.

Bishop, M.P., Shroder, J.F., Jr., and Colby, J.D., 2003, Remote sensing and geomorphometry for studying relief production in high mountains: Geomorphology, v. 55, p. 345–361.

Bishop, M.P., Shroder, J.F., Jr., and Hickman, B.L., 1999, SPOT panchromatic imagery and neural networks for information extraction in a complex mountain environment: Geocarto International, v. 14, p. 17–26.

Bishop, M.P., Shroder, J.F., Jr., Hickman, B.L., and Copland, L., 1998a, Scale-dependent analysis of satellite imagery for characterization of glacier surfaces in the Karakoram Himalaya, in Walsh, S., and Butler, D., eds., Special volume on Remote Sensing in Geomorphology: Geomorphology, v. 21, p. 217–232.

Bishop, M.P., Shroder, J.F., Jr., Sloan, V.F., Copland, L., and Colby, J.D., 1998b, Remote sensing and GIS science and technology for studying lithospheric processes in a mountain environment: Geocarto International, v. 13, p. 75–87.

Bishop, M.P., Shroder, J.F., Jr., and Ward, J.L., 1995, SPOT multispectral analysis for producing supraglacial debris-load estimates for Batūra Glacier, Pakistan: Geocarto International, v. 10, no. 4, p. 81–90.

Brozovik, N., Burbank, D.W., and Meigs, A.J., 1997, Climatic limits on landscape development in the northwestern Himalaya: Science, v. 276, no. 5312, p. 571–574.

Burbank, D., Leland, J., Fielding, E., Anderson, R.S., Brozovik, N., Reid, M.R., and Duncan, C., 1996, Bedrock incision, rock uplift and threshold hillslopes in the northwestern Himalaya: Nature, v. 379, no. 6565, p. 505–510.

Bush, A.B.G, 2000, A positive feedback mechanism for Himalayan glaciation: Quaternary International, v. 65–6, p. 3–13.

Bush, A.B.G., 2002, A comparison of simulated monsoon circulations and snow accumulation in Asia during the mid-Holocene and at the Last Glacial Maximum: Global and Planetary Change, v. 32, p. 331–347.

Cao, M.S., 1998, Detection of abrupt changes in glacier mass balance in the Tien Shan mountains: Journal of Glaciology, v. 44, no. 147, p. 352–358.

Chi Jian-mei and Ren Bing-hui, eds., 1980, Glaciers in China: Shanghai Scientific and Technical Publishers, unpaginated.

Cogley, J.G., and Adams, W.P., 1998, Mass balance of glaciers other than the ice sheets: Journal of Glaciology, v. 44, no. 147, p. 315–325.

Conway, W.M., 1894, Climbing and exploration in the Karakoram-Himalayas: New York, Appleton & Co., 709 p.

Dainelli, Giotto, 1932, Italia Pass in the eastern Karakoram: Geographical Review, v. 22, no. 3, p. 392–402.

DeFilippi, Filippo, 1912, Karakoram and western Himalaya, 1909: London, Constable and Co., 469 p.

Derbyshire, E., Li Jijun, Perrot, F.A., Xu Shuying, and Waters, R.S., 1984, Quaternary glacial history of the Hunza Valley, Karakoram mountains, Pakistan, in Miller, K.J., ed., The International Karakoram Project, v. 2, p. 456–495.

Desinov, L.V., Ivanchenkov, A.S., Kotlyakov, V.M., and Nosenko, G.A., 1982, Resul'taty eksperimenta po izucheniyu oledeniya Karakoruma s borta orbital'noi stantsiy "salyut-6" [Results of

experimental studies of Karakoram glaciers from the Salyut-6 orbital station]: Materialy Glyatsiologicheskikh Issledovaniy, Pub. 42, p. 22–40.

Desio, Ardito, Marussi, Antonio, and Caputo, Michele, 1961, Glaciological research of the Italian Karakoram Expedition 1953–1955, in General Assembly of Helsinki, 1960: Association Internationale d'Hydrologie Scientifique (AIHS), Pub. 54, p. 224–232.

Dozier, J., and Marks, D., 1987, Snow mapping and classification from Landsat Thematic Mapper data: Annals of Glaciology, v. 9, p. 97–103.

Dyurgerov, M.B., and Meier, M.F., 2000, Twentieth century climate change — Evidence from small glaciers: Proceedings of the National Academy of Science, v. 97, no. 4, p. 1406–1411.

Edwards, J.I., 1960, The Batūra Muztagh Expedition, 1959: The Alpine Journal, v. 65, no. 300, p. 48–52.

Elson, J.A., 1980, Glacial geology, in Siegel, B.S., and Gillespie, A.R., eds., Remote sensing in geology: New York, John Wiley, p. 505–551.

Finsterwalder, Richard, 1937, Die Gletscher des Nanga Parbat, Glaciologische Arbeiten der Deutschen Himalaya Expedition 1934 und ihre Ergebnisse: Zeitschrift für Gletscherkunde, v. 25, p. 57–108, and topographic map at 1:100,000.

Finsterwalder, Richard, 1960, German glaciological and geological expeditions to the Batūra Mustagh and Rakaposhi Range: Journal of Glaciology, v. 3, no. 28, p. 787–788.

Finsterwalder, Richard, and Pillewizer, W., 1939, Photogrammetric studies of glaciers in high Asia: The Himalayan Journal, v. 11, p. 107–113.

Finsterwalder, R., Raechl, W., and Misch, P., 1935, The scientific work of the German Himalayan expedition to Nanga Parbat, 1934: The Himalayan Journal, v. 7, p. 44–52.

Fujita, K., Nakawo, M., Fujii, Y., and Paudyal, P., 1997, Changes in glaciers in Hidden Valley, Mukut Himal, Nepal Himalayas, from 1974 to 1994: Journal of Glaciology, v. 43, no. 145, p. 583–588.

Gardner, J.S., 1986, Recent Fluctuations of Rakhiot Glacier, Nanga Parbat, Punjab Himalaya, Pakistan: Journal of Glaciology, v. 32, no. 112, p. 527–529.

Gardner, J.S., and Jones, N.K., 1993, Sediment transport and yield at the Rāikot Glacier, Nanga Parbat, Punjab Himalaya, in Shroder, J.F., Jr., ed., Himalaya to the Sea: Geology, Geomorphology and the Quaternary, p. 184–197.

Gilchrist, A.R., Summerfield, M.A., and Cockburn, H.A.P., 1994, Landscape dissection, isostatic uplift, and the morphologic development of orogens: Geology, v. 22, no. 11, p. 963–966.

Gillespie, A., and Molnar, P., 1995, Asynchronous maximum advances of mountain and continental glaciers: Reviews of Geophysics, v. 33, p. 311–364.

Goudie, A.S., Jones, D.K.C., and Brunsden, Denys, 1984, Recent fluctuations in some glaciers of the western Karakoram mountains, Hunza, Pakistan, in Miller, K.J., ed., The International Karakorum Project, v. 2, p. 411–455.

Haeberli, W., and Beniston, M., 1998, Climate change and its impacts on glaciers and permafrost in the Alps: Ambio, v. 27, no. 4, p. 258–265.

Haeberli, W., Hoelzle, M., and Suter, S., 1998, Into the second century of worldwide glacier monitoring — Prospects and strategies: Paris, UNESCO, 227 p.

Haefner, H., Seidel, K., and Ehrler, H., 1997, Applications of snow cover mapping in high mountain regions: Physics and Chemistry of the Earth, v. 22, p. 275–278.

Hall, D.K., Chang, A.T.C., Foster, J.L., Benson, C.S., and Kovalick, W.M., 1989, Comparison of in situ and Landsat derived reflectance of Alaskan glaciers: Remote Sensing of the Environment, v. 28, p. 23–31.

Hall, D.K., Chang, A.T.C., and Siddalingaiah, H., 1988, Reflectances of glaciers as calculated using Landsat-5 Thematic Mapper data: Remote Sensing of the Environment, v. 25, p. 311–321.

Hall, D.K., Kaminski, M., Cavalieri, D.J., Dickinson, R.E., and others, 2005, Earth observing system snow and ice products for observation and modeling: EOS (Transactions, American Geophysical Union), v. 86, no. 7, p. 67.

Hallet, B., Hunter, L., and Bogen, J., 1996, Rates of erosion and sediment evacuation by glaciers — A review of field data and their implications: Global and Planetary Change, v. 12, p. 213–235.

Hambrey, Michael, 1994, Glacial environments: London, UCL Press, 296 p.

Harbor, J., and Warburton, J., 1992, Glaciation and denudation rates: Nature, v. 356, no. 6372, p. 751.

Harbor, J., and Warburton, J., 1993, Relative rates of glacial and nonglacial erosion in alpine environments: Arctic and Alpine Research, v. 25, p. 1–7.

Hayden, H.H., 1907, Notes on certain glaciers in northwest Kashmir: Geological Survey of India, Records, v. 35, p. 127–137.

Henderson-Sellars, A., and Pitman, A.J., 1992, Land-surface schemes for future climate models — Specification, aggregation, and heterogeneity: Journal of Geophysical Research, v. 97, no. D3, p. 2687–2696.

Hewitt, Kenneth, 1969, Glacier surges in the Karakoram Himalaya (Central Asia): Canadian Journal of Earth Sciences, v. 6, no. 4, p. 1009–1018.

Hewitt, Kenneth, 1988a, Catastrophic landslide deposits in the Karakoram Himalaya: Science, v. 242, no. 4875, p. 64–67.

Hewitt, Kenneth, 1988b, The snow and ice hydrology project — Research and training for water resource development in the Upper Indus Basin: Journal of Canada-Pakistan Cooperation, v. 2, no. 1.

Hewitt, Kenneth, 1990, Snow and ice hydrology project, Upper Indus Basin, Canada-Pakistan — Final Report for the Hydrology Research Division, Water and Power Development Authority (WAPDA), Pakistan and International Development Research Centre (IDRC), Ottawa: Waterloo, Ontario, Wilfrid Laurier University, 9 v.

Hewitt, Kenneth, 1998, Catastrophic landslides and their effect on the Upper Indus streams, Karakoram Himalaya, northern Pakistan: Geomorphology, v. 26, p. 47–80.

Hewitt, Kenneth, 1999, Quaternary moraines vs catastrophic rock avalanches in the Karakoram Himalaya, northern Pakistan: Quaternary Research, v. 51, p. 220–237.

Hewitt, Kenneth, Wake, C.P., Young, G.J., and David, C., 1989, Hydrological investigations at Biafo Glacier, Karakoram Himalaya — An important source of water for the Indus River: Annals of Glaciology, v. 13, p. 103–108.

Horvath, Eva, 1975, Glaciers of the Hindu Kush, *in* Field, W.O., ed., Mountain glaciers of the northern hemisphere: Hanover, New Hampshire, U.S. Army Cold Regions Research and Engineering Laboratory, v. 1, p. 361–370.

Holdsworth, Gerald, Howarth, P.J., and Ommanney, C.S.L., 2002, Quantitative measurements of Tweedsmuir Glacier and Lowell Glacier imagery, *in* Williams, R.S., Jr., and Ferrigno, J.G., eds., Satellite image atlas of glaciers of the world: U.S. Geological Survey Professional Paper 1386–J (North America), p. J312–J324.

Hubbard, A.L., 1997, Modelling climate, topography and paleoglacier fluctuations in the Chilean Andes: Earth Surface Processes and Landforms, v. 22, p. 79–92.

Kääb, A., 2005, Combination of SRTM3 and repeat ASTER data for deriving alpine glacier flow velocities in the Bhutan Himalaya: Remote Sensing of Environment, v. 94, p. 463–474.

Kääb, A., Paul, F., Maisch, M., Hoelzle. M., and Haeberli, W., 2002, The new remote sensing derived Swiss glacier inventory — II. First results: Annals of Glaciology, v. 34, p. 362–366.

Kamb, Barclay, Raymond, C.F., Harrison, W.D., Engelhardt, Hermann, and others, 1985, Glacier surge mechanism — 1982–1983 surge of Varigated Glacier, Alaska: Science, v. 227, no. 4686, p. 469–479.

Kaser, G., 2001, Glacier-climate interaction at low latitudes: Journal of Glaciology, v. 47, no. 157, p. 195–204.

Kaser, G., and Fountain, A., 2001, A manual for monitoring the mass balance of mountain glaciers, with particular attention to low latitude characteristics — A contribution from ICSI to the UNESCO HKH-Friend program: ICSI/UNESCO/HKH-Friend glacier mass balance manual 12.01, draft December 2001.

Kick, W., 1962, Variations of some central Asiatic glaciers, *in* Symposium of Obergurgl: Association Internationale d'Hydrologie Scientifique (AIHS), Pub. 58, p. 223–229.

Kick, W., 1975, Application of geodesy, photogrammetry, history and geography to the study of long-term mass balances of Central Asiatic glaciers, Snow and Ice Symposium (Proceedings of Moscow Symposium, August 1971): IAHS-AISH Publication No. 104, p. 150–160.

Kick, W., 1980, Material for a glacier inventory of the Indus drainage basin — The Nanga Parbat Massif, *in* World Glacier Inventory, Proceedings of the Reideralp workshop: IAHS-AISH Publication, v. 126, p. 105–109.

Kieffer, H., Kargel, J.S., Barry, R., Bindschadler, R., Bishop, M.P., and others, 2000, New eyes in the sky measure glaciers and ice sheets: EOS (Transactions, American Geophysical Union), v. 81, no. 24, p. 265, 270–271.

Knizhnikov, Yu.F., Osipova, G.B., Tsvetkov, D.G, and Kharkovets, E.G., 1997, Measurements of the movement of surging glaciers by the method of aeropseudoparallaxes (Using the Medvezhiy Glacier as an example): Materialy Glyatsiologicheskikh Issledovaniy, Pub. 81, p. 55–60.

Koons, P.O., 1995, Modeling the topographic evolution of collisional belts: Annual Review Earth and Planetary Science, v. 23, p. 375–408.

Kotlyakov, V.M., 1980, Problems and results of studies of mountain glaciers in the Soviet Union, *in* World glacier inventory, Proceedings of the Reideralp workshop: IAHS-AISH Publication 126, p. 129–137.

Kotlyakov, V.M., 1997, Atlas snezhno – ledovykh resursov mira [World atlas of snow and ice resources]: Moscow, Rossiiskaya Akademiya Nauk, 3 v., 392 p.

Kotlyakov, V.M., Serebrjanny, L.R., and Solomina, O.N., 1991, Climate change and glacier fluctuations during the last 1,000 years in the southern mountains of the USSR: Mountain Research and Development, v. 11, p. 1–12.

Kravtsova, V.I., 1982, Ispol'zovanie kosmicheskikh shimkov v kartografirovaniy gornogo oledeneniya [The use of space images in the mapping of mountain glaciers]: Materialy Glyatsiologicheskikh Issledovaniy, Pub. 42, p. 18–22.

Kravtsova, V.I., and Lebedeva, I.M., 1974, Ispol'zovanie kosmicheskikh shimkov dlya izucheniya glyatsiologicheskikh v gornykh regionov [Using satellite images for glaciological investigations of mountain regions], *in* Issledovanie prirodnoi sredny kosmicheskimisredstvami [Investigation of the Natural Environment by Space Means]: Academy of Sciences of the USSR, Committee on Natural Resources, Investigation from Spacecraft, v. 3, p. 57–68.

Krimmel, R.M., Post, Austin, and Meier, M.F., 1976, Surging and nonsurging glaciers in the Pamir Mountains, U.S.S.R., *in* Williams, R.S., Jr., and Carter, W.D., eds., ERTS–1, a new window on our planet: U.S. Geological Survey Professional Paper 929, p. 178–179.

Lambeck, K., and Chappel, J., 2001, Sea level change through the last glacial cycle: Science, v. 292, no. 5517, p. 679–686.

Lebedeva, I.M., 1993, Let'nyaya temperatura vozdukha v nival'no-glyatsial'nom poyase tsentral'no Aziatskogo gornogo massiva [Summer air temperature in the nival-glacial band of central Asian mountain massifs]: Izvestia RAN Seriya Geograficheskaya, no. 6, p. 20–39.

Lebedeva, I.M., 1995, Shirotnye faktory izmenchivosti rezhima lednikovykh sistem tsentral'no Aziatskogo gornogo massiva [Latitude-induced factors underlying the changeability of the regime of glacier systems within the Central Asia mountain massif]: Materialy Glyatsiologicheskikh Issledovaniy, Pub. 79, p. 86–94.

Lebedeva, I.M., and Kislov, A.V., 1993, Atmosfernye osadki I vysota granitsy pitaniya lednikov v subtropicheskom tsentral'no-Aziatskom regione [Atmospheric precipitation and the equilibrium line altitude on glaciers of subtropical Central Asian region]: Materialy Glyatsiologicheskikh Issledovaniy, Pub. 76, p. 60–76.

Liestøl, Olav, 1993, Glaciers of Svalbard, Norway, *in* Williams, R.S., Jr., and Ferrigno, J.G., eds., Satellite image atlas of glaciers of the world: U.S. Geological Survey Professional Paper 1386–E (Europe), p. E127–E151.

Loewe, F., 1959, Some observations of the radiation budget and of the ablation of glacier ice in the Nanga Parbat region: Pakistan Journal of Science, v. 11, no. 5, p. 227–236.

Loewe, F., 1961, Glaciers of Nanga Parbat: Pakistan Geographical Review, v. 16, p. 19–24.

MacGregor, K.R., Anderson, R.S., Anderson, S.P., and Waddington, E.D., 2000, Numerical simulations of glacial-valley longitudinal profile evolution: Geology, v. 28, no. 11, p. 1031–1034.

Maisch, M., 2000, The long term signal of climate change in the Swiss Alps: Glacier retreat since the end of the Little Ice Age and future ice decay scenarios: Geografia Fisica e Dinamica Quaternaria, v. 23, no. 2, p. 139–151.

Mason, Kenneth, 1930, The glaciers of the Karakoram and neighborhood: Geological Survey of India, Records, v. 63, pt. 2, p. 214–278.

Mason, Kenneth, 1935, The study of threatening glaciers: Geographical Journal, v. 85, no. 1, p. 24–41.

Mattson, L.E., 2000, The influence of a debris cover on the midsummer discharge of Dome Glacier, Canadian Rocky Mountains, *in* Nakawo, M., Raymond, C.F., and Fountain, A., eds., Debris-Covered Glaciers — Proceedings of a workshop, Seattle, Washington, 13–15 September 2000: International Association of Hydrological Sciences Publication 264, p. 25–33.

Maull, Otto, 1938, Geomorphologie: Leipzig and Vienna, Franz Deuticke, 294 p.

Mayewski, P.A., and Jeschke, P.A., 1979, Himalayan and trans-Himalayan glacier fluctuations since AD 1812: Arctic and Alpine Research, v. 11, no. 3, p. 267–287.

Mayewski, P.A., Pregent, G.P., Jeschke, P.A., and Ahmad, Naseeruddin, 1980, Himalayan and trans-Himalayan glacier fluctuations and the south Asian monsoon record: Arctic and Alpine Research, v. 12, no. 2, p. 171–182.

McClung, D.M., and Armstrong, R.L., 1993, Temperate glacier time response from field data: Journal of Glaciology, v. 39, no. 132, p. 323–326.

Meier, M.F., 1976, Monitoring the motion of surging glaciers in the Mount McKinley massif, Alaska, *in* Williams, R.S., Jr., and Carter, W.D., eds., ERTS-1, a new window on our planet, U.S. Geological Survey Professional Paper 929, p. 185–187.

Meier, M.F., 1984, Contribution of small glaciers to global sea level: Science, v. 226, no. 4681, p. 1418–1421.

Meier, M.F., and Dyurgerov, M.B., 2002, How Alaska affects the world: Science, v. 297, no. 5580, p. 350–351.

Meier, M.F., Dyurgerov, M.B., and McCabe, G.J., 2003, The health of glaciers — Recent changes in glacier regime: Climate Dynamics, v. 59, p. 123–135.

Meier, M.F., and Wahr, J.M., 2002, Sea level is rising — Do we know why?: Proceedings of the National Academy of Science, v. 99, no. 10, p. 6524–6526.

Menzies, John, 2002, Modern and past glacial environments: Oxford, U.K, Butterworth Heinemann, 543 p.

Mercer, J.H., 1963, Glacier variations in the Karakoram: Glaciology Notes, World Data Center, American Geographical Society, v. 14, p. 19–33.

Mercer, J.H., 1975, Glaciers of the Karakoram, *in* Field, W.O., ed., Mountain glaciers of the northern hemisphere: Hanover, NH, U.S. Army Cold Regions Research and Engineering Laboratory, v. 1, p. 371–409.

Miller, K.J., ed., 1984, The International Karakoram Project: Cambridge, U.K., Cambridge University Press, v. 1, 412 p., v. 2, 635 p.

Molnar, Peter, and England, P., 1990, Late Cenozoic uplift of mountain ranges and global climate change — Chicken or egg?: Nature, v. 346, no. 6279, p. 29–34.

Montgomery, D.R., 1994, Valley incision and the uplift of mountain peaks: Journal of Geophysical Research, v. 99, no. B7, p. 13,913–13,921.

Mool, P.K., Bajracharya, S.R., and Joshi, S.P., 2001, Inventory of glaciers, glacial lakes and glacial lake outburst floods, Nepal: Kathmandu, Nepal, International Center for Integrated Mountain Development, 363 p.

Mool, P.K., Wangda, D., Bajracharya, S.R., Kunzang, K., Gurung, D.R., and Joshi, S.P., 2001, Inventory of glaciers, glacial lakes and glacial lake outburst floods, Bhutan: Kathmandu, Nepal, International Center for Integrated Mountain Development, 227 p.

Mott, P.G., 1950, Karakoram survey, 1939: A new map: Geographical Journal, v. 116, nos. 1–3, p. 89–95.

Nakawo, M., Fujita, K., Ageta, U., Shankar, K., Pokhrel, P.A., and Yao Tandong, 1997, Basic studies for assessing the impacts of the global warming on the Himalayan cryosphere: Bulletin of Glacier Research, v. 15, p. 53–58.

Nosenko, G.A., 1991, Otsenka raspredeleniya rezhmia lednikov Karakoruma po materialam kosmicheskikh semok [Evaluation of the distribution and regime of Karakoram glaciers from the data of space images]: Materialy Glyatsiologicheskikh Issledovaniy, Pub. 72, p. 87–94.

Odell, N.E., 1937, The glaciers and morphology of the Franz Josef Fjord region of north-east Greenland: Geographical Journal, v. 90, no. 2, p. 111–125.

Osipova, G.B., and Tsvetkov, D.G., 1998, Opyt katalogizatsiy pul'siruyushchikh lednikov Pamira [Inventorying surging glaciers of the Pamirs]: Materialy Glyatsiologicheskikh Issledovaniy, Pub. 85, p. 223–232.

Osipova, G.B., and Tsvetkov, D.G., 2002, Issledovanie dinamiki slozhnykh lednikov po kosmicheskim snimkam [Investigations of complex glacier dynamics on the basis of space images]: Izvestia RAN, Seriya Geograficheskaya, no. 3, p. 29–38.

Osipova, G.B., and Tsvetkov, D.G., 2003, Chto daet monitoring pul'siruyushchikh lednikov? [What is the benefit of monitoring surging glaciers?]: Priroda, v. 4, p. 3–13.

Owen, L.A., Finkel, R.C., Caffee, M.W., and Gualtieri, L., 2002, Timing of multiple late Quaternary glaciations in the Hunza Valley, Karakoram Mountains, northern Pakistan: Defined by cosmogenic radionuclide dating of moraines: Geological Society of America Bulletin, v. 114, no. 5, p. 593–604.

Owen, L.A., Scott, C.H., and Derbyshire, E., 2000, The Quaternary glacial history of Nanga Parbat, Quaternary International, v. 65–66, p. 63–79.

Paul, F., Huggel C., and Kääb, A., 2004, Combining satellite multispectral image data and a digital elevation model for mapping debris-covered glaciers: Remote Sensing of Environment, v. 89, no. 4, p. 510–518.

Paul, F., Kääb, A., Maisch, M., Kellenberger, T., and Haeberli, W., 2002, The new remote sensing derived Swiss glacier inventory — I. Methods: Annals of Glaciology, v. 34, p. 355–361.

Pecci, M., and Smiraglia, C., 2000, Advance and retreat phases of the Karakorum glaciers during the 20th century — Case studies in Braldu Valley (Pakistan): Geografia Fisica e Dinamica Quaternaria, v. 23, p. 73–85.

Phillips, W.M., Sloan, V.F., and Shroder, J.F., Jr., Sharma, P., Clarke, M.L., and Rendell, H.M., 2000, Asynchronous glaciation at Nanga Parbat, northwestern Himalaya Mountains, Pakistan: Geology, v. 28, no. 5, p. 431–434.

Pillewizer, Wolfgang, 1956, Der Rakhiotgletscher am Nanga Parbat im Jahr 1954: Zeitschrift für Gletscherkunde und Glazialgeologie, v. 3, no. 2, p. 181–199.

Porter, S.C., 1970, Quaternary glacial record in Swat Kohistan, West Pakistan: Geological Society of America Bulletin, v. 81, no. 5, p. 1421–1446.

Post, Austin, Meier, M.F., and Mayo, L.R., 1976, Measuring the motion of the Lowell and Tweedsmuir surging glaciers of British Columbia, Canada, *in* Williams, R.S., Jr., and Carter, W.D., eds., ERTS-1, A new window on our planet: U.S. Geological Survey Professional Paper 929, p. 180–184.

Raymo, M.E., and Ruddiman, W.F., 1992, Tectonic forcing of the Late Cenozoic climate: Nature, v. 359, no. 6391, p. 117–122.

Raymo, M.E., Ruddiman, W.F., and Froelich, P.N., 1988, Influence of Late Cenozoic mountain building on geochemical cycles: Geology, v. 16, no. 7, p. 649–653.

Richards, B.W., Benn, D.I., Owen, L.A., Rhodes, E.J., and Spencer, J.Q., 2000, Timing of late Quaternary glaciations south of Mount Everest in the Khumbu Himal, Nepal: Geological Society of America Bulletin, v. 112, no. 10, p. 1621–1632.

Roohi, Rakhshan, 2007, Research on global changes in Pakistan, *in* Baudo, R., Tartari, G., Vuillermoz, E., and Shroder, J.F., Jr., eds., Mountains, witnesses of global changes — Research in the Himalaya and Karakoram — Developments in Earth Surface Processes, v.10, p. 329–340: Amsterdam, Netherlands, Elsevier.

Roohi, Rakhshan, Ashraf, A., Hussain, S., Naz, R., Mool, P.K., and Bajracharya, S.R., 2005, Indus basin, Pakistan, Hindu Kush-Karakoram-Himalaya. Inventory of glaciers and glacier lakes and the identification of potential glacial lake outburst floods (GLOFS) affected by global warming in the mountains of the HKH region: Water Resources Research Institute, National Agricultural Research Centre, Final Report to Government of Pakistan, CD-ROM, unpublished.

Ruddiman, W.F., 1997, Tectonic uplift and climate change: New York, Plenum Press, 535 p.

Schaper, J., Martinec, J., and Seidel, K., 1999, Distributed mapping of snow and glaciers for improved runoff modeling: Journal of Hydrological Processes, v. 13, no. 12–13, p. 2023–2036.

Scott, C.H., 1992, Contemporary sediment transfer in Himalayan glacial systems: Implications for the interpretation of the Quaternary record: unpublished Ph.D. thesis, University of Leicester, U.K., 356 p.

Searle, M.P., 1991, Geology and Tectonics of the Karakoram Mountains: Chichester, John Wiley, 358 p.

Seltzer, G.O., 1993, Late-Quaternary glaciation as a proxy for climate change in the central Andes: Mountain Research and Development, v. 13, p. 129–138.

Shi Yafeng, and Wang Wenying, 1980, Research on snow cover in China and the avalanche phenomena of Batūra Glacier in Pakistan: Journal of Glaciology, v. 26, no. 94, p. 25–30.

Shipton, Eric, 1938, The Shaksgam expedition, 1937: Geographical Journal, v. 91, no. 4, p. 313–339.

Shipton, Eric, 1940, Karakoram, 1939: Geographical Journal, v. 95, no. 6, p. 409–427.

Shroder, J.F., Jr., 1980, Special problems of glacier inventory in Afghanistan, *in* World Glacier Inventory, Proceedings of the Riederalp workshop: IAHS–AISH Publication No. 126, p. 149–154.

Shroder, J.F., Jr., 1989, Hazards of the Himalaya: American Scientist, v. 77, no. 6, p. 564–573.

Shroder, J.F., Jr., and Bishop, M.P., 1998, Mass movement in the Himalaya — New insights and research directions, *in* Shroder, J.F, Jr., ed., Special volume on "Mass Movement in the Himalaya": Geomorphology, v. 26, p. 13–35.

Shroder, J.F., Jr., and Bishop, M.P., 2000, Unroofing the Nanga Parbat Himalaya, *in* Khan, M.A., Treloar, P.J., Searle, M.P., and Jan, M.Q., eds., Tectonics of the Western Himalaya and Karakoram: Geological Society of London Special Publication 170, p. 163–179.

Shroder, J.F., Jr., and Bishop, M.P., 2009, Glaciers of Afghanistan, *in* Williams, R.S., Jr., and Ferrigno, J.G., eds., Asia, U.S. Geological Survey Professional Paper, 1386–F, p. F167–F199.

Shroder, J.F., Jr., Bishop, M.P., Copland, L., and Sloan, V., 2000, Debris-covered glaciers and rock glaciers in the Nanga Parbat Himalaya, Pakistan: Geografiska Annaler, v. 82A, no. 1, p. 17–31.

Shroder, J.F., Jr., DiMarzio, C.M., Bussom, D.E., and Braslau, David, 1978, Remote sensing of Afghanistan: Afghanistan Journal, v. 5, no. 4, p. 123–128.

Shroder, J.F., Johnson, R., Saqib Khan, M., and Spencer, M., 1984, Batūra Glacier terminus, 1984, Karakoram Himalaya: University Peshawar (Pakistan), Geological Bulletin, v. 17, p. 119–126.

Shroder, J.F., Jr., Kahn, M.S., Lawrence, R.D., Madin, I.P., and Higgins, S.M., 1989, Quaternary glacial chronology and neotectonics in the Himalaya of northern Pakistan, *in* Malinconico, L.L., Jr., and Lillie, R.J., eds., Tectonics of the western Himalaya: Geological Society of America Special Paper, v. 232, p. 275–294.

Shroder, J.F., Jr., Scheppy, R.A., and Bishop, M.P., 1999, Denudation of small alpine basins, Nanga Parbat Himalaya, Pakistan: Arctic, Antarctic, and Alpine Research, v. 31, no. 2, p. 121–127.

Taylor, P.J., and Mitchell, W.A., 2000, Late Quaternary glacial history of the Zanskar Range, northwest Indian Himalaya: Quaternary International, v. 65, no. 5, p. 81–99.

Thompson, L.G., Yao T., Davis, M.E., Henderson, K.A., Mosley-Thompson, E., Lin, P.N., Beer, J., Synal, H.A., Cole-Dai, J., and Bolzan, J.F., 1997, Tropical climate instability — The last glacial cycle from a Qinghai-Tibetan ice core: Science, v. 276, no. 5320, p. 1821–1825.

Tomkin, J.H., and Braun, J., 2002, The influence of alpine glaciation on the relief of tectonically active mountain belts: American Journal of Science, v. 302, no. 3, p. 169–190.

Tsvetkov, D.G., Osipova, G.B., Zichu, X., Zhongtai, W., Ageta, Y., and Baast, P., 1998, Glaciers in Asia, *in* Haeberli, W., Hoelzle, M., and Suter, S., eds., Into the second century of worldwide glacier monitoring — Prospects and strategies: Paris, UNESCO, p. 177–196.

Visser, P.C., and Visser-Hooft, J., eds., 1938, Wissenschaftliche Ergebnisse der Neiderlandischen Expeditionen in den Karakoram und die angrenzenden Gebiete in den Jahren 1922, 1925, 1929/30 und 1939, v. 2, Glaziologie: Leiden, E.J. Brill, 216 p.

Wake, C.P., and Searle, M.P., 1993, Rapid advance of Pumarikish Glacier, Hispar Glacier basin, Karakoram Himalaya: Journal of Glaciology, v. 39, no. 131, p. 204–206.

Wang, W., Huang, M., and Chen, J., 1984, A surging advance of Balt Bare Glacier, *in* Miller, K.J., ed., The International Karakoram Project, v.1, p. 76–83.

Washburn, A.L., 1939, Karakoram glaciology: American Journal of Science, v. 237, no. 2, p. 138–146.

Whipple, K.X., Kirby, E., and Brocklehurst, S.H., 1999, Geomorphic limits to climate-induced increases in topographic relief: Nature, v. 401, no. 6748, p. 39–43.

Whipple, K.X., and Tucker, G.E., 1999, Dynamics of the stream-power river incision model — Implications for height limits of mountain ranges, landscape response timescales, and research needs: Journal of Geophysical Research, v. 104, no. B8, p. 17,661–17,674.

Williams, R.S., Hall, D.K., and Benson, C.S., 1991, Analysis of glacier facies using satellite techniques: Journal of Glaciology, v. 37, no. 125, p. 120–128.

Workman, F.B., and Workman, W.H., 1910, The Hispar Glacier: Geographical Journal, v. 35, no. 2, p. 105–132.

Workman, W.H., and Workman, F.B., 1911, The call of the snowy Hispar: New York, Charles Scribner's Sons, 297 p.

Zeitler, P.K., Koons, P.O., Bishop, M.P., Chamberlain, C.P., and others, 2001, Crustal reworking at Nanga Parbat, Pakistan: Metamorphic consequences of thermal-mechanical coupling facilitated by erosion: Tectonics, v. 20, no. 5, p. 712–728.

Zeitler, P.K., Meltzer, A.S., Koons, P.O., Craw, D., and others, 2001, Erosion, Himalayan geodynamics, and the geomorphology of metamorphism: GSA Today, v. 11, p. 4–8.